JOURNAL OF ENERGY IN SOUTHERN AFRICA

Volume 27 Number 2 • May 2016

Sponsored by the Department of Science and Technology

JOURNAL OF ENERGY IN SOUTHERN AFRICA

Submissions

It is the policy of the *Journal of Energy in Southern Africa* to publish papers covering the technical, economic, policy, environmental and social aspects of energy research and development carried out in, or relevant to, Southern Africa. Only previously unpublished work will be accepted; conference papers delivered but not published elsewhere are also welcomed. Short comments, not exceeding 500 words, on articles appearing in JESA are invited. Relevant items of general interest, news, statistics, technical notes, reviews and research results will also be included, as will announcements of recent publications, reviews, conferences, seminars and meetings.

Those wishing to submit contributions should refer to the guidelines given on the JESA website (although these are currently under review).

The Editorial Committee does not accept responsibility for viewpoints or opinions expressed here, or the correctness of facts and figures.

The *Journal of Energy in South Africa* is accredited by the South African Department of Higher Education and Training for university subsidy purposes. It is abstracted and indexed in Environment Abstract, Index to South African Periodicals, and the Nexus Database System. JESA has also been selected into the Science Citation Index Expanded by Thomson Reuters (as from Volume 19 No 1). It is also on the Scientific Electronic Library Online SA platform and is managed by the Academy of Science of South Africa.

The Editorial Committee does not accept responsibility for viewpoints or opinions expressed here, or the correctness of facts and figures.

Website: www.erc.uct.ac.za/journals/jesa

Sponsored by the Department of Science & Technology

JOURNAL OF ENERGY IN SOUTHERN AFRICA

Volume 27 Number 2 • May 2016

CONTENTS

Editorial

Thank you to all the authors and all who helped make Issue 2 of Volume 27 of the *Journal of Energy in Southern Africa* a success! Much consideration will preferentially be given to research designed or set up in the southern African region and to studies associated with energy-related matters in the southern African region.

A literature review on the potential of renewable electricity sources for mining operations in South Africa

Roman Günter Votteler*[a]

Alan Colin Brent[b]

a. *School of Public Leadership, and the Centre for Renewable and Sustainable Energy Studies, Stellenbosch University, Stellenbosch, South Africa*
b. *Department of Industrial Engineering, and the Centre for Renewable and Sustainable Energy Studies, Stellenbosch University, Stellenbosch, South Africa*

Abstract
The economic situation of mining corporations operating in South Africa has in recent years created considerable challenges in staying globally competitive. One reason for this is the increase in average electricity costs from 7% to 20% of total operational expenses since 2007. Forecasts for the next decade predict that this development will continue at similar rates. The reliability of Eskom has also decreased, with self-generation being increasingly considered. In addition, the South African government plans to launch a carbon tax in 2016, which will further add to the costs of current electricity sources. This paper investigates the potential of renewable electricity sources for mining operations in South Africa. It is based on an extensive literature analysis, which was conducted in the form of a conceptual review. The investigation of electricity usage patterns reveals that mining operations commonly have a relatively constant day and night consumption. One of the prerequisites for a suitable source is its ability to supply electricity constantly. Most renewable sources can therefore only be used in hybrid versions, owing to relatively high intermittencies, especially with electricity supply from solar photovoltaic and wind generation. Nevertheless, the levelised costs are substantially lower than diesel generators and are already similar to Eskom tariffs, whilst also lowering carbon emissions. The business case of self-generation is shown to be positive. An on-site project can be realised through a power purchase agreement or through own investments.

Keywords: mining; South Africa; renewable energy

Corresponding author. *Tel:* 021 8089530; *Email:* acb@sun.ac.za

1. Introduction

The cost of electricity for mining corporations in South Africa has substantially increased in recent years. The average percentage of annual expenditure on electricity costs for members of the Energy Intensive User Group of Southern Africa, of which 47% are mining companies, has risen from 7% in 2007 to 20% in 2014, (Energy Intensive User Group of Southern Africa, 2014).[1] Power rarely constitutes less than 10% of mining operating costs and often exceeds 25% (Banerjee et al., 2015). The current commonly used electricity sources are on-site diesel generators and the electrification grid of the national utility supplier, Eskom (Boyse, Causevic, Duwe & Orthofer, 2014). Electricity price escalations, past and future, will damage the global competitiveness of these companies (Creamer, 2012). Moreover, uncertainty around reliable electricity supply and carbon emissions management hinders the possible future development of these companies (Kohler, 2014).

The current situation of these companies demands an investigation of alternative sources of electricity, in order to lower costs, to create greater independence and to decrease the carbon footprint of their operations.[2] The enormous technological and economic development of renewable sources of electricity in recent years has increased their attractiveness as a possible option for mining operations in South Africa to diversify electricity sources (Mulaudzi, Muchie & Makhado, 2012; Cornish, 2013).

As Figure 1 shows, the investigation, summarised in the paper, looks at how renewable sources could fit into the electricity usage patterns of mining operations, the technological attractiveness of different renewable and current sources, the most

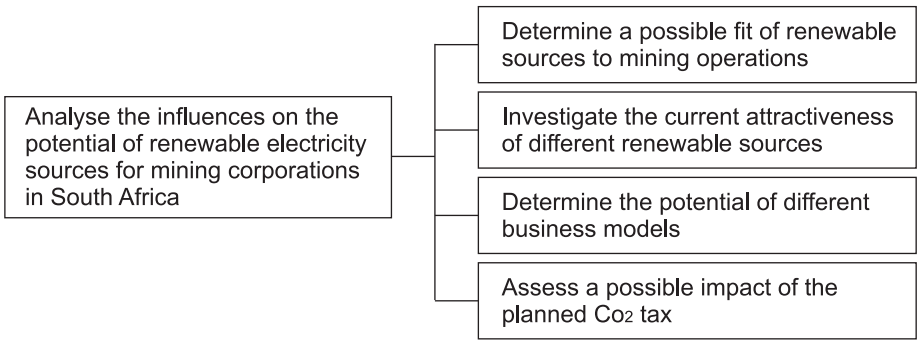

Figure 1: Research objectives

beneficial business model is investigated, and possible impacts of the CO_2 tax. No previous study combining all the macroeconomic elements that influence the project realisation of renewable electricity projects with mining corporations in South Africa could be found through a literature review. Three papers – by Boyse et al. (2014), Gets and Mhlanga (2013), and Brodsky et al. (2013) – do, however, cover some of the elements.

2. Methodology

Petticrew and Roberts (2006) identify six different types of literature reviews, namely: systematic review, narrative review, conceptual review, traditional review, critical review and state of the art review. For this paper a conceptual review was conducted. A conceptual review aims to synthesise areas of conceptual knowledge that can contribute to a better understanding of these issues. The objectives of these syntheses are to provide an overview of the literature in a given field, including the main ideas, models and debates (Petticrew & Roberts, 2006). The literature – conference and journal papers, theses and dissertations, and industry reports from 2008 onwards – was researched until the information was repeated in new texts. This approach assisted in identifying all key factors and their potential effect on the realisation of renewable electricity projects by mining corporations in South Africa. Based on the fact that the element topics are broad, and that there is a vast amount of information, this approach was deemed most suitable. Other approaches, such as a systematic review, would be too detailed and extensive.

3. Mining operations

3.1 Electricity pattern of mining operations

The current development of lower commodity prices hinders the widespread adoption of renewables, as falling profits and lower fuel prices maintain barriers (Crespo, 2015). In addition, the long-term investment into renewables is hindered by the investors' pressure for short-term capital appreciations (Elliott, 2014). As a result, one of the main outcomes of several renewables and mining summits worldwide is the recognition that mining corporations have to be better educated about the concept of renewable sources in the context of their unique operational demands (Judd, 2014b).[3]

Electricity consumption patterns greatly influence the selection of electricity sources (Klein and Whalley, 2015). The majority of mining locations operate day and night, which often creates a relatively constant baseload demand (Levesque et al., 2014). The required amount of electricity depends on the type of mineral and even more on the extent of processing or beneficiation. (Banerjee et al., 2015). Every type of mineral mined has its specific processes, and it is not necessary for all to undergo all processes to be ready for use in manufacturing. The main processing stages are as follows (Banerjee et al., 2015):

- Extracting the resource by digging, sorting and crushing – generally known as mining.
- Concentration of the mineral using various techniques, the majority either based on gravity, or using a chemical process to separate elements, or using magnetism to separate waste from the mineral.
- Smelting of the concoction at high temperatures to separate slag from metal.
- Refining, often through electrolysis, to achieve a higher level of purity.

Figures 2–4 are based on a database of 168 mining operations in Africa (World Bank Group, 2015a). Figure 2 provides an overview of the cumulative power requirements for mining operations at stages of beneficiation. By far the most electricity-intense ones are the platinum group, gold and aluminium. Gold and platinum is illustrated in ounces and it needs 35 273 oz to fill up a tonne (Metric Conversion, 2015). Nickel, ilmenite, cobalt, copper and chromium also have a relatively high electricity demand with a more mixed consumption profile.

The overall contribution in the different periods to the mining electricity demand of the sample can be seen in Figure 3. The smelting and refining processes are the most electricity-intensive and were responsible in all periods for more than three quarters of the demand. Mining in South Africa is the

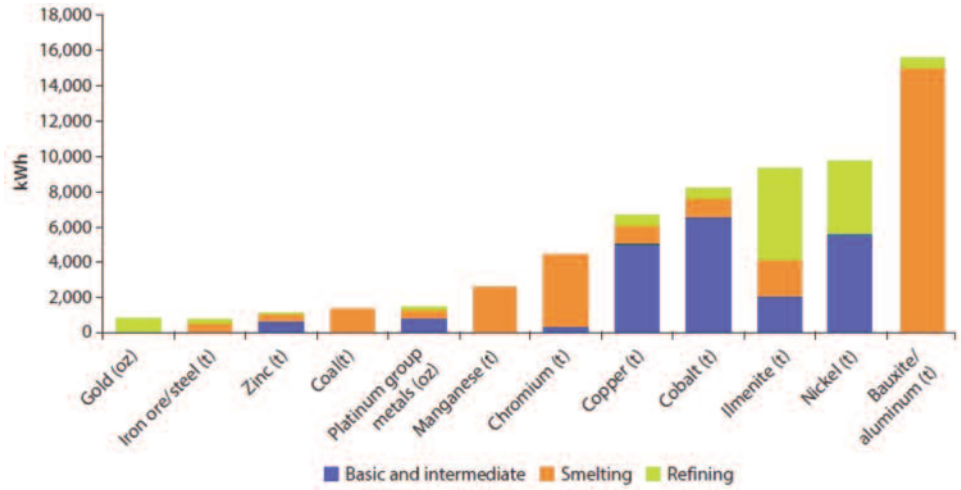

Figure 2: Cumulative power requirements at stages of beneficiation

Source: Banerjee et al. (2015)

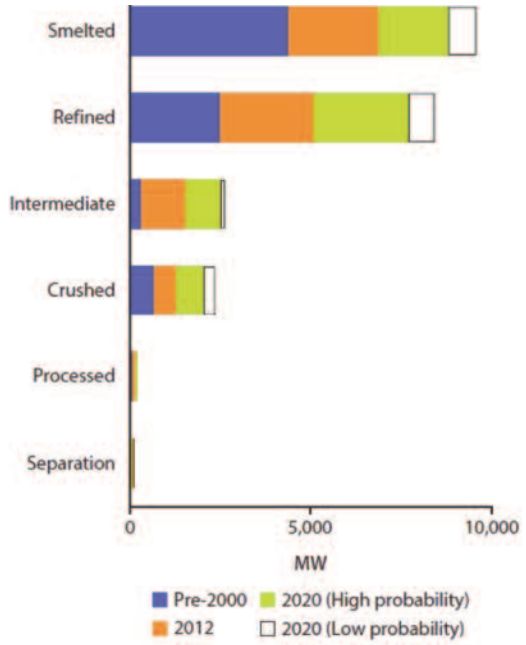

Figure 3: Electricity demand by processing stage

Source: Banerjee et al. (2015)

most electricity-intense industry in Sub-Saharan Africa, with 70% of the demand in 2000 and 66% in 2012. The contribution is, however, forecast to decline to 56% if all high- and low-probability projects are completed (Banerjee et al., 2015).

Another factor affecting electricity demand is whether mining operations are underground or at the surface. Underground mining operations require significantly higher quantities of electricity, due to a great rise in hauling requirements, ventilation, water-pumping and other operations (Toledano, 2012). Figure 4 provides an indication of the difference in electricity demand for coal, copper, gold and platinum. It can be seen that surface mining consumes 30% to 40% less electricity.

3.2 The demand profile

This section introduces the 24-hour demand profiles of five different mining operations in South Africa. The purpose is to gain a better understanding of the consumption patterns and how renewable electricity sources could fit in.

The demand profile in Figure 5 illustrates the

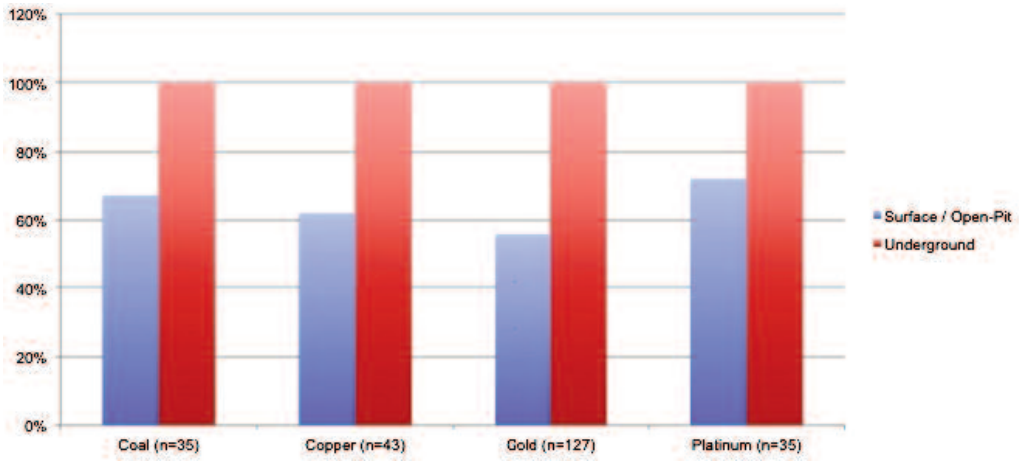

Figure 4: Underground and surface mining electricity demand

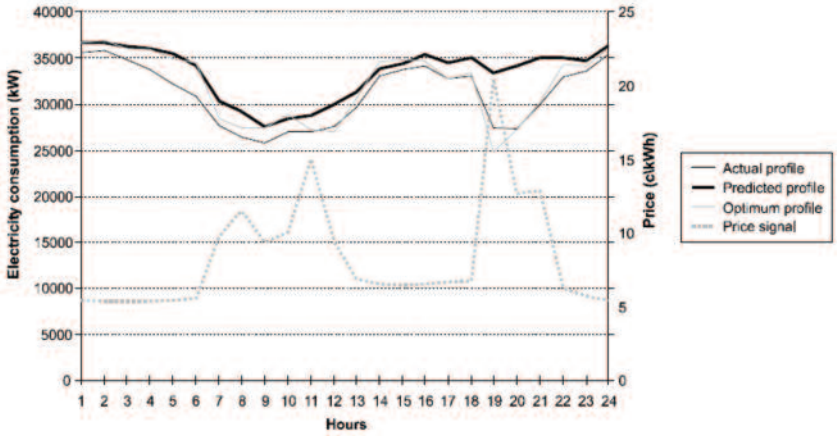

Figure 5: Electricity demand profile of an underground gold mine
Source: Mathews (2005)

electricity consumption pattern of an underground grid connected gold mine in South Africa. The 24-hour electricity demand is relatively constant, with two visible reductions at approximately 9am and 7pm. The purpose of these reductions is to save costs and to shift loads to other times if possible. The reason for shifting consumption is Eskom's Megaflex tariff structure, which is used for large electricity consumers and is more expensive at these times, as can be seen on the price signal line. In addition, Eskom's demand response programme invites large customers to reduce their demand when requested in return for financial rewards, which improves grid stability (Williams, 2014). This demand-side management (DSM) strategy is commonly used in South Africa to lower operating costs by optimising time schedules of systems like pumping and refrigerating (Mathews, 2005).

Figure 6 illustrates another average weekday and Sunday consumption profile of a large grid-connected underground gold mine in South Africa. The purpose of the consumption reduction around 8:00 and 18:00 is again to save costs by shifting demand to other times (Wouter, 2014). Apart from the two reductions, the day and night electricity consumption remains relatively constant. The demand profile in Figure 7 illustrates the 24-hour electricity usage of an underground grid-connected coalmine in South Africa. The usage dip between 2am and 7am is due to operating processes and not a DSM strategy, but the reduction at 6pm is load-shifting to reduce costs. The consumption on weekends is lower than during the week (van Staden, 2015). The electricity demand profile of the third mine does not exist in the form of a graph, as the consumption is not recorded on an hourly base.

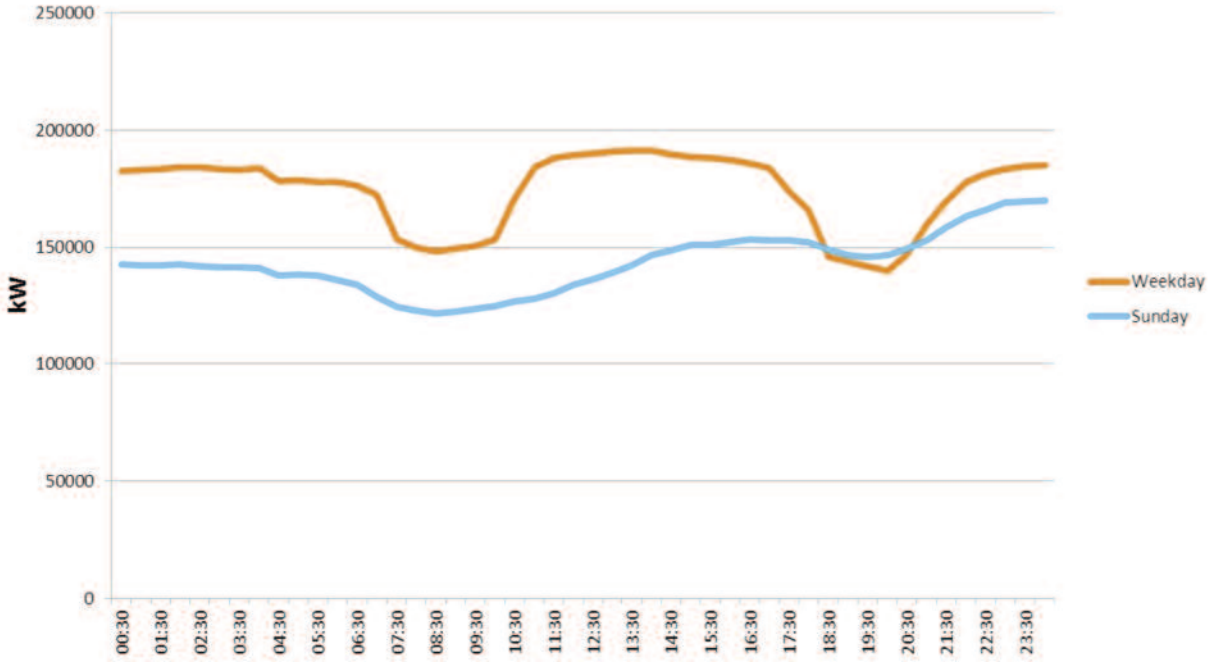

Figure 6: Electricity demand profile of an underground gold mine
Source: Wouter (2014)

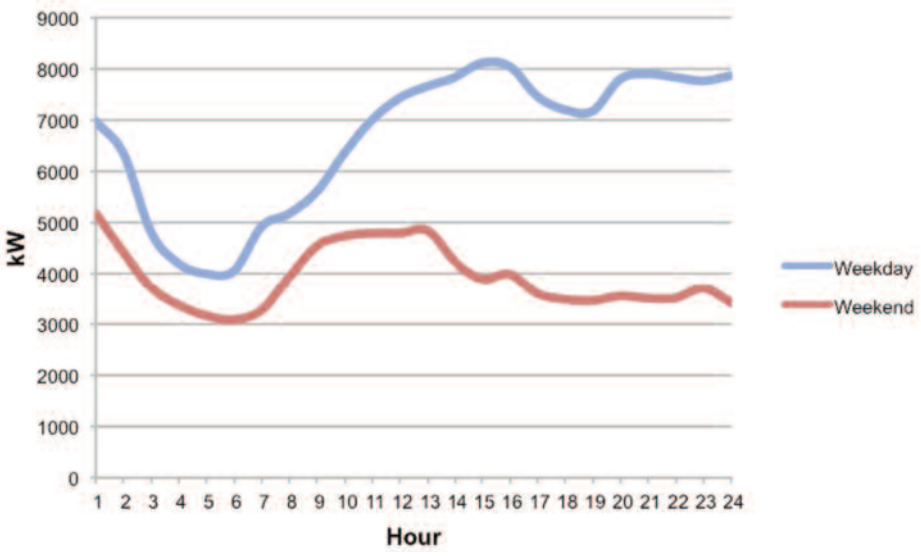

Figure 7: Electricity demand profile of an underground coal mine
Source: Van Staden (2015)

The operation is not grid-connected and runs on diesel generators day and night. The 24-hour consumption is constant. The mining is conducted on the surface and the main mineral extracted is zircon (Beukman, 2015).

Four demand profiles in this section and in Figure 9 in the next section show a relatively constant 24-hour consumption. The profile in Figure 7 has only one reduction in the early morning, to half the amount used after midday. The mine still uses 3MW at the lowest point of the curve. Consequently, the fundamental prerequisite for an electricity source to be suitable for a mining location is its baseload capacity to be able to cover the electricity need for 24 hours a day. The intermittency of most renewable sources like wind or solar photovoltaic (PV) renders it impossible to use these sources individually to cover the electricity demand of mining operations (Judd, 2014a; Mostert, 2014).

3.3 Hybrid concepts

This section introduces the concept of hybrid solutions in accordance with the demand profile. It is difficult to generalise to all mining operations, as every profile has its own characteristics, but the concept of a 24-hour demand, and commonly with a relative constant usage, is also provided in the previous section.

Without a grid connection, there are three technical options to be able to use renewable sources with lower capacity factors at mining locations: renewables with storage, a hybrid system, and a hybrid system with storage. A detailed report on the opportunities of renewables at mining locations in South Africa (Boyse et al., 2014) identifies a hybrid version combined with a baseload capacity source as most cost-effective. The model recommended is that the supply/demand profiles have to be optimised, which means that all renewable energy goes to the primary load. Ideally, at peak output the supply should not exceed the mine's demand. Grid-connected mining operations can add a single renewable source for purposes like decreasing costs, increasing independence and lowering CO_2 emissions (Levesque et al., 2014).

The basic principle of a hybrid system is illustrated and explained in Figure 8, although the hybrid project can also be realised with other renewable sources like wind. Where there is a grid-connection to Eskom it is, for example, possible to replace the diesel generator (Wirth, 2015).

The demand profile of the first renewable electricity project at the non-grid-connected Cronimet Chrome Mining's Thaba mine is presented in Figure 9 and was finalised at the end of 2012. The project is a hybrid solution, and uses a 1 MW PV system (60% penetration ratio) and a 1.6 MVA diesel generator. The diesel generator provides the back-up electricity. The time span from concept to commissioning took six months. The initial capital outlay was EUR 2.42 million for the PV plant in 2012, with annual 1% operating and maintenance costs. The annual diesel burn was 1.9 million litres, of which 450 000 litres can be saved through the solar PV plant. It was calculated that the breakeven point would be achieved at 3.6 years owing to the savings on diesel. The calculation included the assumption of an annual 12% diesel inflation rate on initially EUR 1.05 per litre. The net present value was calculated at EUR 2.86 million, with a discount rate of 15% and a lifetime of 20 years (Ambros, 2014).

The demand profile in Figure 9 is relatively constant, with a slightly increase between 8am and 5pm; the sudden drop at 11am is due to operational processes. As stated at the beginning of this section, the general solar peak supply does not

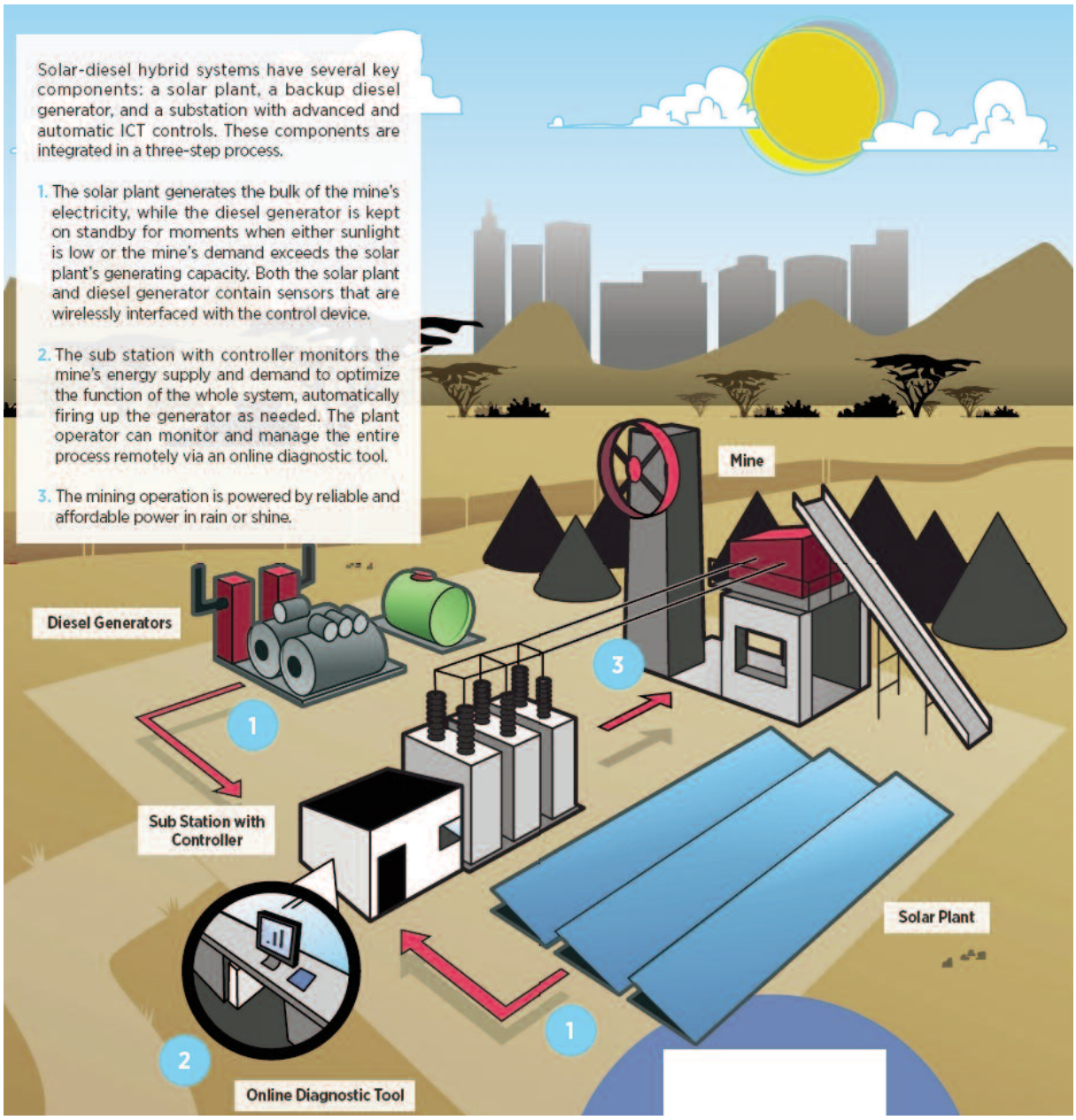

Figure 8: Principle of a hybrid system
Source: Boyse et al. (2014)

exceed the mining demand. The solar PV profile represents a clear sky throughout the whole day. As the solar PV generation increases, the diesel generator production decreases and vice versa. It is important to note that the diesel generator has a lower load limit of 25% to prevent damage. Below this limit it suffers from poor combustion, which reduces efficiency, increases maintenance costs and can cause permanent damage that reduces its life span. A control unit manages the supply levels of solar and diesel generator (International Renewable Energy Agency [IRENA], 2013). A hybrid version with Eskom requires only a 5% minimum base load to keep the electricity supply stable (Wirth, 2015).

The principles for hybrid versions with wind and geothermal power are similar, but the different generation profiles have to be considered. Wind generation is possible throughout the whole day. Variations between no wind and strong wind are possible, which makes it important to create a wind profile of the area through measurements (Rehman et al., 2012). Geothermal energy, on the other hand, is not dependent on the weather and has a constant 24-hour electricity output. Both sources require lower spinning limits for a diesel generator due to their more constant supply levels (Wirth, 2014).

3.4 South African landscape

South Africa's economy is the second-biggest on the African continent, with a GDP of EUR 3.18 billion in 2014. The GDP of Nigeria surpassed the South African one in 2011 (World Bank Group, 2015c; Statistics South Africa, 2015a). Since 2013,

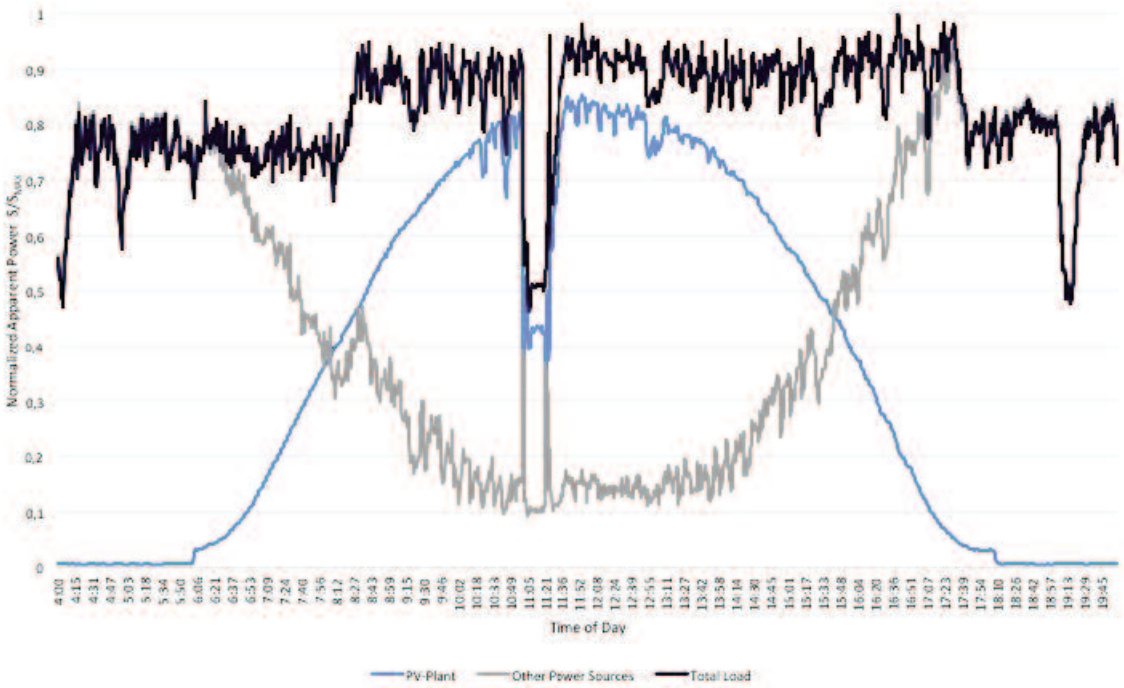

Figure 9: Electricity demand profile of a surface chromium ore mine
Source: Wirth (2015)

the mining sector in South Africa has contributed about 8% to the GDP, with a long-term downward trend since 1970's 21%. Despite the decline in the growth rate of real investment, mining is still responsible for nearly 19% of private sector investment. Today, minerals account for 30% of South Africa's total merchandise export (Chamber of Mines, 2014).

As illustrated in Figure 10, South Africa has sill one of the most reliable electricity supplies in Sub-Saharan Africa. The electricity crisis, including Eskom's power outages, contributed to economic growth dropping by 1.5% to 3.5% in 2008. The mining sector suffered the most, and plunged by 22.1% in the first quarter of 2008. The Eskom crisis in 2015 caused economic growth to contract by 1.3% in the second quarter to 1.2%. The production of the mining sector decreased by 4.8% from 2014 to 2015 (Maasdam, 2008; Statistics South Africa, 2015b).

Eskom's Megaflex tariff, commonly charged to mines because of their high consumption, increased by 346% from 2007 to 2015. As can be seen in Figure 11, however, South Africa still has one of the cheapest tariffs in Africa (the statistics are from 2014). The South African mining sector consumes 15% of Eskom's annual output. Within the mining industry, gold mining uses 47% of the total, followed by platinum at 33%, with all other sectors combined consuming the remaining 20% (Eskom, 2010).

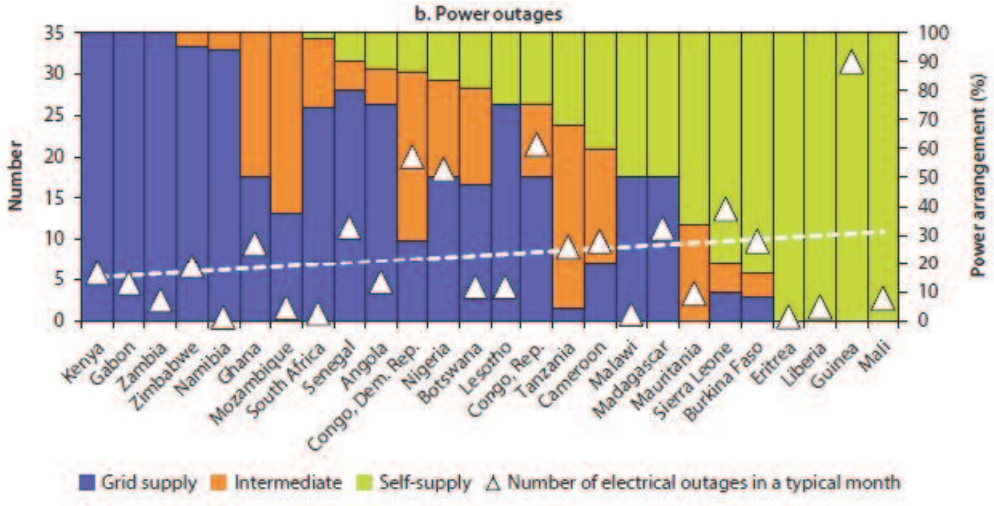

Figure 10: African comparison of security of electricity supply
Source: Banerjee et al. (2015)

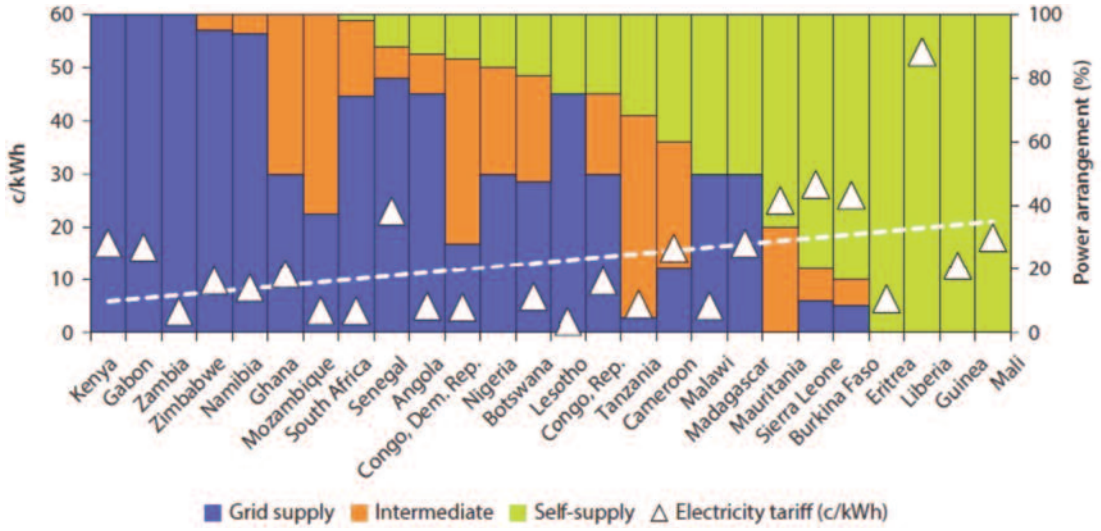

Figure 11: African comparison of electricity tariffs for mines firms
Source: Banerjee et al., 2015

3.5 A global overview of existing projects

Worldwide, 21 operating renewable energy projects were identified, and these are introduced and categorised in Table 1. The market is relatively young, with the first wind project being commissioned in 2010 and the first solar project in 2012. An overwhelming 91% of the electricity sources are solar PV (n=11) and wind (n=8) installations. Half the projects are in Chile, of which the majority are grid-connected and financed through a power purchase agreement. Table 1 shows the projects that are not connected (1–11) and those that are connected (12–21) to their countries' national grids. The following conclusions can be drawn:

Off-grid projects
- They can be found in various countries.
- Seven out of twelve are based on the mining corporation's own investment.
- The largest project is 6.7 MW.

On-grid projects
- Eight out of ten are in Chile.
- 90% are financed through a power purchase agreement; and
- Sizes range up to 115 MW.

3.2 Attractiveness of electricity sources

This section discusses technological factors of currently used and possible renewable electricity sources for mining operations in South Africa. Table 2 represents an overview of the results.

Two types of technical factors were selected. These were identified according to the main factors used to analyse electricity sources in the papers investigated for Table 2. Only experience and project size were added to the specifications of this research. The first type provides indicative data for generating technologies, namely initial investment costs, levelised costs of energy and capacity factor.[5] The second type indicates the suitability for the purpose of mining operations in South Africa. The selected factors are: the experience with the source in the global mining industry; the availability of the energy source or fuel in South Africa to power the system; the service infrastructure in South Africa; and the possibility to realise medium-scale projects of 1–10 MW. The location of mining regions in South Africa is indicated in Figure 12. This will give a better understanding of the natural fuel availability to power the renewable technology.

Gas generators were not selected, as the fuel supply infrastructure in South Africa is not sufficient and is currently not used by South African mines (Boyse et al., 2014; IRENA, 2015c). The black blocks on the maps indicate the mining areas where the source can be used. The non-renewable and renewable electricity-generating technologies, which have the potential to be used on-site or via grid connection by mining corporations, are now briefly introduced.

Diesel generator

The usage of diesel generators at mining operations in South Africa is common. The reason for this is their high reliability due to solid service and fuel infrastructure. Projects of all sizes can be executed, according to the need of the mine (Global Data, 2014). The average annual diesel price increase is a combination of the forecasted global real annual increase of 2% (OPEC, 2014; World Bank, 2015b) and a South African average annual inflation rate of 5% (International Monetary Fund, 2014; Organisation for Economic Co-operation and Development, 2014).

Eskom

Eskom is responsible for South Africa's electricity production. The country's electricity is produced with coal-fired plants (93%), renewables (1%),

Table 1: Global operating renewable energy projects at mining locations

No.	Mining cooperation	Mine	Developer	Financing	Connection	Location	Size	Source	Date of first operation	Reference
1	Antofagasta Minerals	El Tesoro	Soitec Solar	Own investment	Off-grid	Chile	0.06 MW	CPV	2013	Soitec (2015)
2	Royal Gold	El Toqui	Vergnet	Own investment	Off-grid	Chile	1.65 MW	Wind / Hydro / Diesel	2010	Vergnet Wind Turbines (2014)
3	Rio Tinto	Diavik	Enercon	Own investment	Off-grid	Canada	2.3 MW	Wind / Diesel	2012	Enercon 92015)
4	Cronimet Mining AG	Thabazimbi	Cronimet Power Solutions	Own investment	Off-grid	South Africa	1 MW	Solar PV / Diesel	2012	Cronimet Power Solutions (2015)
5	Galaxy Resources	Mt Cattlin	Swan Energy	Own investment	Off-grid	Australia	3.6 MW / 1 MW	Wind / Solar PV / Diesel	2012	Galaxy Re-sources (2015)
6	Barrick Gold	McCarran	Stellar Energy	Own investment	Off-grid	USA	1.51 MW	Solar PV / Gas	2014	Stellar Energy (2013)
7	Glencore	Reglan	Enercon	Own investment	Off-grid	Canada	3 MW	Wind / Diesel	2014	Glencore (2015)
8	Mandalay Resources	Cerro Bayo	Rame Energy	Power purchase agreement (PPA)	Off-grid	Chile	1.8 MW	Wind / Diesel	2015	Rame Energy (2014)
9	Barrick Gold	Veladero	Rame Energy	PPA	Off-grid	Argentina	2 MW	Wind / Diesel	2014	Rame Energy (2014)
10	Rio Tinto	Weipa bauxite	First Solar	PPA	Off-grid	Australia	6.7 MW	Solar PV / storage / Diesel	2014	First Solar (2015)
11	Shanta Gold	New Luke	Redavia Solar	Rental	Off-grid	Tanzania	1 MW	Solar PV / Diesel	2014	Redevia (2015)
12	Société Nationale Industrielle et Minière de Mauritanie	Nouadhibou	Vergnet	Own investment	On-grid	Mauritania Nigeria	4.5 MW	Wind	2012	SNIMM (2013)
13	Antofagasta Minerals	Los Pelambres	Pattern Energy	PPA	On-grid	Chile	115 MW	Wind	2014	Pattern Energy (2015)
14	Antofagasta Minerals	El Tesoro	Abengoa	PPA	On-grid	Chile	10.5 MW	CSP	2012	Abengoa Solar (2015)
15	Xstrata / Anglo American	Collahuasi	Solarpack	PPA	On-grid	Chile	25 MW	Solar PV	2012	Solarpack (2012b)
16	Quiborax	El Aguila	E-CL	PPA	On-grid	Chile	2.3 MW	Solar PV	2013	E-CL (2015)
17	Barrick Gold	Punta Colorada	Rame Energy	PPA	On-grid	Chile	20 MW	Wind	2011	Rame Energy (2014)
18	Imagold	Rosebel	Renewable Energy Resource Corp	PPA	On-grid	Suriname	5 MW	Solar PV	2014	Renewable Energy Re- source Corp. (2014)
19	Antofagasta Minerals	Chuquicamata	Solarpack	PPA	On-grid	Chile	1 MW	Solar PV / Diesel	2012	Solarpack (2012a)
20	Minera Dayton	Andacollo	Solairedirect	PPA	On-grid	Chile	1.26 MW	Solar PV	2013	Solairedirect (2012)
21	CAP Group	Copiapo	Sunedison	PPA	On-grid	Chile	100 MW	Solar PV	2014	Sun Edison (2013)

Table 2: Electricity-generating technologies for South African mines

	Initial investment USD/kW	*LCOE USD/kWh*	*Capacity factor in %*	*Annual forecast until 2020*	*Experience*	*Availability of power / fuel source*	*Service infrastructure*	*Project size 1–10 MW*
Diesel generator[1,2,3,4,5]	500–800	0.35–0.4	<95	8% increase	Excellent	Good	Very good	Yes
Eskom[16, 17,18, 19]	400–450	0.07–0.075	<99	12% increase	Excellent	Good	Very good	Yes
Solar PV[1,6,7]	1 500– 2 000	0.072–0.22	<30	3.4% decrease	Good	Good	Very good	Yes
CSP[1,6,7,8,9]	3 500–8 700	0.18–0.3	<80	3.5% decrease	Limited	Medium	Good	Not commercial
Wind on-shore[6,7,10]	1 300–2 200	0.06–0.12	<48	2% decrease	Good	Medium	Very good	Yes
Geothermal[7, 12,15,16]	3 000–5 500	0.08– 0.14	<90	0%	No	Medium–good	Low	Yes
Biomass[2,6,13]	2 600– 4 500	0.04–0.14	<80	0%	No	Medium–low	Low	Yes
Battery storage[1,15]	2 000–4 000	0.42–0.6		10.6% decrease	Limited	/	Low	Yes
Hydro power[2,6]	1 500–3 500	0.04–0.15	<60	0%	Limited	Medium–low	Medium–low	Yes

(1)Lazard, 2014; (2) International Energy Agency [IEA], 2014; (3) Gielen, 2012; (4) Organisation of the Petroleum Exporting Countries [OPEC], 2014; (5) World Bank Group, 2015b; (6) IRENA, 2015a; (7) IRENA, 2014; (8) Hinkley, Curtin, Hayward, Wonhas, Boyd, Grima, Tadros, Hall, Naicker & Mikhail, 2011; (9) Fichtner, 2010; (10) Fraunhofer, 2013; (11) MAKE Consulting, 2013; (12) Tshibalo, Dhansay, Nyabeze, Chevallier, Musekiwa & Olivier, 2015; (13) Bole-Rentel & Bruinsma, 2013; (14) IRENA, 2015b; (15) IEA, 2011; (16) Ngugi. 2012; (16) Department of Energy [DOE], 2013; (17) Deutsche Gesellschaft für Internationale Zusammenarbeit [GIZ], 2014; (18) Fouche, 2013; (19) Wernecke, 2015.

pumped storage (1%), gas (1%) and nuclear power (5%) (Eskom, 2014). Eskom's experience and practical knowledge is extensive, as numerous mines use Eskom as a supplier (Boyse et al., 2014). The availability of Eskom as a source can be seen in Figure 13. The thin lines represent the power grid (availability of power source), which is not ideally developed in the central and western regions. The service infrastructure is well established, as Eskom owns the /national grid. Applications can be made for medium- and large-scale connections (Eskom, 2015a).

Solar photovoltaic

The data for solar photovoltaic (PV) technology are based on single-axis tracking devices. The global experience with solar PV technology at mining operations is considerable (see Table 1). The areas with high mining activity are indicated in Figure 14; the majority have an annual radiation of more than 2 000 kW/m^2. The modular technology enables medium-sized projects. The service infrastructure is well established owing to an established market in South Africa (South African Photovoltaic Industry Association, 2013; Global Data, 2014).

Concentrating solar power

The data presented for concentrating solar power (CSP) are based on the technology of parabolic trough with synthetic oil and power tower with molten salt, as both technologies are commercially proven and available (Gauché, Brent & Von Backström, 2014). The initial investment is strongly positively correlated with the capacity factor. The global experience with CSP and mining operation is limited, with one grid-connected project in Chile (Table 1). The sun radiation in mining areas shows high potential to use CSP as a power source, as discussed with solar PV in Figure 14. The service infrastructure is established with several companies in South Africa, which have realized seven projects (National Renewable Energy Laboratory, 2015). Projects of up to 10 MW exist, but are not commercial as costs are too high (Fraunhofer ISE, 2013).

Wind power

For the purpose of this paper, only on-shore wind technology was considered, as it is easier to carry out wind parks closer to the mining operations. The international experience with wind and mining operations is advanced, with nine established off- and on-grid projects (see Table 1). Figure 15 illustrates mining areas with the highest wind potential in South Africa. The overall power availability is medium, as wind conditions in the centre of South Africa are generally less favourable (Department of Trade and Industry, 2015). The service infrastructure in South Africa is well established, as several wind farms have been established and the respon-

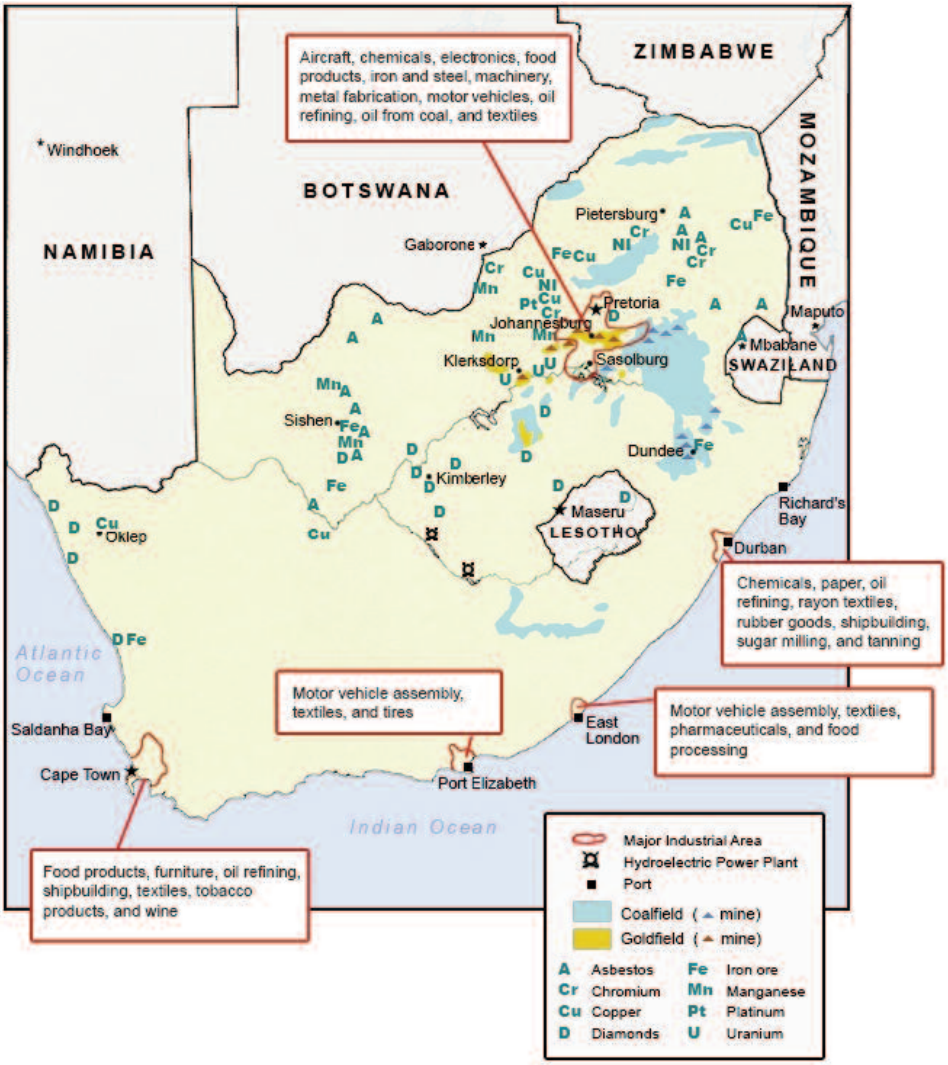

Figure 12: Industrial areas, mines and ports in South Africa
Source: Michigan State University (2006)

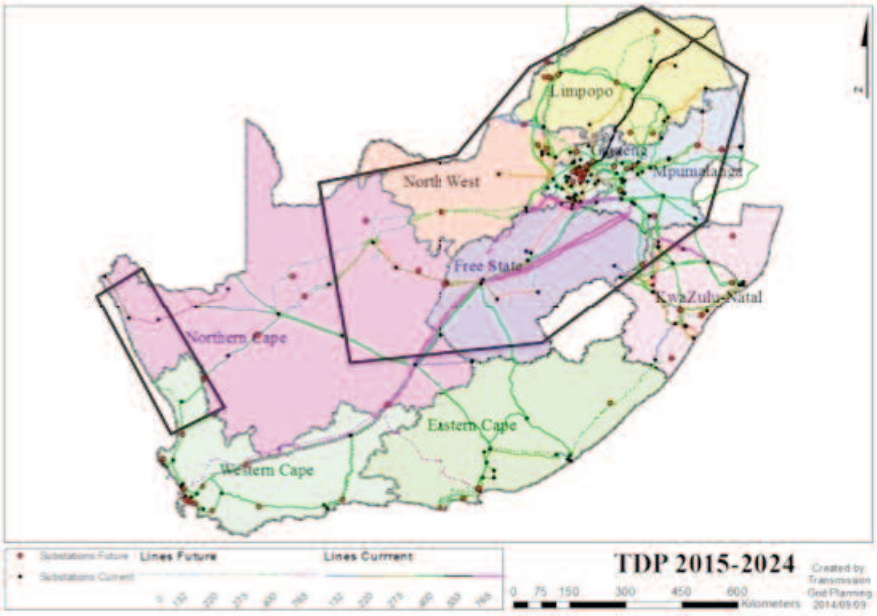

Figure 13: Eskom power stations and grid
Source: Eskom (2013)

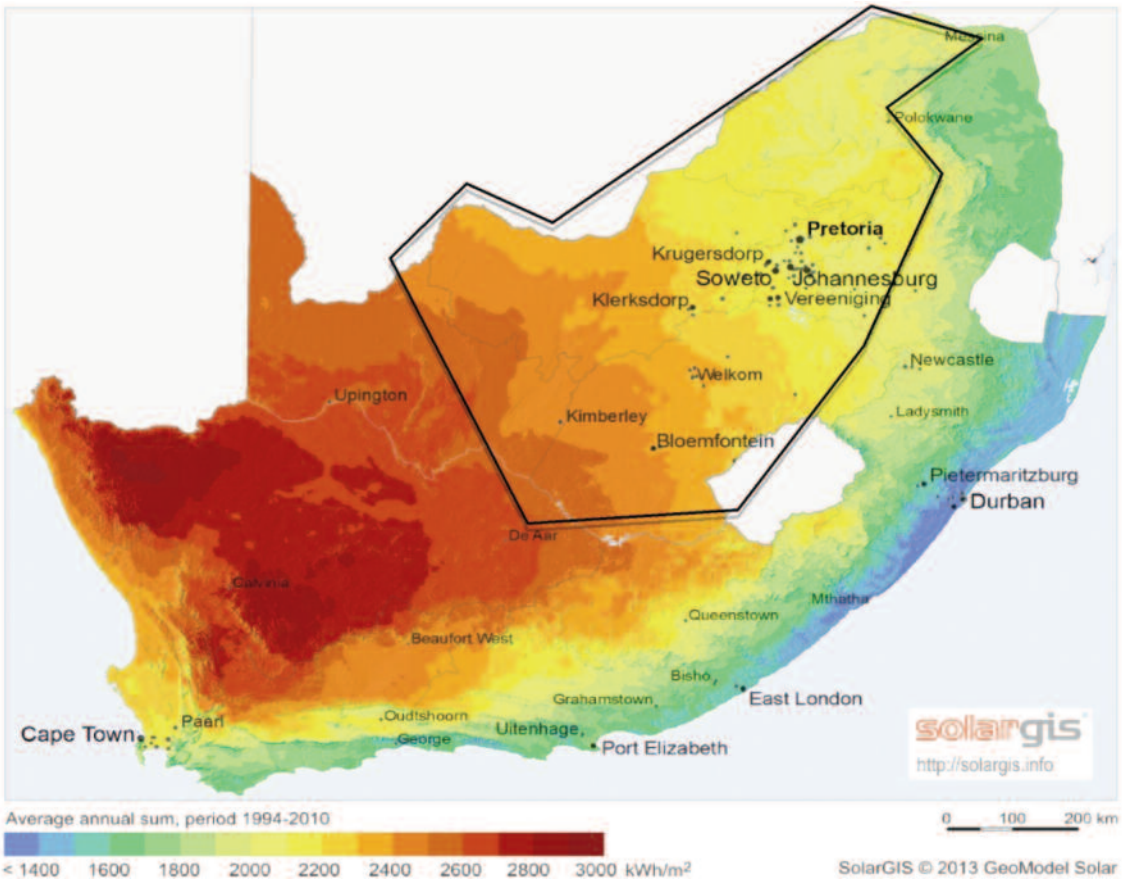

Figure 14: Solar resource quality across South Africa
Source: SolarGis (2013)

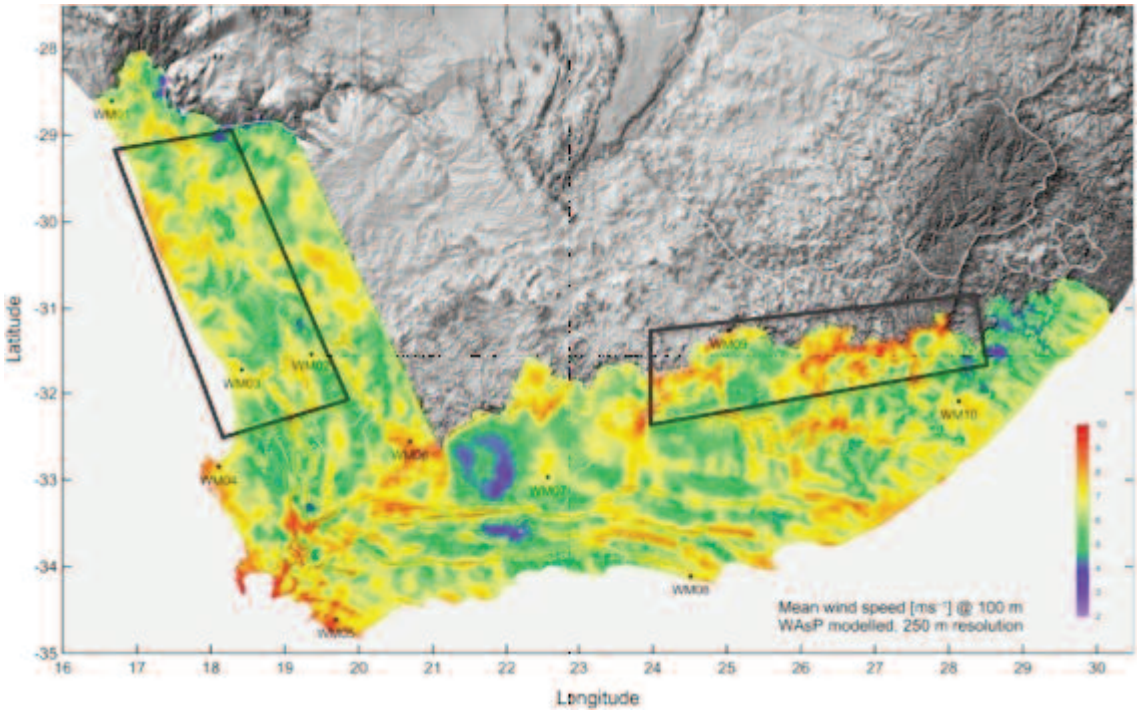

Figure 15: Wind resource quality in South Africa
Source: WASA (2014

sible companies are located in the country. Projects can be realised on a small-to-utility scale (IEA, 2014; SA Wind Energy Association, 2015).

Geothermal

For the data of this paper, only the 'hot dry rock' method was considered, because it has the highest potential for electricity generation and future development (IRENA, 2014; Geothermal Energy Association, 2013). No experience with mining operations could be identified (see Table 1). Figure 16 indicates the mining locations with the highest potential. In granite areas, 3 000 m to 5 000 m have to be drilled. The service infrastructure is limited, as there are no larger projects in the country. Projects can be realised on a small to utility scale (Tshibalo et al., 2015).

Biomass

The data for electricity generation with biomass focuses on the matured technologies, including direct combustion in stoker boilers, low-percentage co-firing, anaerobic digestion, municipal solid waste incineration, landfill gas, and combined heat and power (IRENA, 2015a). No experience with biomass electricity generation could be identified globally (see Table1). As can be seen in Figure 17, South Africa is a water-scarce country, which makes fuel availability medium with some potential in the north-east area. The service infrastructure is still a challenge, which lowers the reliability of the system and fuel supply (van Zyl, 2010; Bole-Rentel & Bruinsma, 2013; IRENA, 2012).

Battery storage

The data for lithium-ion and lead-acid batteries is presented, as cost and performance levels are improving, especially in comparison to sodium-sulphur batteries (IRENA, 2015b). Batteries can extend the capacity factors of non-baseload technologies, like solar PV and wind power (Dickens et al., 2014). Global experience is limited, with one operational project in Australia (see Table 1), as is service infrastructure. Two operational projects were identified with 10 kW and 20 kW (DOE, 2015; IRENA, 2015b).

Hydro power

The data represented for hydro power excludes pumped storage. At present, one project in Chile represents limited experience with mining (see Table 1). Figure 18 shows that power source availability, especially for micro projects, is moderate in south-western regions of South Africa. The service infrastructure is improving as more projects are being introduced, but it is still in its infancy. It is possible to realise projects on a small to utility scale (Klunne, 2012; Rycroft, 2014a). On-site executions are highly constrained, however, as the mining operation has to be close to the hydro facility.

3.3 Attractiveness business models

This section focuses on business models of renewable energy projects at mining operations, as initial expenses are considerably higher and the experience with present sources is well established. Table 3 provides a summary of the main organisations

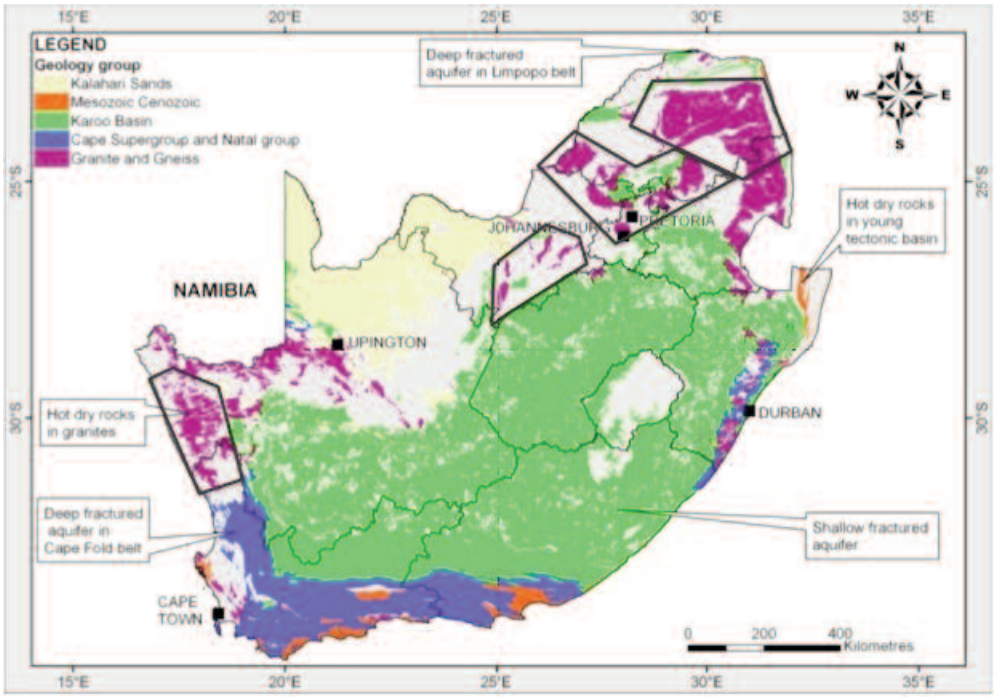

Figure 16: Geological map of South Africa
Source: Tshibalo et al. (2015)

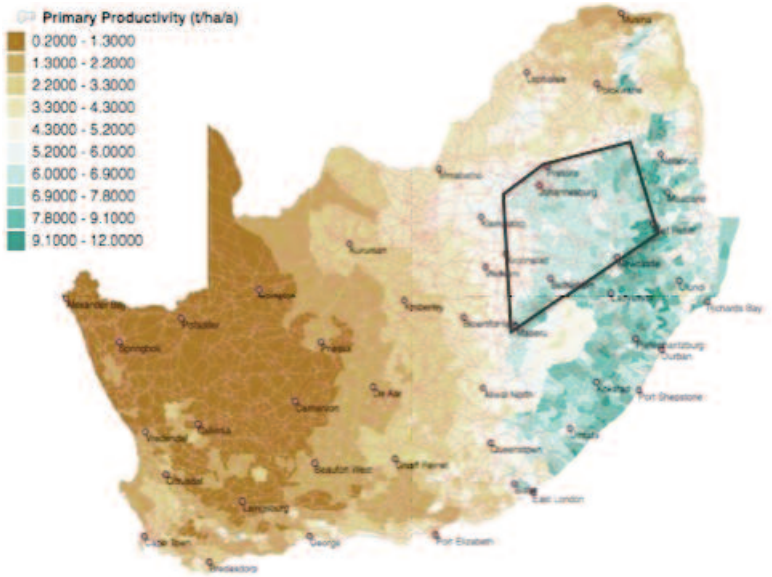

Figure 17: Net primary productivity of the land
Source: Schulze (2007)

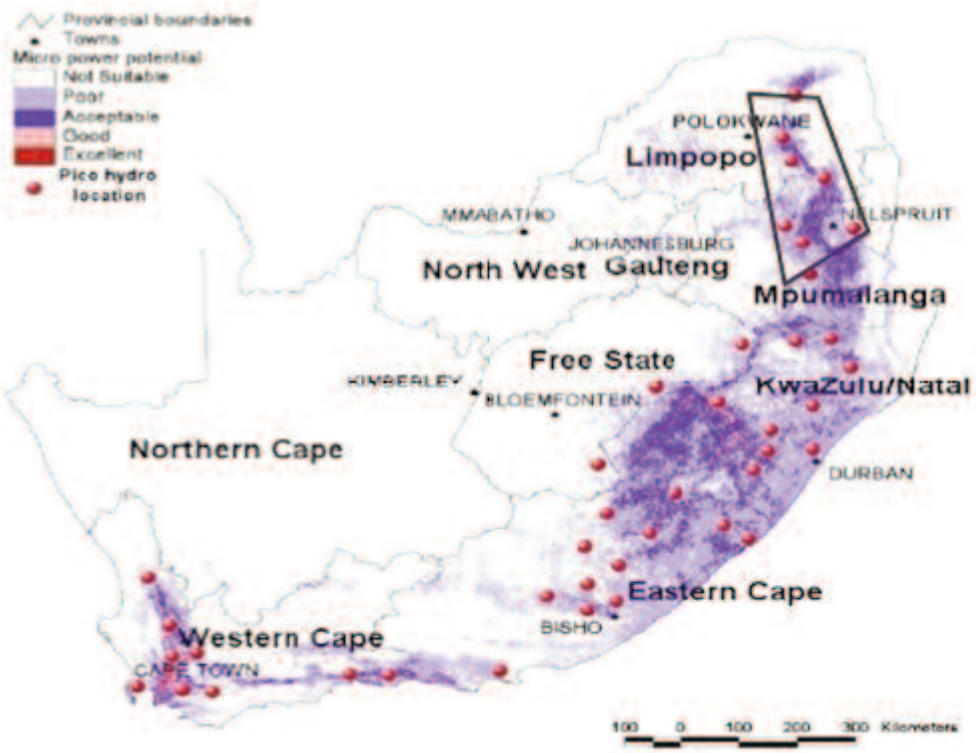

Figure 18: Hydro power potential
Source: Kusakana (2014)

and the regulatory and policy framework for renewable energy in South Africa.

In South Africa, the government is presently not supporting the implementation of off-grid industrial electricity generation from renewable sources. However, there are plans to implement subsidies until 2020 for solar photovoltaic electricity generation (Ahlfeldt, 2013).

This section discusses the attractiveness of the different business models for South African mining corporations to execute renewable energy projects. Business models entailing wheeling agreements with Eskom were not considered, as costs can add up to 18% to the kWh price (Rycroft, 2014b; Haw, 2013). The models investigated are self-generation, industrial pooling, net metering, and self-generation for powering townships (Boyse et al., 2014; GIZ, 2014; Banerjee et al., 2014):

Self-generation model

In the case of the self-generation model, the mining corporation develops a renewable generation

Table 3: Governmental and regulatory structure for renewable energy in South Africa
Source: Boyse et al. (2014); DoE (2015); Department of Environmental Affairs (2015)

Organisation	*Purpose*
Department of Energy	The governmental body in South Africa that is responsible for creating policies and strategies regarding energy production and administration.
Department of Environmental Affairs	The governmental body to ensure the protection of the environment and conservation of natural resources, in balance with a sustainable development of the country.
Energy Development Corporation	Governmental agency to support the development of renewable energy and alternative fuels through investment.
National Energy Regulator of South Africa	Regulating authority that supervises over the electricity supply industry.

Policy	*Purpose* ``	*Introduction*
White Paper on Energy Policy	General energy policy. Set goal of developing renewable energy by reforming fiscal, legislative and regulatory regimes.	1998, renewed 2009
White Paper on Renewable Energy	Laid the foundation for the widespread implementation of renewable energy, and set target of 10 000 GWh by 2013.	2003
National Cleaner Production Strategy	Framework (non-binding) to promote sustainable energy production and consumption across South African industries.	2004
Energy Act	Contained strategy for increased generation and consumption planning (renewable and conventional energy sources).	2009
Renewable Energy Feed-in Tariff programme	Set tariffs for wind, small hydro, concentrated solar, and landfill gas technologies. The tariffs were aligned with falling technology costs in 2011.	2009
Integrated Resource Plan	A national, long-term plan on electricity supply, based on nuclear power, coal and renewables. Total PV capacity goal is 8 400 MW. The REIPPP falls under this plan.	2010–2030
Renewable Energy Bids	Independent power producers bid for on-grid production capacity. In the first round (2012), 1 415 MW was allocated across concentrated solar PV, concentrated solar PV, and biogas.	2011

source to reduce electricity costs and to increase independence. Grid-connected mines use this model as a separate electricity source, which is only connected to the mine. It is possible to implement this model in two ways. The first is for the mine to develop, finance and operate the plant on its own land, using a subcontractor for the development. The second is to lease its own land to an independent power producer (IPP), who sells the electricity to the mine. The benefit of the self-generation model is that the smallest number of actors is involved, so that experts presently prefer it. The disadvantage is the high initial investment cost – which represents a shift from operating expenses (diesel fuel or Eskom electricity costs) to capital expenses (plant costs), making this model rewarding only in the long term. The risk for an IPP is the long-term commitment to only one client, the mine. Factors like changing commodity prices or operational expenses can lead, in the worst case, to the closure of a mine (Jamasmie, 2014).

Industrial pooling model
The industrial pooling model entails several corporations, with mining operations situated close to one another, forming a partnership to reduce electricity generation costs. The foundation of this model is the building of a consortium to enter a long-term power purchase agreement with shared renewable energy assets. As in previous models, the project can be realised by using combined financial investments and a subcontractor to build the plant. The plant would be situated on the land of one of the mining operations. Another option is to use an IPP. A mini-grid would be used to distribute the electricity. The advantage would be a lowering of the electricity costs as a result of a higher economy of scale than in the case of self-generation. The difficulty lies in the planning process of the model. Experience has shown that a joint capital investment of competitors is difficult to achieve, owing to different interests, diverse lifespans of the mines, and a lack of education about renewables.

Net metering model
The net metering model can only be implemented by grid-connected mines, which purchase electricity from the national supplier. Its purpose is to lower long-term electricity expenses, avoid potential electricity interruptions and use cleaner electricity. This model can be installed by the mine itself, using a subcontractor, or by an IPP. Eskom purchases the excess electricity produced by the renewable source. The benefit of the system is in gaining addi-

tional revenue for the operator of the system. In addition, no electricity is wasted, as all energy generated is used. The disadvantage of the model is that net metering is currently not formally supported by the regulatory framework in South Africa and is therefore not attractive.

Self-generation model for powering rural settlements

The self-generation model for powering rural settlements is especially for off-grid mines running on diesel generators. In this case, a rural settlement would be situated close to the mine. The community could be connected via a mini-grid through an own investment or an IPP. The outcome would be the reduction of electricity expenses for the mining corporation and rural electrification. The renewable electricity plant can be installed via a subcontractor, by the mine itself, or through an IPP. The neighbouring community would apply for government support to run a transmission line.

The advantage of the model is that selling the unused electricity to the community creates extra revenue – with the mine also contributing to one of the government target of expanding electrification. A difficulty presented by the model is the deviation of active mines from their core business. In addition, the process of obtaining the required permits from Eskom, NERSA and environment or land management offices is lengthy and difficult. The regulatory difficulties make this model unfeasible.

3.5 Carbon emissions tax

The South African government has announced its intention to launch a carbon emissions tax (Republic of South Africa, 2013). The bill is part of the commitment to reduce greenhouse gas emissions below business as usual by 34% by 2020 and 42% by 2025. The tax is planned to be introduced at a marginal rate of EUR 8.61 (ZAR 120) per ton of CO_2. Taking into account the listed tax-free threshold, the effective carbon tax rate will vary between EUR 0.43 (ZAR 6) and EUR 3.44 (ZAR 48) per tonne CO_2. All calculations are closely linked to the Department of Environmental Affair's mandatory reporting requirements. Entities will be liable for fossil fuel combustion emissions, industrial processes and product use emission, and fugitive emissions (National Treasury of South Africa, 2015; Swart, 2015).

According to the latest publication from the Treasury, the Draft Carbon Tax Bill includes the following features (National Treasury of South Africa, 2015):

1. Basic 60% tax-free threshold during the first phase of the carbon tax, from implementation date up to 2020.
2. Additional 10% tax-free allowance for process emissions.
3. Additional tax-free allowance for trade exposed sectors of up to 10%.
4. Recognition for early actions and/or efforts to reduce emissions that beat the industry average in the form of a tax-free allowance of up to 5%.
5. A carbon offsets tax-free allowance of 5–10%.
6. To recognise the role of carbon budgets, an additional 5% tax-free allowance for companies participating in phase 1 (up to 2020) of the carbon budgeting system.
7. The combined effect of all of the above tax-free thresholds will be capped at 95%.

There is, however, still much controversy about the actual design of the tax, the date of implementation and even if it will actually be implemented. A scenario analysis by Roger Baxter, CEO of the Chamber of Mines of South Africa (2015), offers two case scenarios of how the tax would affect two deep underground gold mines close to Johannesburg, owned by AngloGoldAshanti and SibanyeGold. The Sibanye case predicts a further 30% price increase from 2014 till 2017. The Anglo case forecasts its electricity tariff to increase from EUR 4.3 c/kWh in 2013 to EUR 10.9 c/kWh in 2020 (ZAR 60–152 c/kWh); without the tax an increase to EUR 10.4 c/kWh (ZAR145 c/kWh) is projected.

The treasury claims the tax will not affect the cost of Eskom electricity, as the utility might be excluded, or the existing environmental levy included in tariffs will be replaced by the tax. In addition, plans are still uncertain about a levy reduction and other 'revenue recycling' measures, which will be specifically aimed at not increasing costs in distressed sectors such as mining (Van Rensburg, 2015; Peyper, 2015; Dhawan, 2015; Seccombe, 2015).

4. Results and discussion

4.1 A possible fit of renewable sources to mining operations

Several renewable sources have half the levelised costs of diesel generators and are close to parity with Eskom, even without including forecast future price changes, which are also in favour of renewables. In the case of own investment, however, the disadvantage of renewables is the high initial capital expense, instead of current operational expenses. It can therefore be seen as an investment for long-term success.

The risk factor of high initial capital expenses, combined with limited global experience, necessitates the further education of decision-making leaders of mining corporations. The global renewable energy market only started to evolve in 2011, with the first and so far only project in South Africa being realised in 2012.

Most mines have a relatively constant baseload

consumption, so that, considering the intermittency of most renewable sources, it is only possible to use such sources in hybrid versions. For a mine that is not grid-connected, a hybrid version with the currently used diesel generator was identified as most promising, as storage facilitates are still too expensive.

4.2 Current attractiveness of different renewable sources

The renewable technology with the highest potential for the majority of mining corporations in South Africa is solar PV. Initial investment costs are low in comparison to other renewable energy technologies, besides wind power, but roughly three times the price of present sources. As stated before, however, current levelised costs are half the amount of diesel generators and close to parity with Eskom. The global experience in this market is the most highly established, with 11 projects, demonstrating the success of the model (Table 1). The availability of the power source is also the best compared to the other renewable technologies. Furthermore, owing to the numerous companies situated in South Africa, the service infrastructure is well developed. Wind energy is selected as the second-best option. The disadvantage, in comparison to solar PV, is the lower availability of the power source, which decreases the potential for on-site realisations. The third and last option selected for its potential is geothermal technology. Though the initial investment costs are high, the levelised costs are low. Disadvantages are that there is no experience with this technology within mining operations, service infrastructure is low, and the technology is relatively new, especially in South Africa. The geothermal option does, however, have the potential for a baseload source with a capacity factor of up to 90%. Solar PV and wind, on the other hand, have to be used as a hybrid version to achieve baseload characteristics.

All other renewable energy technologies were evaluated as unsuitable at the current state of development. The initial investment costs for CSP and battery storage are too high. There is no experience and a low service infrastructure with biomass. A combination of low power-source availability, little experience within mining operations, and a very young service infrastructure are the reasons for not selecting hydro power as an option.

4.3 Potential of different business models

The business model of self-generation is selected as the most attractive one in South Africa. The model entails the least actors, which simplifies the realisation process. As far as the regulatory framework is concerned, this is the most feasible option, as no additional organisations are involved or licences needed. Wheeling options were not considered, as additional costs are up to 18% of the electricity price and levelised costs of renewables are close to parity with Eskom. The option of using an IPP is limited, especially for smaller, remote mines. Some of the reasons are the elevated risk factor of international institutions investing in South Africa, the risk that the mine as the only customer may close down, and limited global experience with renewable projects at mining operations (Reeves, Whittaker & Ellinghaus, 2015; Baker & McKenzie, 2013).

4.4 Possible impact of the CO_2 tax

The planned South African CO_2 tax of EUR 8.61 (ZAR 120) with an actual effective impact of EUR 0.43–3.44 (ZAR 6–48) still involves a lot of controversy regarding its realisation and it is not yet certain if or when it will be implemented. A case study by two large mining corporations operating in South Africa states that the tax would spur their current negative economical development; the tax would, however, add to the attractiveness of renewable sources to reduce CO_2 emissions (Forer *et al*., 2014).

5. Conclusion

This paper set out to determine the influences shaping the market potential of renewable sources of electricity at mining operations in South Africa. It argued that the most attractive renewable electricity sources for the corporations are, in descending order of suitability, solar PV, on-shore wind, and geothermal technology. Owing to the electricity usage patterns of mining operations and the intermittency of, especially, solar PV and wind, a hybrid version with current sources must be used. To execute a project, the business model of self-generation was identified as the most promising, and can be realised through own investment or an IPP agreement.

The past and projected future economic situation of mining corporations operating in South Africa creates the opportunity for renewable electricity sources to contribute to their long-term success. The advantages would be greater independence from diesel and Eskom's electricity supply, lower electricity costs and reduced CO_2 emissions. Considering the shift from operational to capital expenses, however, there are some key challenges: firstly, the need to foster greater trust in investors so that power purchase agreement projects may be realised, and, secondly and of greater importance, the need to encourage further education for decision-making leaders of mining corporations so that they are able to understand the emerging opportunity presented by renewable electricity sources (Judd, 2014b). Further research should, therefore, be conducted to help these leaders to better understand the concept of renewable electricity in relation to their specific needs. Ideally, the research should

be conducted from the perspective of these mining leaders in order to make the knowledge more plausible and accessible. Possible strategic approaches that could add value and structure to the research are the multi criteria decision analysis methods, the strategic planning process, and Porter's value chain (Grant & Jordan, 2012; Hough et al., 2011).

Notes

1. The Energy Intensive User Group of Southern Africa (2014a) is a non-profit organisation whose members are energy-intensive consumers – of which 47% are involved in mining and quarrying.
2. efers to the amount of carbon dioxide gas (CO_2) that is emitted as a result of, among other things, the consumption of fossil fuels (Reddy & Jorgensen, 2014).
3. Summits of mining corporations and renewable energy companies started in 2013, to develop and discuss the market of renewables in mining operations (Energy and Mines, 2015).
4. For the purpose of this study the following exchange rates from the 13.07.2015 were used: EUR 1 = USD1.10 (CNN Money, 2015a); EUR 1 = ZAR 13.94 (CNN Money, 2015b).
5. This method considers the predicted lifetime-generated energy and estimates a price per unit of electricity produced (Branker et al., 2011). The different sources assumed: share of equity of 20–40%; share of debt of 60–80%; cost of capital of 8–10%; cost of debt of 6–8% and a lifespan of 20–25 years.

References

Abengoa Solar. 2015. Industrial installation of concentrating solar power in Chile. [Online]. Available: www.abengoasolar.com/web/en/nuestras_plantas/plantas_para_terceros/chile/index.html [2015, January 31].

Ahlfeldt, C. 2013. *The localisation potential of photovoltaic PV and a strategy to support large scale roll-out in South Africa*. South Africa: WWF, SAPVIA, Department of Trade and Industry, Pretoria.

Alton, T., Arndt, C., Davies, R., Hartley, F., Markrelov, K., Thurlow, J. & Ubogu, D. 2014. Introducing carbon taxes in South Africa. *Applied Energy* 116, March:344–354.

Ambros, D. 2014. *Project 'zimbi': PV/diesel hybrid power case study*. Final report. Unterhaching: Cronimet Power Solutions Gmbh.

Baker & McKenzie. 2013. *The future of clean energy in Africa*. Final report. Chicago: Green Energy Pipeline.

Banerjee, G.S., Romo, Z., McMahon, G., Toledano, P. & Robinson, P. 2014. The power of the mine: A transformative opportunity for sub-Saharan Africa. Final report. Washington D.C.: World Bank Group, ESMAP, Africa Region Sustainable Development.

Baxter, R. 2015. Presentation of Chamber position on carbon tax to the Davis Tax Committee. Johannesburg: Chamber of Mines of South Africa.

Beukman, H. 2015. Mineral sand resources. Presentation. Johannesburg: MSR.

Bole-Rentel, T. & Bruinsma, D. 2013. *The bioenergy sector in South Africa*. Den Haag: tbr Consulting, ECN, Bruinsma Solutions.

Boyse, F., Causevic, A., Duwe, E. & Orthofer, M. 2014. *Sunshine for mines: Implementing renewable energy for off-grid operations*. Washington, DC: Carbon War Room.

Branker, K., Pathak, M.J.M. & Pearce, J.M. 2011. A review of solar photovoltaic levelized cost of electricity. *Renewable and Sustainable Energy Reviews,* 159: 4470–4482.

Brodsky, S., Curnow, P., Fevre, M., Ghannam, M., Nasrollah, K. & O'Brien, J.P. 2013. *The future of clean energy in Africa*. Chicago: Baker & McKenzie.

Chamber Of Mines. 2014. *Facts and figures 2014*. Johannesburg: Chamber of Mines of South Africa.

Cornish, L. 2013. Energy management – delivering operational excellence. *Inside Mining* 61:60-61.

Creamer, T. 2012. Big users urge hard line on Eskom costs, as utility delays tariff submission. *Mining weekly.* Available at www.miningweekly.com/article/big-users-urge-hard-line-on-eskom-costs-as-utility-delays-tariff-submission-2012-08-31 [2015, January 26].

Crespo, T. 2015. Despite barriers to adopting, costs pressure driving renewed mining interest in renewable energy. Toronto: Energy and Mines.

Cronimet Power Solutions. 2015. Project Thabazimbi chromium mine. Available: www.crm-ps.com/en/thabazimbi.php [2015, January 30].

Department of Environmental Affairs. 2015. *Department of Environmental Affairs, Republic of South Africa*. Available: www.environment.gov.za [2015, April 6].

Dhawan, R. 2015. Carbon tax in the mining sector. *Business media live*. Available: www.businessmedialive.co.za/the-distributional-impacts-of-a-carbon-tax-in-the-mining-sector/. [2015, November 25].

Dickens, A., Singh, C., Bosset, P., Mitchell, V., Cosgrove, J., McLoughlin, S. & Cuadrado, P. 2014. *Energy storage: Power to the people*. London: HSBC Global Research.

Department of Energy. 2013. *Integrated resource plan for electricity IRP 2010–2030*. Johannesburg: Department of Energy, Republic of South Africa.

Department of Energy. 2015. Department of Energy, Republic of South Africa. Available: http://www.doe-irp.co.za [2015, April 6].

Department of Trade and Industry. 2015. *The wind energy industry localisation roadmap in support of large-scale roll-out in South Africa*. Johannesburg: Department of Trade and Industry, Republic of South Africa.

Deutsche Gesellschaft für Internationale Zusammenarbeit. 2014. *Alternative energy in mining*. Pretoria: German Cooperation; Deutsche Gesellschaft für Internationale Zusammenarbeit; South African Institute of International Affairs.

E-CL. 2015. E-CL and Quiborax to build solar PV plant. Available: www.e-cl.cl/prontus_ecl/site/artic/20130705/pags/20130705115312.php [2015, January 30].

Elliott, M. 2014. Business risks facing mining and metals. London: Ernst & Young Global Mining & Metals

Center.
Enercon. 2015. Windenergieanlagen. Available: http://www.enercon.de/de-de/windenergieanlagen.htm [2015, January 31].
Energy and Mines. 2015. Introduction to renewable energy with mining operations. Available: http://energyandmines.com [2015, March 17].
Energy Intensive User Group of Southern Africa. 2014b. *Electricity cost as a percentage of annual expenditure.* Available: www.eiug.org.za/about/membership/ [2014, December 27].
Eskom. 2010. *The energy efficiency series: Towards an energy efficiency mining sector.* Johannesburg: Eskom Demand Side Management Department.
Eskom. 2013. *Map of Eskom power stations*. Available: www.eskom.co.za/ Whatweredoing/ ElectricityGeneration/PowerStations/Pages/Map_Of_Eskom_Power_Stations.aspx [2015, April 4].
Eskom. 2014. *Environmental management*. Available: http://financialresults.co.za/ 2012/eskom_ar2012/fact-sheets/013.php. [2015, April 4].
Eskom. 2015a. *Transmission development plan 2015–2024*. Johannesburg: Eskom.
Fichtner. 2010. Technology assessment of CSP technologies for a site specific project in South Africa, final report. Johannesburg: The World Bank & ESMAP.
First Solar. 2015. Rio Tinto's project. Available: www.firstsolar.com/en/about-us/projects [2015, January 30].
Forer, G., Warren, B., O'Flynn, B., Elliott, M., Mitchell, P. & Downham, L. 2014. *Mining: The growing role of renewable energy*. London: Ernst & Young.
Fouché, N. 2013. Palabora mining company: The effect of power tariff increases. Management presentation. Phalaborwa: Palabora Mining Company.
Fraunhofer ISE. 2013. *Levelized cost of electricity: Renewable energy technologies*. Freiburg: Fraunhofer Institute for Solar Energy Systems.
Galaxy Resources. 2015. Mt Cattlin mining location. Available: www.galaxyresources.com.au/pro_raven_mt_cattlin.shtml [2015, January 31].
Gauché, P., Brent, A. & Von Backström, T.W. 2014. Concentrating solar power: Improving electricity cost and security of supply, and other economic benefits. *Development Southern Africa* 315:692–710.
Geothermal Energy Association. 2013. *Geothermal power: International market overview*. Washington D.C.: Geothermal Energy Association.
Gets, A. & Mhlanga, R. 2013. *Powering the future: Renewable energy roll-out in South Africa*. Johannesburg: Greenpeace South Africa.
Gielen, D. 2012. *Power sector costing study*. Abu Dhabi: International Renewable Energy Agency.
Glencore. 2015. Powering a mine on wind. Available: http://www.glencore. com/sustainability/case-studies/p/powering-a-mine-on-wind [2015, February 1].
Global Data. 2014. *Diesel generator market – global market size, equipment share and competitive analysis to 2020*. London: Global Data Research Institute.
Haw, H. 2013. *Overview of solar PV in South Africa*. Cape Town: South African Photovoltaic Industry Association.
Hinkley, J., Curtin, B., Hayward, J., Wonhas, A., Boyd, R., Grima, C., Tadros, A., Hall, R., Naicker, K. & Mikhail, A. 2011. *Concentrating solar power-drivers and opportunities for cost-competitive electricity*. Victoria: CSIRO.
International Energy Agency. 2011. *Geothermal heat and power roadmap*. Paris: International Energy Agency.
International Energy Agency. 2014. *Africa energy outlook: A focus on energy prospects in Sub-Saharan Africa.* Paris: International Energy Agency.
International Monetary Fund. 2014. *World economic outlook*. Washington D.C.: International Monetary Fund.
International Renewable Energy Agency. 2012. *Biomass for power generation*. Abu Dhabi: International Renewable Energy Agency.
International Renewable Energy Agency. 2013. *Hybrid power systems.* Abu Dhabi: International Renewable Energy Agency.
International Renewable Energy Agency. 2014. *Estimating the renewable energy potential in Africa: A GIS approach*. Bonn: International Renewable Energy Agency.
International Renewable Energy Agency. 2015a. *Renewable power generation costs in 2014*. Bonn: International Renewable Energy Agency.
International Renewable Energy Agency. 2015b. *Battery storage for renewables: Market status and technology outlook*. Bonn: International Renewable Energy Agency.
International Renewable Energy Agency. 2015c. *Africa power sector: Planning and prospects for renewable energy*. Bonn: International Renewable Energy Agency.
Jamasmie, C. 2014. Anglo American considers closing platinum mines in South Africa. *Mining.* Available: www.mining.com/anglo-american-considers-closing-platinum-mines-in-s-africa-98146/ [2015, April 6].
Judd, E. 2014a. Positioning mines to meet the mining industry's energy needs. Toronto: Energy and Mines.
Judd, E. 2014b. Sincerity and patience required for renewables in mining sector. Toronto: Energy and Mines.
Klein, S.J.W. & Whalley, S. 2015. Comparing the sustainability of U.S. electricity options through multi-criteria decision analysis. *Energy Policy* 79 April:127–149.
Klunne, W.J. 2012. Current status and future developments of small and micro hydro in Southern Africa. *Journal of Energy in Southern Africa* 243:14–25.
Kohler, M. 2014. Differential electricity pricing and energy efficiency in South Africa. *Energy* 641:524–532.
Kusakana, K. 2014. A survey of innovative technologies increasing the viability of micro-hydro power as a cost effective rural electrification option in South Africa. *Renewable and Sustainable Energy Reviews,* 37, September:370–379.
Lazard. 2014. *Levelized cost energy analysis – version 8.0*. New York: Lazard Asset Management.
Levesque, M., Millar, D. & Paraszczak, J. 2014. Energy and mining. *Journal of cleaner production* 84

(December):233-255.
Maasdam, R. 2015. Energy crisis – The case of South Africa. Johannesburg: Rabobank Economic Research Department.
MAKE Consulting. 2013. Global wind turbine trends 2012: Lowering the levelized cost of electricity. Aahhus: MAKE Consulting.
Mathews, E.H. 2005. Implementation of DSM strategies at the Kopanang Mine. *Journal of Energy in Southern Africa* 162:32-37.
Metric Conversion. 2015. Metric tons to ounces. Available: http://www.metric-conversions.org/weight/metric-tons-to-ounces.htm [2015, December 1].
Michigan State University. 2006. South Africa: Industrial areas, mines, and ports. Available: http://overcomingapartheid.msu.edu/image.php?id=65-254-103 [2015, April 3].
Mostert, M. 2014. A quantitative method for selecting renewable energy projects in the mining industry based on sustainability. Master's thesis, University of the Witwatersrand, Johannesburg, South Africa.
Mulaudzi, S.K., Muchie, M. & Makhado, R. 2012. Investigation of the solar energy production and contribution in South Africa. *African Jurnal of Science, Technology, Innovation and Development,* 44:233–254.
National Treasury of South Africa. 2015. *Publication of the Draft Carbon Tax Bill for public comment.* Pretoria: Department of National Treasury of South Africa.
Ngugi, P.K. 2012. What does geothermal cost? – the Kenya experience. El Salvador: United Nations University.
National Renewable Energy Laboratory. 2015. Concentrating solar power projects in South Africa. Colorado, USA: National Renewable Energy Laboratory.
Organisation for Economic Co-operation and Development. 2014. *Economic Outlook no 95 – long term baseline projections*. Paris: Organisation for Economic Co-operation and Development.
Organisation of the Petroleum Exporting Countries. 2014. *World Oil Outlook*. Vienna: Organisation of the Petroleum Exporting Countries.
Pattern Energy. 2015. *El Arrayán wind*. Available: http://patternenergy.com/ en/operations/projects/ el_arrayan [2015, January 30].
Petticrew, M. & Roberts, H. 2006. *Systematic reviews in the social science: A practical guide*. Oxford: Blackwell.
Peyper, L. 2015. Can a carbon tax still fly as SA mining sinks? *Miningmx,* 13 August. Available: www.miningmx.com/page/special_reports/mining-yearbook/mining-yearbook-2015/1653564-Can-a-carbon-tax-still-fly-as-SA-mining-sinks#.VlXD_LSZaI. [2015, November 25].
Rame Energy. 2014. Past projects. Available: www.rame-energy.com/ operations/past-projects [2015, January 30].
Reddy, V. & Jorgensen, P. 2014. Managing greenhouse gas emissions in mining: Opinion. *ReSource* 163:12–13.
Redevia. 2015. Mining location in Tanzania. Available: www.redaviasolar.com/mines [2015, January 31].
Rehman, S., Alam, M., Meyer, J.P. AND Al-Hadhrami, L.M. 2012. Feasibility study of a wind-pv-diesel hybrid power system for a village. *Renewable Energy* 38:258-268.
Reeves, R., Whittaker, S. & Ellinghaus, S.D. 2015. Conference Interview, 24 February. Johannesburg: Energy and Mining Summit.
Renewable Energy Resource Cooperation. 2014. Suriname solar project. Available: www.rerc.us/projects.htm [2015, January 30].
Republic of South Africa. 2013. *Reducing greenhouse gas emissions and facilitating the transition to a green economy*. Carbon Tax Policy Paper. Pretoria: National Treasury.
Rycroft, M. 2014a. The potential of small hydro power plants in southern Africa. *Energize* May 2014:18–22.
Rycroft, M. 2014b. Wheeling and dealing: Connecting electricity suppliers and customers. *Energize* April 2014:44–48.
Seccombe, A. 2015. Chamber of mines says carbon tax will damage industry. *Business Day,* 20 May. Available: www.bdlive.co.za/business/mining/2015/05/20/chamber-of-mines-says-carbon-tax-will-damage-industry [2015, November 25].
Schulze, R.E. 2007. Primary production, in R.E. Schulze ed. *South African atlas of climatology and agrohydrology*. Water Research Commission, Pretoria, RSA, WRC Report 1489/1/06, Section 14.1.
Société Nationale Industrielle et Minière de Mauritanie. 2013. Inauguration of SNIM's wind power plant. Available: http://www.snim.com/e/index.php/news-a-media/news/10-inauguration-of-snims-wind-power-plant.html [2015, February 1].
Soitec. 2015. Concentrix™ technology in action around the world. Available: www.soitec.com/en/products-and-services/solar-cpv/our-references [2015, February 1].
Solairedirect. 2012. The Dayton project. Available: www.solairedirect. com/international-presence/chile [2015, January 31].
SolarGis. 2013. Direct normal irradiation – South Africa. Available: http://solargis.info/doc/postermaps [2016, April 19].
Solarpack. 2012a. Calama solar 3 project. Available: www.solarpack. es/ing/calama.aspx [2015, January 30].
Solarpack. 2012b. Pozo Almonte solar project. Available: www.solarpack. es/ing/pozo-almonte.aspx [2015, January 31].
South African Photovoltaic Industry Association. 2013. *South Africa PV industry – overview*. Johannesburg: South African Photovoltaic Industry Association.
South African Wind Energy Association. 2015. *Wind industry growth.* Available: http://www.sawea.org.za/resource-library/useful-information/109-industry-growth.html [2015, March 25].
Statistics South Africa. 2015a. *Gross domestic product: Second quarter 2015*. Pretoria: Stats SA publications.
Statistics South Africa. 2015b. *Mining: Production and*

Sales, September 2015. [Online}. Available: www.statssa.gov.za/?page_id=1856&PPN=P2041&SCH=6230. [2015, November 15].
Stellar Energy. 2013. Barrick-Western power plant. Available: www. stellarenergy.com/case-studies/commercial-solar/commercial/item/barrick-western-power-plant.html [2015, January 31].
Sun Edison. 2013. Amanecer solar CAP. Available: www.sunedison.cl/chile [2015, January 31].
Swart. I. 2015 Draft Carbon Tax Bill released: South Africa moves to reduce greenhouse gas emissions. Johannesburg: Deloitte and Touche.
Toledano, P. 2012. Leveraging the mining industry's energy demand to improve host countries' power structure. Working paper. New York: Colombia University.
Tshibalo, A.E., Dhansay, T., Nyabeze, P., Chevallier, L., Musekiwa, C. & Olivier, J. 2015. Evaluation of the geothermal energy potential for South Africa. *Proceedings World Geothermal Congress 2015 Melbourne*. Johannesburg: University of South Africa.
Van Rensburg, D. 2015. Carbon tax? What carbon tax? *Fin24,* 8 November. Available: www.fin24.com/Economy/Carbon-tax-What-carbon-tax-20151106. [2015, November 25].
Van Staden, P. 2015. Energy management Sasol. Presentation. Johannesburg: Sasol.
Van Zyl, E. 2010. Bioenergy potential in sub-Saharan Africa. Stellenbosch: Stellenbosch University, Department of Microbiology.
Vergnet Wind Turbines. 2014. El Toqui. Available: www.vergnet.com/en/ centrale-eltoqui.php [2015, January 30].
WASA. 2014. Wind atlas for South Africa. Available: http://www.wasaproject.info [2015, April 2].
Wernecke, G. 2015. Senior Project Manager, Cronimet Mining Power Solutions SA. Johannesburg: Personal interview, [May, 6].
Williams, N.C. 2014. Demand reduction and responsive strategies for underground mining. PhD thesis, University of Exeter, Exeter, England.
Wirth, G. 2015. Technical manager at Cronimet Power Solutions. Unterhaching: Cronimet Power Solutions. Personal interview.
World Bank Group. 2015a. *Africa Power-Mining projects database.* Washington D.C.: World Bank Group.
World Bank Group. 2015b. *Commodity markets outlook.* Washington D.C.: World Bank Group.
World Bank Group. 2015c. *Economic data South Africa*. Available: http://data.worldbank.org/country/south-africa. [2015, November 13].
Wouter, F. 2014. Energy management AGA. Presentation. Johannesburg: AngloGold Ashanti.

Incorporating a three dimensional photovoltaic structure for optimum solar power generation – the effect of height

Olufunmilayo Alice Mafimidiwo

Akshay Kumar Saha*

School of Electrical, Electronic and Computer Engineering, University of KwaZulu-Natal, Durban

Abstract

In a renewable energy system, incorporating three-dimensional technology in solar power generation takes advantage of the three-dimensional nature of the biosphere so that energy collection occurs in a volume, contrary to what is commonly obtained in planar or flat photovoltaic panel. Three-dimensional photovoltaic technologies are capable of generating more power from the same base area when compared to the conventional flat solar panels. This investigation examines methodologies for computation and analyses the effect of height per unit volume compared with a plain surface arrangement. The results show remarkable increase in the energy generated by the three-dimensional photovoltaic structure over the two-dimensional planar structures.

Keywords: Three-dimensional technology, solar energy, height per unit volume, power output

Corresponding author. *Tel:* (+27) 031-260-2725; *Email:* saha@ukzn.ac.za

1. Introduction

Solar power is a major energy source, capable of making a substantial contribution to fulfilling the world's future energy requirements. According to literature, the average cost of commercial photovoltaic (PV) modules stands at an average of about USD 1.89–2.50 /Wp (Sahay et al., 2013; Candelise et al., 2013, May 2012; Bernardi et al., 2012; Gaudiana, 2010). A photovoltaic system is a method of converting solar energy or irradiation directly into useful energy with the use of an electronic device called a semiconductor (Usama et al., 2012). At present, PV energy costs less than 1% of what it used to be in the past. In spite of a substantial decline in PV system costs, however, the levelised cost of electricity (LCOE) of PV remains high. As at 2011, the LCOE for residential systems without storage and with assumption of a 10% cost of capital was in the range USD 0.25–0.65 /kWh. With the addition of electricity storage added, the cost range increases to USD 0.36–0.71/kWh. In 2011, for thin-film systems, the LCOE of current utility-scale was estimated to be between USD 0.26 and USD 0.59/kWh. The cost for the crystalline solar PV system is higher (Candelise et al., 2013). For the PV solar energy conversion technology to be affordable and for building-integrated photovoltaics (BiPV) technology to become economically attractive for building applications, this cost can be brought down to at most USD 1/Wp (Shaari, 1998). This can only be made possible if the appropriate solar energy conversion technology were employed (Suto and Yachi, 2011) and a solar incentive programme and net metering were implemented (United States Department of Energy [DoE], 2008). Different types of solar cells are available for use for energy conversion technology. However, crystalline silicon (Si) dominates around 90% of the current PV market (Ismail et al., 2013).

Convectional PV modules have relatively low energy density and this is worsened by the fact that

the output of the devices is dependent on the latitude of the installation and the weather conditions of the location; besides, the peak insolation hours available in most locations is limited (Bernardi, 2012; Aglietti *et al.*, 2008), In achieving the energy conversion target, the use of low-cost base material, optimal device design and affordable device processing technology are vital (Gharghi *et al.*, 2006b). Conventionally, for low-scale solar energy generation, flat PV panels are installed in residential and commercial rooftop installations. In cases where the rooftop is not adequate for use or the plants are too large for roof-mounting, solar modules can also be placed on the ground, either as a fixed mount or a tracking mount that follows the sun to orient the PV modules. Other options include mounting as structures that create covered parking or provide shade as window awnings. This is often used in multifamily or commercial applications (DoE, 2008). There is the need for establishing improved technology in order to optimise power generation per installation area. For more effective use of the sunlight energy, the number of hours the solar cells are in trajectory with the sun for peak power generation can be lengthened by incorporating sun-trackers (Mousazadeh *et al.*, 2009; Moradi & Reisi, 2011), although the tracking has the disadvantage of introducing additional costs. It also requires larger space for operation thereby causing interference with other panels and possible shading and is also subject to occasional maintenance and disruptions. Furthermore, it is not suitable for residential or commercial installations due to its bulky moving parts (Yahyavi *et al.*, 2010; Mafimidiwo & Saha, 2014). However, it is still being used for the fact that its price has reduced considerably (Philipps *et al.*, 2015). A tracking system can be more cost efficient if the cost of its tracker is less than total costs of that system by a factor of $(T_c - 1)/T_c$ where T_c is the tracking factor, which tends to unity as it improves the output power generated and this varies from location to location (Yahyavi *et al.*, 2010). In addition to this, it can generate more energy with fewer solar panels, lower electrical device ratings and a smaller structure on about the same land area (Yahyavi *et al.*, 2010; Philipps *et al.*, 2015). Nevertheless, there is a need for improved technology for solar energy optimisation.

2. Three-dimensional photovoltaic structure

Three-dimensional photovoltaic (3DPV) technology is a new technology in PV energy generation that mimics the pattern found in nature of structures that collect sunlight in three dimensions (Suto & Yachi, 2011; Gharghi *et al.*, 2006b; Yuji & Yachi, 2010). Three main physical reasons underlying the advantages of collecting light in 3D are the multiple orientations of the absorbers that allow for the effective capturing of off-peak sunlight, the avoidance of inter-cell shading, and the re-absorption of light reflected within the 3D structure (Suto & Yachi, 2011; Yahyavi *et al.*, 2010; Bernardi *et al.*, 2012). These benefits enable the measured generated energy densities (energy per base area) to be higher by a factor of 2–20 than the stationary flat PV panels. The 3DPV is a new approach for achieving optimum solar energy that will yield a cost-effective, more reliable and most economically friendly alternative energy source (Aglietti *et al.*, 2009; Bernardi *et al.*, 2012q; Yuji & Yachi, 2010).

The 3DPV technology utilises the 3D nature of the dimensional structures such as the spherical or cubic system to absorb power in the entire volume of that material. Hence, power is measured in Watts per unit volume as against per area measurement as in the planar or two-dimensional system. Furthermore, the impact of height in system efficiency for the 3DPV is remarkable (Aglietti *et al.*, 2009; Yahyavi *et al.*, 2010; Yuji & Yachi, 2010). Some of the research carried out on this technology is briefly discussed in this paper.

2.1 Solar energy generation in three dimensions

According to the Massachusetts Institute of Technology (Myers *et al.*, 2010), it has been established that 3DPV structures can increase the generated energy density in a linear proportion to the structure height, for a given day and location. The optimum shape of the 3D structures was derived using computer simulations such as genetic algorithms for optimising the generated output energy. These 3D structures include a cubic box open at the top, a funnel-shaped cubic box, a sphere, a parallelepiped, or any other 3D shape that in principle is found capable of doubling the daily energy density. The 3DPV structures were found to lessen some of the variability inherent in solar PV as they provide a more regular source of solar energy generation at all latitudes. They are found capable of doubling the number of peak power generation hours as they intensely reduce the seasonal, latitude and weather variations of solar energy generation when compared to a flat panel design (Bernardi *et al.*, 2012; Yahyavi *et al.*, 2010; Myers *et al.*, 2010).

2.2 The 3DPV module assembly by Fibonacci number

The 3DPV technology by Fibonacci number method involves the arrangement of the individual solar cells of the three-dimensional PV module in a leaf-like manner. The arrangement revealed that such a modular design has the benefits of having each solar cell receive the reflected light from the other cells, thereby maximising power generation per installation area (Myers *et al.*, 2010) It also enables solar cells to be stacked in a vertical configuration, which enhances the doubling of daily ener-

gy density (Yuji & Yachi, 2010; Yahyavi et al., 2010).

2.3 Fibonacci number composition for output power characteristics of a 3DPV module

Another research group carried out a test on a 3DPV module whose configuration was based on Fibonacci numbers (Suzumoto et al., 2012; Yuji & Yachi, 2010; Suto & Yachi, 2011). The simulation results revealed that the power generation characteristics of the solar cells depend on the shape and spacing of the solar cells for the most effective use of sunlight energy.

2.4 Spherical silicon solar technology

Accurate 3D technology was found to enable innovative and improved device design, which can result in overall cost effectiveness, improved material processing and system utilisation (Gharghi et al., 2006b, Szlufcik et al., 1997). Of particular interest is the spherical silicon solar technology, which was found to be attractive, ideal and quite inexpensive. It utilises low-cost silicon feedstock for its fabrication process, which is found to be simple and inexpensive (Gharghi et al., 2006a). In addition, self-supporting 3D shapes are discovered to create new schemes for PV installation and increase energy density that can facilitate the use of inexpensive thin film materials in area-limited applications. Hence, harnessing solar energy in three dimensions can open new avenues towards Terawatt-scale generation (Bernardi et al., 2012).

2.5 3D nanopillar-based cell modules

In recent years, much progress has been made in developing PV that can potentially be mass deployed (Fan et al., 2009). An example is 3D nanopillar-based cell modules which were used for the purpose of reducing solar cell cost by utilising novel device structures and materials processing to yield acceptable efficiencies. In this regard, the highly regular, single-crystalline nanopillar arrays of optically active semiconductors are directly grown on aluminium substrates, which are configured as solar modules. An example is the CdTe/CdS PV structure that incorporates 3D, single-crystalline *n*-CdS nanopillars, which is embedded in polycrystalline thin films of *p*-CdTe, to enable high absorption of light and efficient collection of the carriers. The cadmium sulphide cell (CdS) and cadmium telluride cell (CdTe) are chemically different semiconductors with different bandgaps and doping or conductivity type. They form a good pair CdTe/CdS as one of the topmost successful heterojunction for PV applications to overcome the problem of poor junction formation. The prefix n or p attached to each semiconductor indicates the type of doping that is given to it, or it indicates its conductivity type (Green, 2015). Various experiments and modelling exercises proved the potency arising from the geometric configuration of this approach to enable enhanced carrier collection efficiency on both rigid and flexible substrates of the highly versatile nanopillars solar modules (Fan et al., 2009).

3. Effect of height in the Fibonacci method of 3DPV generation

The Fibonacci method of PV module (FPM) installation utilises numbers to attain the height spacing for volumetric adsorption of solar irradiation to optimise solar power generation in an area (Suto and Yachi, 2011, Yuji and Yachi, 2010, Seiji Suzumoto1, 2012). The manifestations of the Fibonacci numbers and the golden ratio are apparently endless and can be found throughout nature in the form and designs of many plants and animals (Grigas, 2013; Koshy, 2011). The Fibonacci sequence can be perceived in nature in the spirals of a sunflower's seeds and the shape of a snail's shell (Grigas, 2013). These numbers have also long been used in various manners in architecture, art and music as well as medicine, science and engineering. In particular, the numbers are widely used in engineering applications including computer data structures and sorting algorithms, financial engineering, audio compression, architectural engineering and solar energy application (Zou et al., 2004; Belegundu & Chandrupatla, 2011; Stakhov, 2005; Koshy, 2011). The numbers highlight the order and mathematical complexity of the natural world (Grigas, 2013). They are present in the leaf or petal arrangement of most plants as shown in Figure 1, frequently in order to maximise the amount of light received on the space allotted for each leaf or petal on the plant (Mafimidiwo & Saha, 2014; Gharghi et al., 2006b; Yuji & Yachi, 2010).

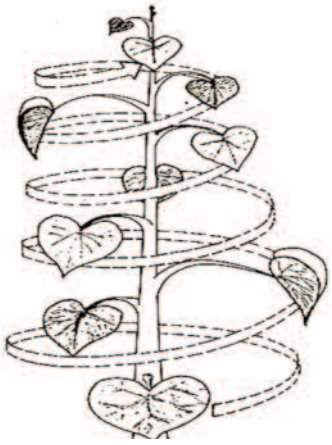

Figure 1. Leaf arrangement on plants by phyllotaxis
Source: Grigas (2013)

In a similar fashion, a mass of silicon with an expanded surface can absorb the solar radiation in layers of its crystallised molecules (Grigas, 2013). Conversely, the leaves are not usually arranged on

a flat surface, but spread through the whole volume of a plant. This is analogous to the reason why trees tend to grow vertically – to access most of the solar rays in a given volume. Solar panels can be arranged in a similar fashion and the solar energy considered in terms of Watt-hours per unit volume. To install PV panels on a tall structure is, however more time-consuming and costly than laying them on the ground (Yahyavi *et* al., 2010). However, depending on the price of land, arranging the solar equipment on a raised structure could be more cost-effective. Another advantage of a vertical arrangement is the possibility of rotating Fibonacci solar panels in order to track the sun for a higher efficiency (Aglietti *et* al., 2009; Suto & Yachi, 2011: Gharghi *et* al., 2006b).

Although 3DPV solar power installations are not common, one such installation, using a FPM approach, exists in Ontario, Canada as shown in Figure 2. The solar-powered tree of about 0.5 kW is installed at Tourism London, Wellington Rd, Ontario Canada and it is funded by the Ontario Power Authority (City of London, 2014). It is 7 m tall and has 27 leaves, each producing power.

Figure 2: A 500 W solar-powered tree at Tourism London, Ontario Canada
Source: City of London (2014)

4. 3DPV structure effect on solar radiation intensity

The generated solar energy density is a function of the solar intensity called irradiance, which is measured in W/m^2 (Boyd, 2013). Many parameters determine the intensity of solar radiation, including latitude, season, altitude, geographical conditions, atmospheric pressure, humidity, time of day, and some other extra-terrestrial effects such as solar storms. On a clear day, the intensity of solar radiation is at its maximum around noon and decreases towards dusk (Bernardi *et* al., 2012). However, the 3DPV structure was found to nearly double the number of peak hours available for solar energy generation and provide a measured increase in the energy density by a factor of about 2–20 without the use of sun-tracking in cloudy weather (Myers *et* al., 2010). The structure is also found to be able to reduce the large variability in solar energy generation with latitude and season, contrary to what is obtained in the case of planar solar configuration (Suto & Yachi, 2011; Yahyavi *et* al., 2010; Yuji & Yachi, 2010; Grigas, 2013). The solar radiation received on the surface of the material is proportional to the power absorbed in the entire volume of the 3DPV structure.

4.1 Energy per unit volume

Generally, some level of physical mass is required for energy of any sort to be absorbed and this energy is found to be proportional to the volume and density of that material (Suto & Yachi, 2011; Yahyavi *et* al., 2010; Bernardi *et* al., 2012). Mathematically, the material surface is two-dimensional, while the physical objects are three-dimensional (Yahyavi *et* al., 2010). It is proper to consider energy in the volume, as well as energy on the surface, in the context of solar energy (Yuji & Yachi, 2010). For energy per unit volume consideration, it is assumed that some solar collectors are effectively arranged within any three dimensional structure such as a cube with arbitrary dimensions *f, g, h* facing northerly with the *x, y, z*-axes (Myers *et* al., 2010). Hence, the cube volume, *V*, is also considered as a vector *V* with three assigned components, as in Equation 1:

$$\begin{cases} V_x = gh \\ V_y = fh \\ V_z = fg \end{cases} \quad (1)$$

These components are assumed to be proportional to the cube's three faces on which the solar beams radiate on the top, front and east or west at any given time.

The solar irradiance is considered a vector with variable components proportional to the absolute values of *x, y, z* components. Hence, solar power, *P*, going into the cube as indicated earlier can be extended and interpreted as the scalar product of the volume and irradiance vectors.

5. Methodology

In order to analyse the energy absorbed by the cube, this investigation considered the cube volume and the vector components of the surfaces as shown in Figure 3, with dimensions *f, g, h* standing northwest with the *x, y, z* – axes. As stated in section 4, the cube volume, V, was considered a vector $\underline{V}$, with three components as given in Equation 1. These components of the volume vector were exposed to the solar beam radiation. It was also considered that the solar irradiance is also a vector, with variable components proportional to the absolute values of *x, y, z* given by Equation 1. The implication of this would be that the solar power going

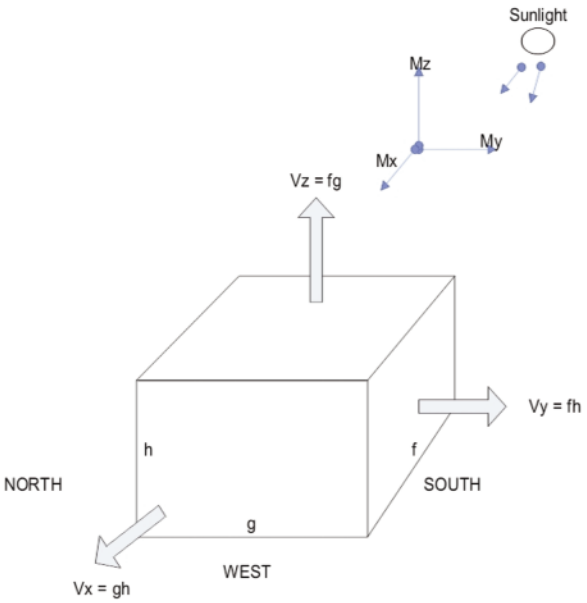

Figure 3: Solar irradiance components to a cube

Source: Yahyavi et al. (2010)

into the cube of a solar tree can be expressed as a scalar product.

Hence,

$$P = \underline{V}.\underline{I} \tag{2}$$

where:

$$P_x = ghl\,[Cos(\beta)(\theta)]$$

$$P_y = fhl[Sin(\alpha)Sin(\beta)Cos(\theta) - Cos(\alpha)Sin(\theta)],$$

and Pz is given by Equation 3

$$P_z = fgl[Cos(\alpha)Sin(\beta)Cos(\theta) + Sin(\alpha)Sin(\theta)] \tag{3}$$

Total power is the vectorial sum of the components as shown by Equation 4:

$$P_{Tot} = P_x + P_y + P_z \tag{4}$$

The value of irradiance and the angles β and θ are functions of time as described by (Kenny et al., 2006, Yahyavi et al., 2010). The module of irradiance *M*, which is defined as the average irradiance in any location at a certain latitude α, is introduced in Equation 5. For the purpose of computation, the *M* value applied here is taken as 62% for location latitude of -29.8833 (South).

Then,

$$Avg[Cos(\beta)Cos(\theta)] = Avg[Sin(\beta)Cos(\theta) = 0.62$$

$$Avg[Sin(\beta)] = 0 \text{ and } f, g, h = 1$$

The module of irradiance for Durban is assumed here as 0.62 for the month of January and it is utilised here as a parameter of average irradiance at the latitude (α) -29.8833 (South). This is specified by the three components, including Equation 5.

$$Mx = 0.621$$

$$My = 0.621Sin(\alpha)$$

$$Mz = 0.621Cos(\alpha)$$

and

$$M = M_x + M_y + M_z \tag{5}$$

The average value of available solar power obtained within the volume is the scalar product of volume vector *V* and module of irradiance, *M* as indicated in Equation 6:

$$P_{Avg} = V \,.\, M \tag{6}$$

Hence, Equation 7 with its associated components and Equation 8 are derived.

$$P_{Avg} = \begin{cases} P_{x\text{-}Avg} = ghlMx \\ P_{y\text{-}Avg} = fhlMy \\ P_{z\text{-}Avg} = fglMx \end{cases} \tag{7}$$

and

$$PTot\text{–}Avg = P_{x\text{-}Avg} + P_{y\text{-}Avg} + P_{z\text{-}Avg} \tag{8}$$

Dimensions f, g, h in these equations are the effective dimensions where 100% of the solar energy is absorbed. However, real dimensions of the occupied space are '*n*' times larger; and *n* relates to the efficiency η of the collectors. The efficiency of the PV panels is assumed to be 16%, therefore, *n* is 2.5 in this case. This was found useful in the optimisation computations carried out on these two different solar panels installation configurations.

A solar power system can be more efficient depending on how it collects solar energy. In order to determine the solar irradiance in volume, it was assumed the solar panel was effectively arranged within a cube as shown in Figure 4. From Equation 4, more energy could enter a volume as compared with entering through a surface such that:

$$(P_{Tot} > P_x, P_y, P_z) \tag{9}$$

The main concept of measuring energy per unit volume is that solar collectors get more irradiance when elevated from the horizontal position as shown in Figure 5 to the vertical position as shown in Figure 4.

The solar cell efficiency depends on the collec-

tivity factor c, defined as the ratio of the collected solar energy to the maximum solar energy available in an effective volume occupied by the solar system installed in an area and at a certain height. The amount of solar energy generated is a function of the collectivity factor and this was found to be in direct proportion with height.

5.1 Computation of solar energy in 3D and 2D

In this investigation, computation of solar energy in 2D and 3D was made with comparison between the results obtained on the power (Watts) generated with the tree-level arrangement (3D) in Figure 4 and power (Watts) generated by its equivalent co-planer arrangement (2D) in Figure 5 and the data was made using Matlab program, version R2012b. Analysis of results is presented according to Figures 6, 7 and 8.

5.2 The 3D configuration of the solar panel

In order to estimate the effect of height, the solar panel was configured in 3D and a 10 kW solar array was assumed for the multilevel fixed structure as shown in Figure 4. The effective volume dimensions occupied by the tree-level system were assumed to be $f = 3.5$; $g = 2.5$; and $h = 3$ m. The index of the real dimensions of the occupied space by the PV panel n was assumed to be 2.5, the assumed irradiation I, was 678 W/m^2 for the solar panels installed at a tilted angle of towards South.

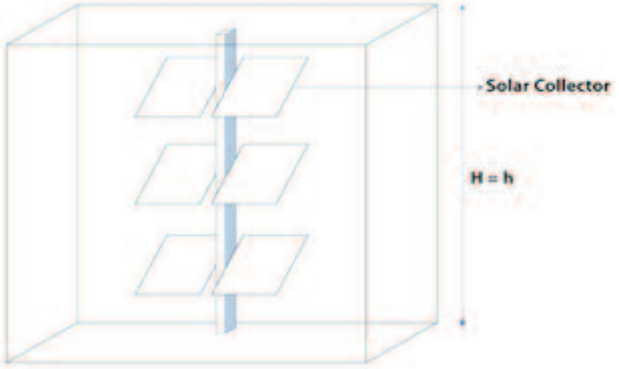

Figure 4: Multilevel panels arranged as a volume

From Equation 5, the modules of irradiance of the solar radiation for the 3D and 2D structures were determined for this location and expressed as Equation 10:

$$M_x = 420\ W/m^2,\ M_x = 292\ W/m^2 \text{ and } M_x = 302\ W/m^2 \quad (10)$$

These values were used for modules of irradiance in the Matlab computations as in Equation 11 and associated components.

$$\begin{cases} P_{x\text{-}Avg} = ghM_x = 0.62ghl \\ P_{y\text{-}Avg} = fhM_y = 0.62fhlSin(\alpha) \\ P_{z\text{-}Avg} = fgM_z = 0.62fglCos(\alpha) \end{cases} \quad (11)$$

5.3 The 2D configuration of the solar panel

It was assumed that the elevation, for the 2D arrangement is one-third of the height h, for the 3D structure. In the 2D arrangement, not all the sides were present (as shown in Figure 5), hence only the front and the pop would receive the solar radiation.

Figure 5: Planar (2D) arrangement of solar panels

Consequently, for the 2D arrangement the average total power in Watts was estimated as according to Equation 12:

$$P_{Tot\text{-}Avg} = P_{y\text{-}Avg} + P_{z\text{-}Avg} \quad (12)$$

where:

$$P_{y\text{-}Avg} = fhM_y = +0.62fhlSin(\alpha)$$

$$P_{z\text{-}Avg} = fgM_z = +0.62fhlCos(\alpha) \quad (13)$$

$$H = 1/3h \quad (14)$$

6. Results and discussion

The variables derived for the solar power in equations 4, 7 and 11 were used to determine generated powers for the 2D and 3D solar structures for height variation of 1 to 6 m. The values are presented in Table 1. The linear appearance of results in Figures 6–7, obtained in 2D and 3D cases was caused by the effects of other factors such as weather, while seasonal variations such as cloud and rain and temperature were not considered, for simplification.

Table 1 shows that, at the height of 1 m, the 2D and 3D solar structures generated output power of 2.983 kW and 4.714 kW respectively, corroborated by Figures 6 and 7, while at the height of 6 m, the 2D and 3D generated output power of 4.686 kW and 15.08 kW respectively, as supported by Figure 8. The percentage increase in the output power between the 2D and 3D solar structures was from 37% to 69% from the minimum height of 1 m to the maximum height of 6 m, respectively. Consequently, power generation in 3D installation got improved with increasing height.

The existence of a linear relationship between solar generated energy and the generated output power substantiated an increase in solar energy

Table 1: Power output values for the 2D and 3D solar installations

Parameter	*Values*					
Height h (m)	1.000	2.000	3.000	4.000	5.000	6.000
Power (2D) kW	2.983	3.324	3.665	4.005	4.345	4.686
Power (3D) kW	4.714	6.786	8.859	10.93	13.00	15.08

generated with increasing height. A solar farm with multiple trees may, however, give different results because of the shading effect from adjacent trees hindering the absorption of the reflected rays by the PV cells, causing a reduction in the generated output power. In order to avoid excessive partial shading of the elements, the solar trees would need to be installed with a relatively large spacing. A new set of equations would therefore be required to accommodate these changes (Sampatakos, 2014).

Figure 6: Energy optimisation by area in a

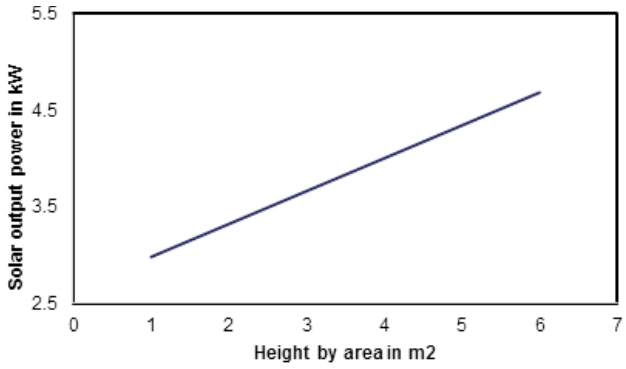

planar system

Figure 7: Energy optimisation by volume in a

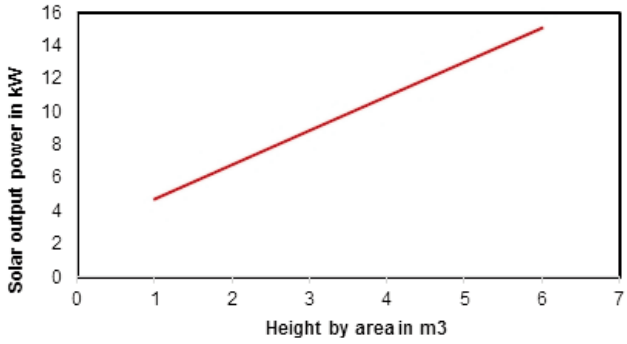

3DPV system

Figure 8: Energy optimisation by volume in a

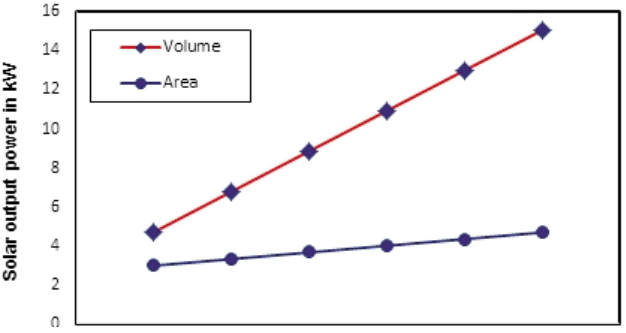

3DPV and by area in a planar system

7. Conclusions

In this investigation, the effects of height on solar generated energy and power were analysed and discussed. All other variable parameters, such as weather conditions and time of the day, were not considered. The concept of energy-per-unit volume for solar energy for solar installation with consideration for height was corroborated by the results. The Module of Irradiance was found to be a simple and useful tool for establishing the per-unit component for the top, front, and the side surfaces of the irradiance into a unit volume. There was an enhanced power output with the use of the Module of Irradiance. The relationship between generated power by volume for the 3DPV system and the generated power by area for the planar system was found to be linear. The power generated by the 3DPV structure over the planar structure increased by 16%. Consequently, the introduction of height to solar power installation increases the performance of the solar device. However, in situations where more than one tree is used, different results might be obtained because of the tendency to experience uneven illumination of solar panels caused by overlapping shades of solar cells. This is a different possible scenario outside this study.

References

Aglietti, G. S., Redi, S., Tatnall, A. R. and Markvart, T., 2008. High altitude electrical power generation. *WSEAS Transactions on Environment and Development* 4**:**1067-1077.

Aglietti, G. S., Redi, S., Tatnall, A. R. and Markvart, T. 2009. Harnessing high-altitude solar power. *IEEE Transactions on Energy Conversion, ,* 24(2)**:**442-451.

Belegundu, A. D., Chandrupatla, T. R. 2011. *Optimization concepts and applications in engineering.* Cambridge: Cambridge University Press.

Bernardi, M., Ferralis, N., Wan, J. H., Villalon, R. and Grossman, J. C., 2012. Solar energy generation in three dimensions. *Energy and EnvironmentalSscience* 5(5)**:**6880-6884.

Boyd, M. 2013. Analytical model for solar irradiance near a planar vertical diffuse reflector: Formulation, validation, and simulations. *Solar Energy* 91**:**79-92.

Candelise, C., Winskel, M. and Gross, R.J., 2013. The dynamics of solar PV costs and prices as a challenge for technology forecasting. *Renewable and Sustainable Energy Reviews 26*: 96-107.

City of London. 2014. Corporate energy conservation and demand management (CDM) Plan. Available:

http://www.london.ca/residents/Environment/Energy/Documents/2014%20CDM%20Plan%20final.pdf [19 April 2016].

Fan, Z., Razavi, H., Do, J.-W., Moriwaki, A., Ergen, O., Chueh, Y.-L., Leu, P. W., Ho, J. C., Takahashi, T., Reichertz, L. A., Neale, S., Yu, K., Wu, M., Ager, J. W. and Javey, A. 2009. Three-dimensional nanopillar-array photovoltaics on low-cost and flexible substrates. *Nature Materials* 8:648–653.

Gharghi, M., Bai, H., Stevens, G. & Sivoththaman, S. 2006. Three-dimensional modeling and simulation of pn junction spherical silicon solar cells. *IEEE Transactions on Electron Devices*, 53(6) **:**1355–1363.

Green, M. A. and Archer, D. A., 2015. *Clean electricity from photovoltaics*. London: Imperial College Press.

Grigas, A., 2013. The Fibonacci Sequence: Its history, significance, and manifestations in nature. Senior Honours thesis, Liberty University, Virginia, USA.

Ismail, H., Mathew, S., Aloka, S., Narayanaswamy, B., Ming, L.C. and Hussain, S.A., 2013. Comparative performance of grid integrated solar photovoltaic systems under the tropical environment. In *Innovative Smart Grid Technologies-Asia (ISGT Asia), 2013 IEEE:*1-6.

Kenny, R. P., Huld, T. A. and Iglesias, S. 2006. Energy rating of PV modules based on PVGIS irradiance and temperature database. *Proceedings of 21st European Photovoltaic Solar Energy Conference and Exhibition, 2006:4-8*.

Koshy, T., 2011. *Fibonacci and Lucas numbers with applications*, John Wiley & Sons.

Mafimidiwo, O. A. and Saha, A. K. 2014. Improving solar energy generation through the use of three dimensional photovoltaics technology. *Proceedings of the Southern African Universities Power Engineering Conference.* University of KwaZulu-Natal, Howard Campus, Durban South Africa: 294-300.

Moradi, M. H. and Reisi, A. R. 2011. A hybrid maximum power point tracking method for photovoltaic systems. *Solar Energy,* 85(11)**:**2965–2976.

Mousazadeh, H., Keyhani, A., Javadi, A., Mobli, H., Abrinia, K. and Sharifi, A., 2009. A review of principle and sun-tracking methods for maximizing solar systems output. *Renewable and sustainable energy reviews* 13(8):1800-1818.

Myers, B., Bernardi, M. and Grossman, J. C., 2010. Three-dimensional photovoltaics. *Applied Physics Letters,* 96(7):071902.

Philipps, S., Bett, A., Horowitz, K. and Kurtz, S. 2015. Current status of concentrator photovoltaic (CPV) technology. *National Renewable Energy Laboratory, Golden, Colorado, USA.*

Russell, G. 2010. Third-generation photovoltaic technology – The potential for low-cost solar energy conversion. Letter to *Journal of physical chemistry* 2010(1):1288-1289.

Sahay, A., Sethi, V. and Tiwari, A., 2013. A comparative study of attributes of thin film and crystalline photovoltaic cells. *International Journal of Mechanical, Civil, Automobile and Production Engineering* 3(7):267–270.

Sampatakos, D. 2014. Development of three dimensional PV structures as shading devices for a decentralized facade unit of the future. TU Delft, Delft University of Technology.

Suzumoto, S., Tayo, L. and Yachi, T., 2012. Output power characteristics of a three-dimensional photovoltaic module using fibonacci number composition. In *IEEE 34th International Telecommunications Energy Conference:*1-7.

Shaari, S. 1998. Photovoltaics in the built environment: an application for Malaysia. Dissertation for De Montfort University, Leicester. Available: https://www.dora.dmu.ac.uk/handle/2086/4157.

Stakhov, A. 2005. The generalized principle of the golden section and its applications in mathematics, science, and engineering. *Chaos, Solitons & Fractals* 26**:**263–289.

Suto, T., Yachi, T. 2011. Power-generation characteristics of an FPM by simulation with shadow-effect analysis. *37th IEEE Photovoltaic Specialists Conference, 19-24 June 2011*.

Szlufcik, J., Sivoththaman, S., Nlis, J., Mertens, R. P. and Van Overstraeten, R. 1997. Low-cost industrial technologies of crystalline silicon solar cells. *Proceedings of the IEEE* 85**:**711–730.

United States Department of Energy. 2008. Energy efficiency and renewable energy. Available: www. fueleconomy.gov/feg/byfueltype.htm.

Usama, S. M., Arif, A. F. M., Kelley, L. and Dubowsky, S. 2012. Three-dimensional thermal modeling of a photovoltaic module under varying conditions. *Solar energy* 86**:** 2620–2631.

Yahyavi, M., Vaziri, M. and Vadhva, S. Solar energy in a volume and efficiency in solar power generation. In *IEEE International Conference on Information Reuse and Integration*:394-399.

Yahyavi, M., Vaziri, M. and Vadhva, S., 2010. Solar energy in a volume and efficiency in solar power generation. Available: http://ieeexplore.ieee.org/stamp/stamp.jsp?tp=&arnumber=5558900.

Yuji, A. and Yachi, T. 2010. A novel photovoltaic module assembled three-dimensional. *35th IEEE Photovoltaic Specialists Conference, 20-25 June 2010*.

Zou, J., Ward, R. K. and Qi, D. 2004. A new digital image scrambling method based on Fibonacci numbers. *Proceedings of the 2004 International Symposium on Circuits and Systems* (Vol. 3). DOI: 10.1109/ISCAS.2004.1328909

Experimental investigation on heat extraction from a rock bed heat storage system for high temperature applications

Denis Okello [*1]

Ole J. Nydal[2]

Karidewa Nyeinga[1]

Eldad J. K. Banda[1]

1 *Department of Physics, Makerere University, PO Box 7062, Kampala, Uganda*
2 *Department of Energy and Process Engineering, Norwegian University of Science and Technology, PO Box 7491, Trondheim, Norway*

Abstract
Solar energy is available in an intermittent way, and integrating an energy storage system with solar energy collection devices may promote uninterrupted supply of energy in the absence of the availability of solar energy. It has been shown that heat can be stored using rocks packed in a bed, but limited work has been reported on heat extraction from a charged rockbed. This paper reports on the heat extraction from a charged rock bed. Discharging tests were performed under different air flow conditions and initial bed temperatures. Without the blower, the discharging rate is very slow. The discharging rate can be increased, and the cooking time controlled by adjusting the air speed through the rock-bed system.

Keywords: rock bed storage, heat extraction, air flow rates, boiling

* Corresponding author. *Tel:* +256 772 59403;
Email: dekello@yahoo.com

1. Introduction

Solar energy offers an alternative solution to the current energy demand from low- to high-temperature domestic and industrial applications. The conversion of solar radiation to thermal energy for direct use is particularly more attractive for both industrial and domestic heating applications. The domestic application of solar thermal systems includes solar water-heating, solar drying, solar cooking and space-heating systems. Most developing countries in sub-Saharan Africa are in dire need of energy for food preparation and yet they are located within the sunbelt region. Most communities in the rural villages rely on woodfuel for cooking. The use of solar energy to cook has several advantages, including: saving rural women and children from the burden of walking long distances in search of firewood; improving the health of these people since they will no longer be as exposed to the danger of inhaling smoke caused by incomplete biomass combustion; and reducing the current high rate of deforestation in most parts of the world. Substantial research has been reported on solar cookers [1]–[6], but these solar cookers still need improvements for them to have a wider acceptance, since their use is restricted to the sunny periods of the day. This can be remedied by integrating a thermal energy storage (TES) system for storing energy during time of availability for later applications.

The use of rock particles to store heat has several advantages compared to other thermal energy storage: they are cheap and locally available, the technology is feasible and the storage containment design is similar to the conventional cooking oven

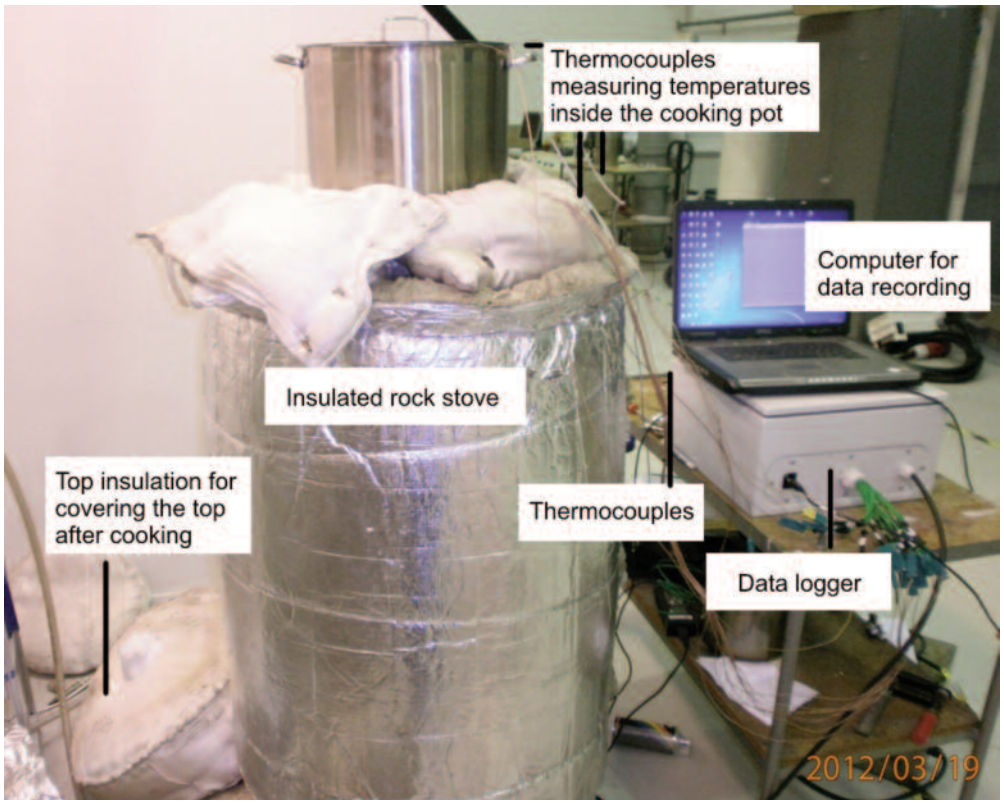

Figure 1: A rock bed stove showing the cooking pot, data logging and recording systems, top insulation for covering the top part after cooking, and thermocouples measuring the temperature inside the cooking pot and that of the rock bed storage as a function of time

which promotes cooking on the top part of the storage. In addition, rocks have fairly good heat transfer characteristics when used with air at low velocities and can withstand high temperatures [7], [8].

Studies have shown that heat in the medium-to-high temperature range (200–400 °C) can be stored in a bed of rocks [9], [10]. There has, however, been limited research reported on heat extraction from a heated rock bed. This paper, investigates heat extraction from a charged bed of rocks and the thermal behaviour of the storage during this process. Since most food preparation in rural homesteads in developing countries involves boiling vegetables in water (mainly cassava, vegetables, maize grain, groundnuts, eggs, pumpkins, matooke, sweet potatoes, etc), and given that these food items do not take long to cook once the boiling point is attained [11], the study on heat extraction is limited to the time it takes to boil a given amount of water.

2. Experimental methods

The rock bed TES was constructed using two vertical co-axial cylinders made from stainless steel. The diameters of the inner and outer cylinders were 30 and 40 cm respectively. Three thin, parallel, and reflecting steel foils were inserted in the space between the cylinders to minimise heat loss by radiation. In attempt to eliminate heat loss to the surroundings, the bed was insulated with additional layers of fibreglass material, as shown in Figure 1. The top part of the experimental TES system reported by Okello et al. was modified as shown in Figure 2 [9]. The top plate was constructed using an aluminum plate of thickness 10 mm, and to it were attached fins made of the same aluminum material, as seen in Figure 2A. Fins were used to enhance the heat transfer from air to the top-plate. The simulated approach described by Chikukwa [12], [13] of using packed thin copper pins attached to a top plate was not considered, since the copper pins were not available. The heat extraction tests were performed by reversing the airflow direction and, from our design, it was not possible to recirculate the airflow. The direction of airflow was reversed by placing the fan at the bottom of the storage. A hole was left at the centre of the plate for letting air in and out during charging and discharging processes, as depicted in Figures 2A and B. This discharging procedure allows the thermal stratification of the storage to be retained and gives a better heat transfer to the cooking pot than by the metallic contact alone. A 20 litre saucepan containing a known amount of water was used for the boiling tests. The change in the temperature of water with time was recorded by placing a thermocouple in the middle of the water. The thermocouple tip was bent upwards to ensure that it did not touch the base of the saucepan. The variations in axial temperatures of the TES unit were also recorded.

The schematic layout of thermocouples at differ-

A: Top plate with fins attached

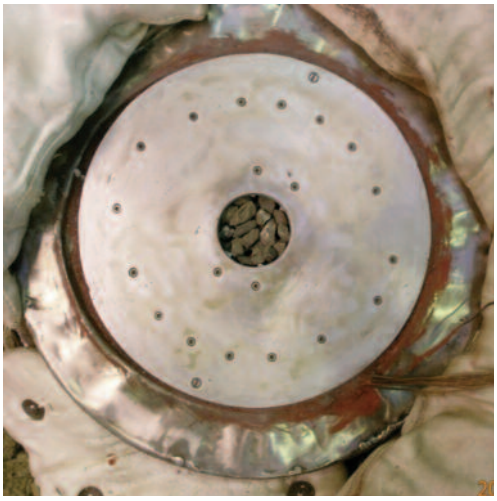

B: Top part used (cooking plate)

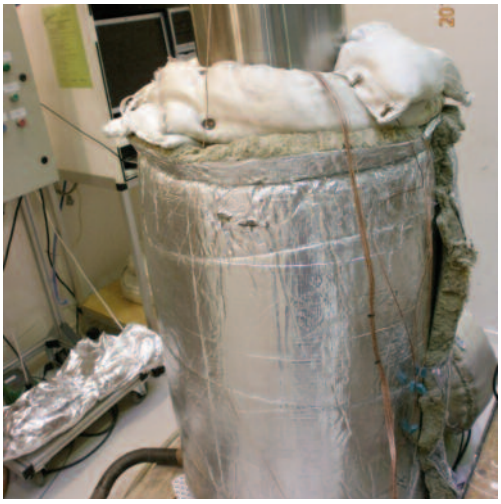

C: Water in saucepan on cooking plate

D: Water boiling on cooking plate

Figure 2: The design and construction of the top plate (A and B), and the complete rock bed storage unit during the cooking test (C); D shows a water boiling test on a rock stove

ent axial bed height is shown in Figure 3. The topmost thermocouple T_1 was placed 2 cm below the top surface of rocks. Thermocouple T_2 was placed 0.18 m below T_1, while the succeeding thermocouples were spaced at equal distances of 0.1 m. The positioning of thermocouples along the bed was made possible with the help of a supporting hollow steel rod. The photograph showing a complete system with data logging systems during boiling test is shown in Figure 1. The thermocouples were connected to an NI CompactPoint DAQ (data aquisition system) that was interfaced with the computer through an RS-232 cable. A LabView program was developed to read and record temperatures every minute. The minute data was displayed on the screen, making it possible to monitor the temperature dynamics at different levels of the bed during the experiment. The uncertainty in the measured temperature is estimated at ±1 . The thermocouple T_7 was not working and was not considered.

The discharging tests were performed under condition of no airflow and under constant and varying airflow rate conditions while monitoring the temperature profiles along the bed length. Known volumes of water were placed in turns and the times taken for each to begin boiling were recorded.

3. Results and discussion

3.1 Constant flow rates

The cooking test on top of a rock bed heat storage was performed by considering the time it takes to bring a known volume of water to boiling point. Figure 4 shows both the temperature of water during the boiling test and the temperature profiles along the rock-bed storage. With a constant airflow rate of 4.95×10^{-3} kg/s, the variation in the temperature of water was observed and recorded. The boiling test started with 12 litres of water and this was followed by adding one litre of water each time the boiling point was reached. The points where water was added are seen as zigzags in the heating curve for water and are marked by A_1 to A_6. In total,

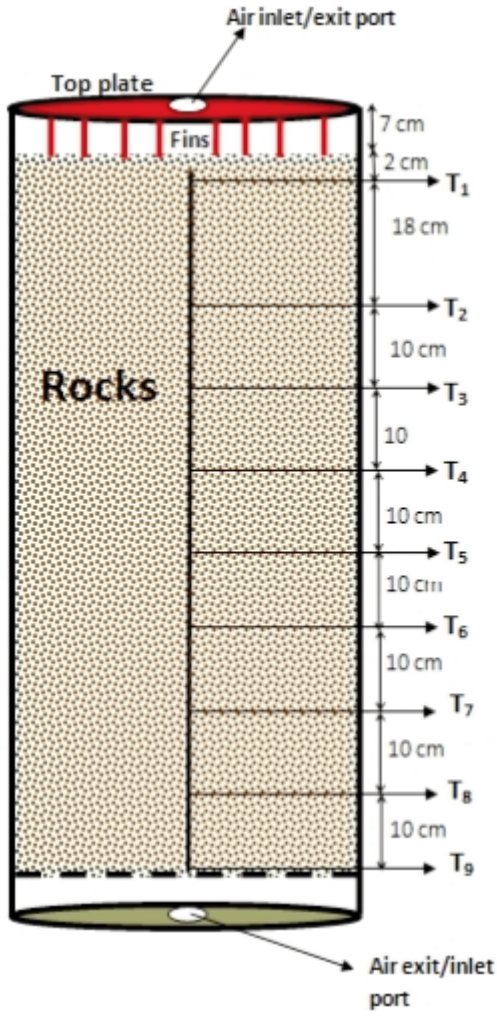

Figure 3: The schematic of the rock bed system with the top (hot) plate installed, outlining the layout of thermocouples along the bed height

18 litres of water could be boiled in about 2 hours. It took 53 minutes to bring to boiling 12 litres of water from an initial temperature of 19.2 . One litre of water was added each time the water in the saucepan began to boil. A_1 and A_2 took about 7 minutes each to begin boiling; A_3 and A_4 took 8 and 9 minutes respectively; A_5 took 12 minutes to begin boiling; while A_6 took 18 minutes to reach a constant maximum temperature of 98 . At this point, most sections of the bed were at temperatures below 100 and the experiment was stopped.

The temperature distribution as a function of bed length during the cooking test is shown in Figure 5. Separations between temperature profiles after every 30 minutes are the same for a constant airflow rate discharging method.

3.2 Varying air flow rates

In this test, the bed was charged with a hot-air blower to almost uniform temperature at 350 and left to stabilise for about 30 minutes. The boiling times were then tested under the conditions of no airflow and varying airflow rates. In Figure 6, the boiling test was carried out by first putting three litres of water in a saucepan on the top plate of the rock bed stove but without initiating air flow. The test started with temperature at the topmost part of the bed (T_1) initially at 320 which had dropped to 215 after 112 minutes. The temperature of the water in the saucepan rose from 19.8 to 85.5 in same time period. The temperature of water was observed to increase faster in the first 40 minutes from 19.8 to 77.5 , but for the next 72 minutes, a very slow rise in temperature was observed, with the thermocouples registering only 8 change. The airflow was

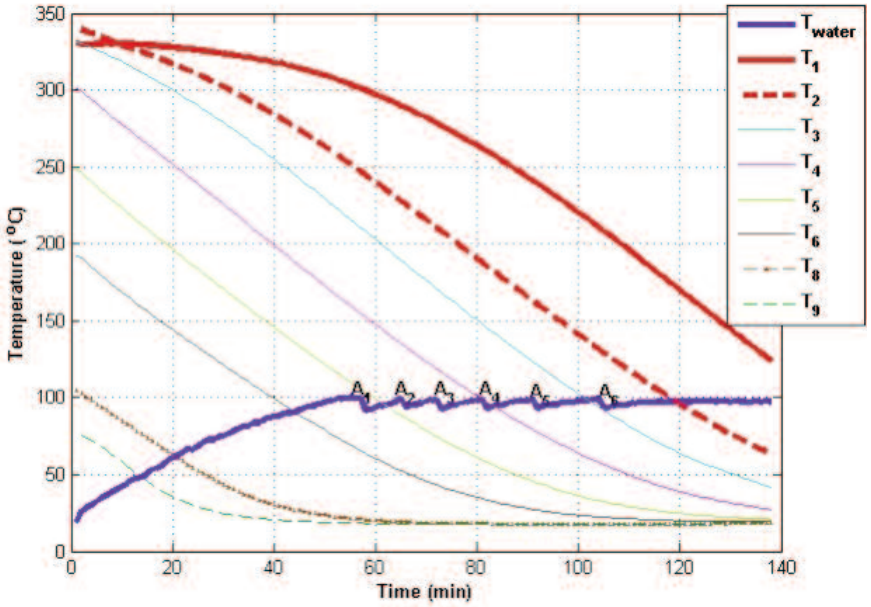

Figure 4: The temperature for water and the temperature profiles along the rock bed TES during the discharging process with a constant air flow rate of 4.95×10^{-3} kg/s. $A_{1\text{-}6}$ indicates points when a litre of water was added to the already boiling water in the cooking pot.

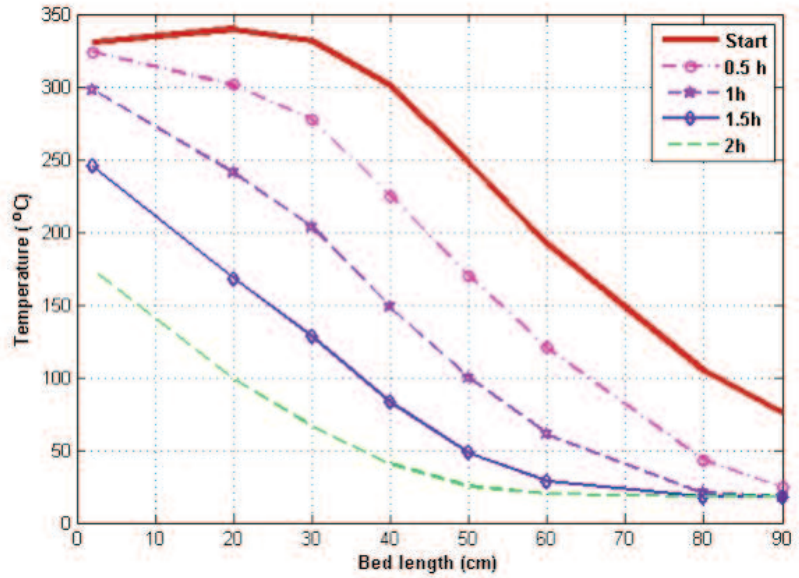

Figure 5: Temperature profiles along the bed during cooking test with a constant air flow rate of 4.95 x 10^{-3} kg/s

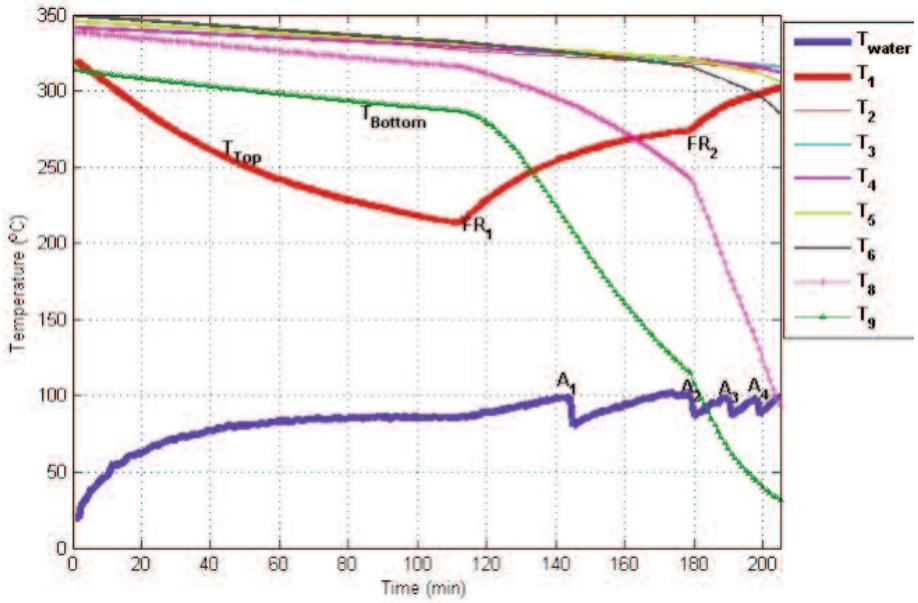

Figure 6: The heating rate of water and temperature profiles along the rock bed TES system for different airflow conditions. FR_1 and FR_2 indicate points when airflow rates were changed to 2.2 × 10^{-3} kg/s and 3.3 × 10^{-3} kg/s respectively, while A_{1-4} indicates points where litres of water were added.

then initiated by turning on the fan, with the airflow speed set to 2.2 × 10^{-3} kg/s. Cold air is blown into the storage at the bottom and hot air exits through the hole at the top plate, under the cooking pot. The temperature of the water immediately started to rise and it boiled after 28 minutes. The temperature of rocks at the upper section of the bed (T_1) started to rise immediately after the fan was switched on at a point marked by FR_1 in Figure 6. A litre of water at a temperature of 19.8 was then added, with the airflow speed kept constant, and it boiled in 25 minutes.

The flow speed was then increased to 3.3 × 10^{-3} kg/s; it was observed to boil a litre of water in 10, 7 and 6 minutes respectively. The points where units of one litre of water were added, with the flow rate changed at point FR_2 to 3.3 × 10^{-3} kg/s, are marked by A_2, A_3 and A_4 on the heating curve for water in Figure 6. In this case, the heating rate is observed to increase with time since the topmost part of the bed was at a lower temperature than its innermost sections.

After the boiling test was completed, the top plate was covered with the well-designed top insulation cover shown in Figure 1, and and bed was left for 13 hours. The temperature profiles showing the thermal behaviour within the bed are shown in Figure 7. The higher temperature at the top is

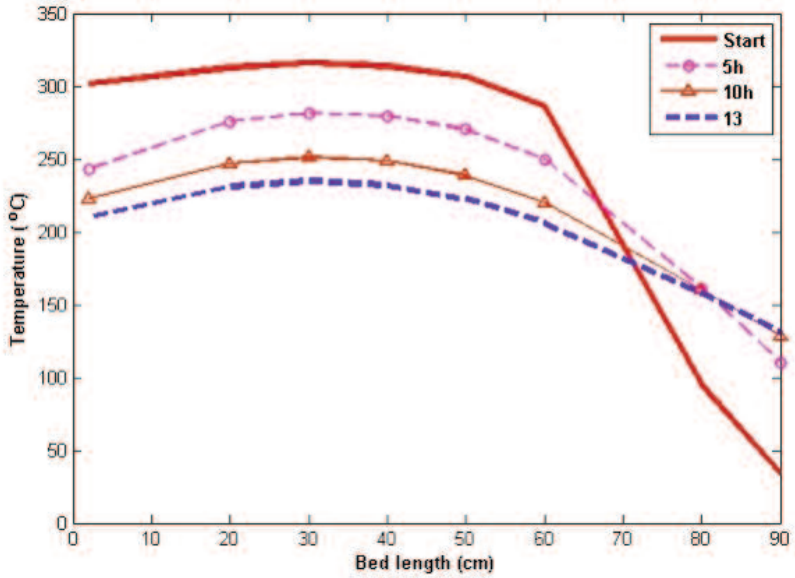

Figure 7: Thermal dynamics of an air-rockbed TES system during storage time

observed to drop as the bed approaches thermal equilibriation.

3.3 Tests on a de-stratified rock bed TES

The boiling test was again performed after the bed was left to equilibriate for 13 hours. Figure 8 shows the temperature profiles exhibited by both water and the rock bed TES system during discharging. The test was started by heating 7 litres of water with a constant airflow rate of 4.9×10^{-3} kg/s and it boiled in 50 minutes. The water was then changed and another 3 litres of water were again poured in the saucepan and the airflow rate was reduced to 2.9×10^{-3} kg/s; it took 44 minutes for it to reach boiling temperature. This was replaced with another 3 litres of water and the air flow rate was reduced further to 0.98×10^{-3} kg/s. The water was observed to heat up to constant temperature of about 86 in about 2 hours. At this point, the airflow rate was increased to 4.9×10^{-3} kg/s, and boiling occurred in 10 minutes. When the pan contents were replaced by another 3 litres of water and the airflow rate increased further to 5.6×10^{-3} kg/s, the water could reach only 86 . At this point all sections of the rock bed TES were at temperatures below 100 , as shown by the bed thermal profiles. These tests show that it is possible to extract heat from a charged rockbed storage by simply reversing the airflow

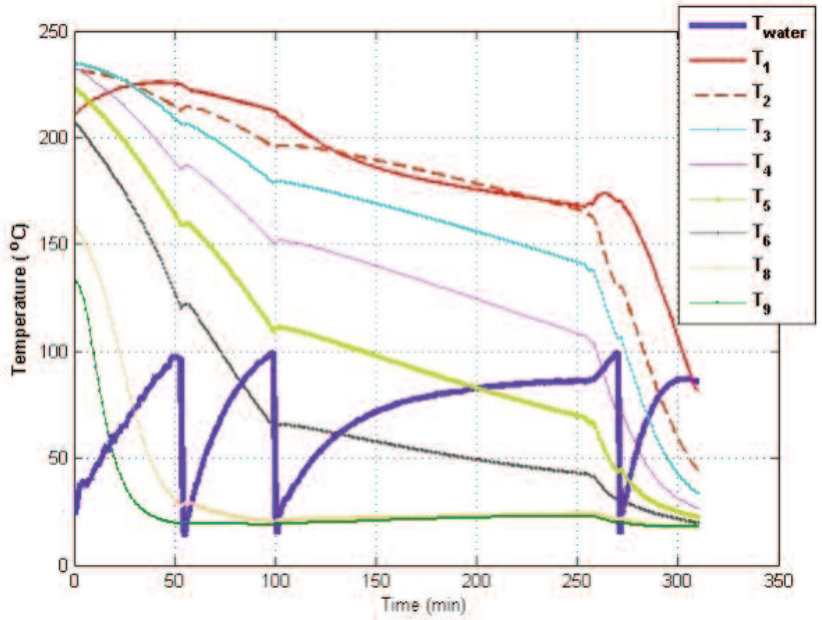

Figure 8: Heating rate of water and temperature profiles along the rock bed TES system for different airflow conditions. Zigzag points in the heating curve for water indicate points when the water was changed. The change in airflow rate is seen by changed temperature profiles along the bed.

direction, and the extraction rates can be varied by simply adjusting the airflow speed.

The temperature profile exhibited in the rock bed TES with varying discharging air flow rates during this boiling test is shown in Figure 9. The effects of varying airflow rates on the temperature profiles of a TES unit plotted after every 30 minutes are seen from the separations between the curves. The curves are closer with slow airflow discharge rate and vice versa.

4. Conclusions

Discharging tests were performed by blowing air into the bottom of a heated rock bed storage under different airflow conditions. A cooking pot with water was placed on top of the heat storage, covering the opening for the hot exit air. The results for constant airflow rate discharging showed a higher rate of energy extraction in a well-stratified bed at the beginning, which then falls off with time. Without the blower, the discharging rate is very slow. The discharge rate can be increased, and the cooking time controlled by adjusting the air speed through the rock bed system. The method of discharging with varying airflow rates seems beneficial to most cooking practices since the rate can be adjusted according to the requirements of the preparation of particular foods.

Acknowledgement

The authors are grateful to the technical staff at the Department of Energy and Process Engineering at the Norwegian University of Science and Technology for the construction of the thermal energy storage system, and for the financial support to the NUFU project on small-scale concentrating solar energy systems with heat storage.

References

1. M. Telkes. 'Solar cooking ovens', *Solar Energy*, vol. 3, pp. 1–11, 1959.
2. B.S. Negi and I. Purohit , 'Experimental investigation of a box type solar cooker employing a non-tracking concentrator'. *Energy Conversion and Management,*, vol. 46, pp. 577–604, 2005.
3. N. M. Nahar, 'Performance and testing of an improved hot box solar cooker', *Energy Convers. Mgmt*, vol. 30, pp. 9–16, 1990.
4. M.A.Mohamad, H.H El-Ghetany and M.A.D Adel, 'Design, construction and field test of hot -box solar cookers for African Sahel region, *Renewable Energy*, vol. 14, pp. 49–54, 1998.
5. N.M. Nahar, 'Design, development and testing of a double reflector hot box solar cooker with a transparent insulation material, *Renewable Energy*,vol. 23, pp. 167–179, 2001.
6. A. Raji Reddy and A.V. Narasimha Roa, 'Prediction and experimental verification of performance of box type solar cooker - Part I: Cooking vessel with central cylindrical cavity', *Energy Conversion and Management.*, vol. 48, pp. 2034–2043, 2007.
7. H.W. Fricker, 'High temperature heat storage using natural rock'. *Solar Energy Materials*, vol. 24, pp. 249–254, 1991.

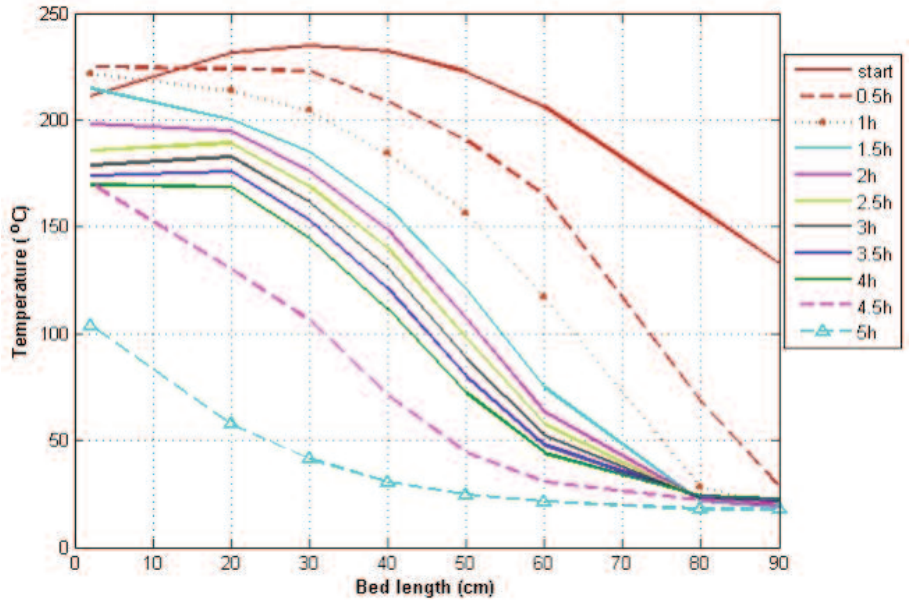

Figure 9: Rock bed temperature profiles during the third cooking test with varying flow rates test shown in Figure 8

8. R. Daschner, S. Binder, and M. Mocker, 'Pebble bed regenerator and storage system for high temperature use', *Applied Energy*, vol. 109, pp.394–401, 2013.
9. D. Okello, C.W. Foong, O.J. Nydal and E.J.K. Banda, 'An experimental investigation on the combined use of phase change material and rock particles for high temperature (350°C) heat storage', *Energy Conversion and Management*, vol. 79, pp. 1–8, 2014.
10. D.Okello, O.J. Nydal and E.J.K. Banda, 'Experimental investigation of thermal de-stratification in rock bed TES systems for high temperature applications'. Energy Conversion and Management, vol. 86, pp.125–131, 2014.
11. B.S.M. Ali, 'Design and testing of Sudanese solar box cooker', *Renewable Energy*, vol. 21, pp. 573–581, 2000.
12. A. Chikukwa. 'Modelling of a solar stove: Small scale concentrating system with heat storage', PhD thesis, Norwegian Univ. of Science and Technology, Trondheim, Norway, 2007.
13. A. Chikukwa and J. Lovseth, 'Optimization and modelling of a high temperature solar thermal storage adapted for hotplate operation', *Proc. ISES Solar World Congress: Renewable energy shaping our future*, pp. 660–669, 2009.

Modelling household electricity consumption in eThekwini municipality

Samantha Reade*

Temesgen Zewotir

Delia North

Statistics Department, School of Mathematics, Statistics and Computer Science, University of KwaZulu-Natal (Westville Campus), Private Bag X 54001, Durban 4000, South Africa

Abstract

South African municipalities are faced with the challenges of growing demand for services. This study models the energy consumption estimation practice within the Durban municipal area. It was found that an estimation technique that accounts for the seasonal and monthly effects, as well as residential type, predicts monthly individual household electricity consumption with minimum error. Models that were developed may be used to estimate electricity consumption for household billings within a municipality.

Key words: electricity consumption, mixed models, municipalities, billing

* Corresponding author: *Tel:* +27 (0)31 260 3011; *email:* 208506871@stu.ukzn.ac.za

1. Background

The eThekwini municipality, which includes the city of Durban, is situated on the East Coast of South Africa, within the province of KwaZulu-Natal. It covers a land area of approximately 2000 km^2, with a population of 3.4 million. The licensed distributor of electricity to the municipality, eThekwini Electricity supplies 655 338 households with electricity, approximately half of which are prepaid customers and half are credit customers. All credit customers have an electricity meter on their property. Ideally, credit customers are charged monthly for the amount of electricity they consumed during the previous month, but for technical and personnel reasons, electricity meter readings are taken at three-month intervals. If the data collector has no access to the meter, the reading is done in the following three-month visit, and, if again the meter is not accessible during that visit, the next reading reads for the last nine months' consumption, and so on. In the meantime, however, the household is obliged to pay the estimated consumption charges and only upon the actual reading are the estimated billings adjusted backwards, with any difference then credited or debited to the household in the following month's billing. Whenever the actual reading is available, the credit or debit accrued from the previous estimates, plus the new measured consumption for that month, will be billed. In other words, the actual consumption values are used to adjust the previous estimates and predict monthly household consumption values for the months until the next reading.

Household electricity consumption is estimated by eThekwini Electricity by means of a cumulative total of weighted previous actual usages, whereby the most recent consumptions carry the highest weightings, while weights of older consumptions decrease in a geometric progression. The method

may be expressed in terms of Equation 1:

$$E(y) = \sum_{k=1}^{n-1} \left(\frac{1}{2}\right)^k lag_k + 2\left(\frac{1}{2}\right)^n lag_n \qquad (1)$$

where n is the total number of actual measurements that each household has; $E(y)$ represents the expected electricity usage, and lag_k represents the k^{th} lagged actual consumption value converted per month.

The lag_1 carries a weight of 0.5, lag_2 carries a weight of 0.25, lag_3 carries a weight of 0.125 and lag_4 carries a weight of 0.0625, etc. Once these weighted lags are summed, it becomes evident that the bulk of the estimate for current electricity usage comes from the first four lags that a household has. This customary estimation method clearly does not allow for any seasonal or cyclical trends in consumption, nor does it take into account individual household electricity consumption variability and patterns.

Little research has been done, in either South Africa or other developing countries, to find models that will assist utilities to better predict monthly household electricity consumption. A primary focus of local research has been the national aggregate electricity demand and the examination of factors likely to influence it. In the 1980s, Pouris (1987) used annual data and an unconstrained distributed lag model to estimate long-run price elasticity of the aggregate electricity demand. More recently, Inglesi (2010) specified variables that could be used to explain aggregate electricity demand in South Africa, and determined that a long-run relationship exists between electricity consumption, electricity price and economic growth. Sigauke and Chikobvu (2011) captured the effect of various short-term demand-influencing factors such as days of the week and temperature, by developing a combination regression-SARIMA-GARCH model to predict daily peak aggregate electricity demand. Further to their 2011 study, Chikobvu & Sigauke (2013) then employed a piecewise linear regression model and applied extreme value theory to model the influence of temperature on South Africa's daily average electricity demand.

Following a model similar to that of Pouris (1987), Ziramba (2008) examined electricity demand as a function of gross domestic product (GDP) per capita and electricity price in the South African residential sector. Ziramba found that, in the long run, income was the main factor that determined residential electricity demand, while the price of electricity was insignificant. Similar studies where residential electricity demand has been modelled as a function of GDP per capita, price and other factors, have been carried out in Australia, the United States, Sri Lanka and Taiwan. In addition to studies where the focus has been price elasticity or forecasting electricity demand, research has also gone into other factors affecting electricity consumption. Firth et al. (2008) identified trends between electricity consumption and appliance usage. Marvuglia and Messineo (2012) used artificial neural networks for short-term electricity forecasting in Italy and focused on how the use of air-conditioning affected electricity consumption. Yohanis et al. (2008) carried out a comprehensive study in Northern Ireland on the patterns of electricity consumption of 27 households, taking into account a wide range of household factors such as dwelling type, location, dwelling size, household appliances, attributes of the occupants and income. They found that each factor had an impact on electricity consumption.

Aside from the small study of 27 households by Yohanis et al. (2008), the problem with studies such as those cited is that they are not able to describe electricity consumption at the level of the individual household. Though such studies are useful to estimate national residential electricity usage, the main challenge in South Africa is service delivery at the municipal and ward levels. The present study therefore initiates and motivates further research on estimating the electricity consumption of a typical household in a given municipality in South Africa. The customary practice in estimating present electricity consumption is based on prior consumptions only. Intuitively, prior consumption should serve as a good estimate for current consumption, but the challenge lies in how to best weight these prior consumption values so as to ensure accurate estimates. This study investigates how to weight prior consumption values in estimate current electricity consumption. A further aim is to ascertain whether all available lags for a household are important or not, and if there is any seasonal pattern in household consumption. The study differs from the literature cited in that the main focus is at a household level, as opposed to modelling and predicting consumption for the entire residential sector. The traditional time series and econometric modelling approaches are replaced by an applied statistical approach.

2. Data description

Data for this study was provided by eThekwini Electricity, from meter readings perpetually carried out at three-month intervals amongst credit customers. Meter readings, reading dates and actual consumption values are all stored on the municipality's database for combined online information systems. Other data that are stored include electrical connection identifiers, property identifiers and dwelling-type classifications. Dwellings are classified into three types: houses, share blocks that are one or two storeys high (e.g. simplex or duplex), and share blocks of more than two storeys (e.g. blocks of flats). This classification information was supplied

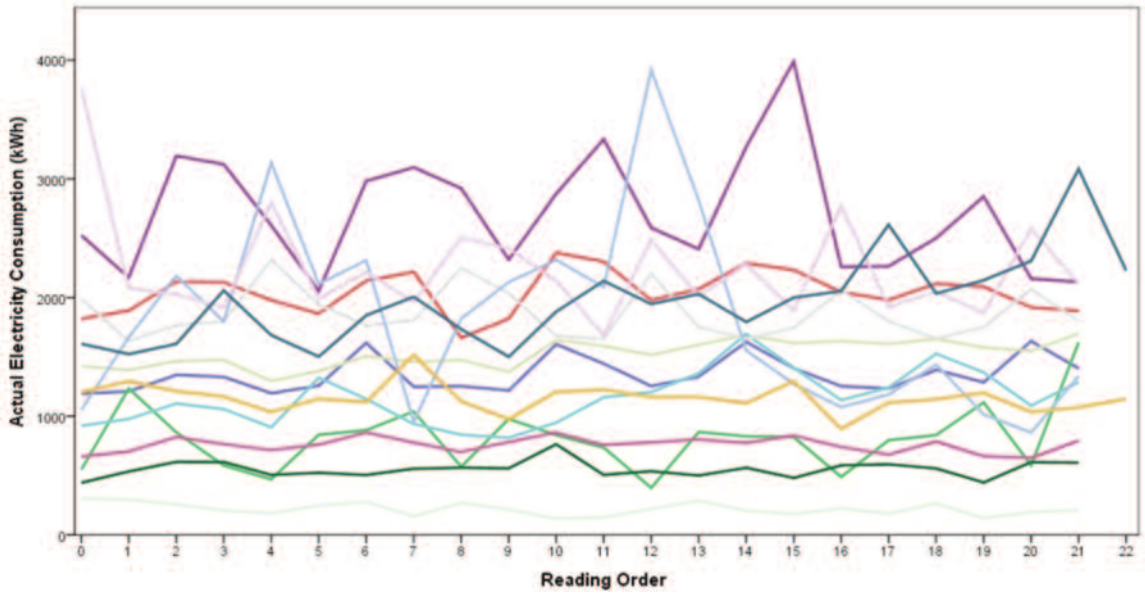

Figure 1: Profile plot of monthly electricity consumption for randomly selected households

by eThekwini Electricity, as well as meter-reading data for the five-year period 2008–2013. For this study individual electricity consumers were identified by their electrical connection identification, and are referred to as households. Additional information, such as month of meter reading and length of usage periods (defined as the time, in days, between two consecutive meter readings), was also extracted from the data provided.

The original data set received from eThekwini Electricity was large, containing information for approximately 300 000 households, along with three-monthly consumption values for each household. Computing power required for processing such large data exceeded the available computing facilities at the University of KwaZulu-Natal, but, as the main focus was modelling electricity consumption so as to enable future prediction, using a randomly selected sample was sufficient. A sampling frame was specified so as to ensure that only households with regular meter readings at three-month intervals were considered and that each dwelling type was represented. Accordingly, a sample of 1 478 households was randomly selected from the data set. Electricity consumption was modelled for the sampled data, demonstrating effective methods that could be implemented on a larger scale (with the necessary computing capacity). A focal point of this study was to investigate the presence of a seasonal effect so as to enable better modelling of electricity usage. The starting point was, therefore, examining a simple profile plot of a few randomly selected households from the sample.

Figure 1 shows that household electricity consumption is a constant function with dominant individual variability. Moreover, this individual variability also shows some systematic cyclic seasonality, which can be accounted for by month-to-month variation. An overall seasonal pattern is, however, difficult to distinguish by simply studying the profile plot. Possible reasons for the obscured seasonality could be that there are both different dwelling types and different measurement batches that exist but are not accounted for in Figure 1. A measurement batch is a particular measurement pattern of three-month intervals that each household follows. For example, if a meter is read in January, subsequent readings will always be done in (approximately) April, July and October, then cycle back into January. As meter readings are carried out in intervals of three months, there are only three measurement batches: Batch 1: January, April, July, October; Batch 2: February, May, August, November; Batch 3: March, June, September, December. In order to better understand factors affecting monthly electricity consumption and any seasonal trends within it, the research proceeded by studying profile plots by dwelling type and measurement batch.

Figure 2 shows a clear difference between the consumption patterns of the three dwelling types, with houses having the highest electricity usage. Although a clearer systematic cyclical pattern in the prior consumption values is observed in Figure 2, it is still difficult to identify an overall seasonal trend, probably because, within each dwelling type, households may be further classified into the different measurement batches. Moreover, minor variations within each batch arise due to eThekwini Electricity following a measurement system of 90 days as opposed to calendar months, as well as factors such as local elections or holidays also leading meter readings to be postponed or brought forward. Although this study was most concerned to model seasonal effects within each household, and not reading-batch variability, it is acknowledged that these batch variations may cause the obscured

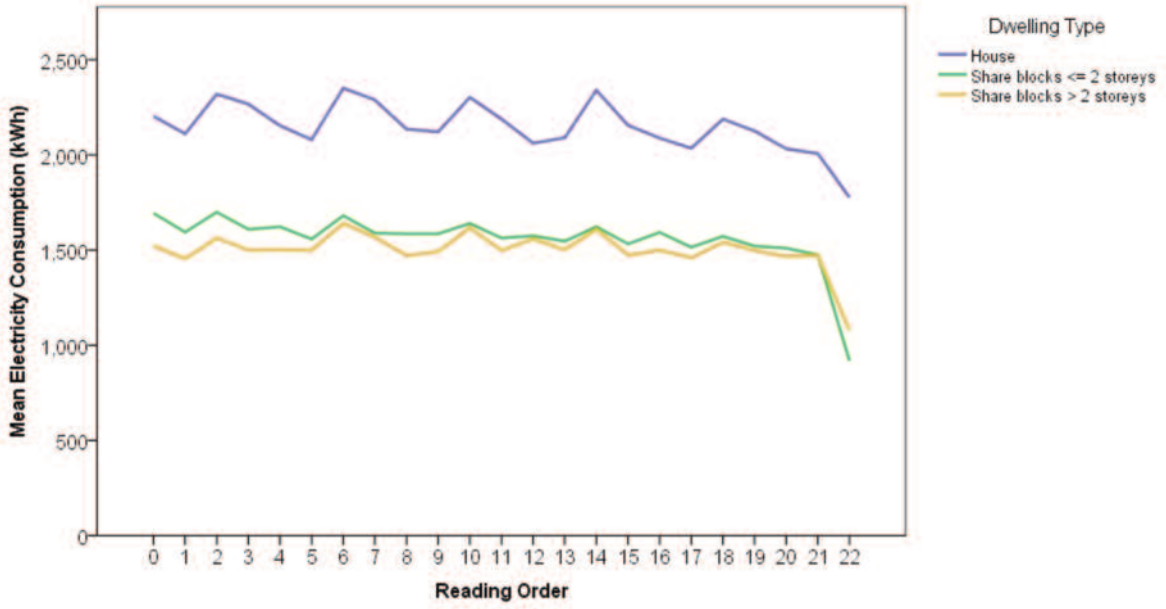

Figure 2: Profile plot by dwelling type and reading order

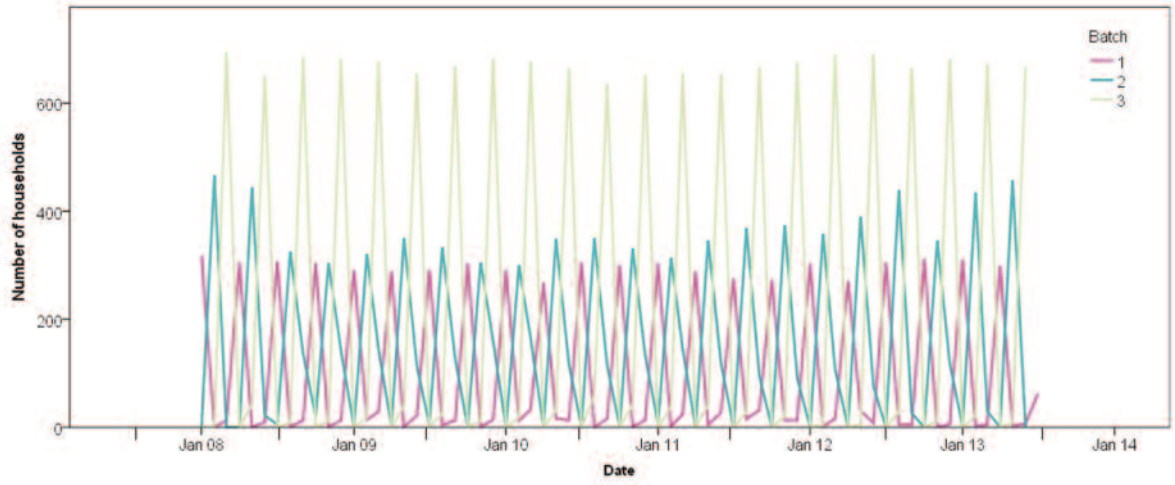

(a)

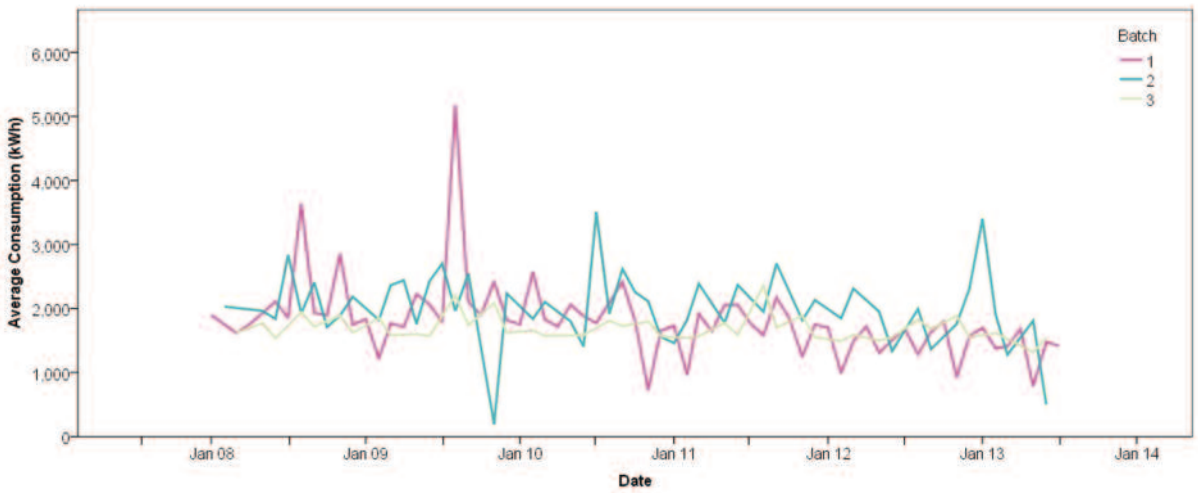

(b)

Figure 3: Batch profiles for (a) number of households (b) average consumption (kWh)

seasonal pattern. A simple way of demonstrating this is to study the batch profiles given in Figure 3, which show the number of households and average consumption by month for the five-year period.

Figures 3(a) and 3(b) show that there is individual batch variability present in both the consumption values and number of households. Figure 3(a) clearly shows three distinct measurement patterns and evidence that meter-readings follow periods of more-or-less three months. Batch 3 appears to have the most number of households, followed by batch 2 and then batch 1. A possible reason for this variation could be that some batches come from more densely populated areas than others, resulting in more meter-readings. From Figure 3(b) it can be observed that, within each batch, some form of monthly effect is taking place, as some months show higher consumption values than others. An overall monthly pattern is difficult to determine in Figure 3(b), however, possibly due to each reading-batch having its actual consumption values recorded at different times. To better understand the month effect, a profile plot of the average electricity consumption of the reading-batches by month over the five-year period was examined; the plot is displayed in Figure 4.

The plot shows that higher electricity consumption values generally occur in July, August and September. Given, however, that meters are read at three-month intervals, the consumption values for the months in Figure 4 also refer to consumption values of approximately two months prior to the month of meter reading. In the 90-day interval, the 'middle' month is the month where the monthly consumption could be deduced. From this understanding it can be seen that the months of high consumption reading, July, August and September, in fact refer to an approximate median June-August period of higher electricity usage. It is necessary to be vigilant with regard to metre-reading months and actual consumption months. The reading month is given, so the inference should be the consumption pattern of two months earlier. Conscious of this, it is essential to examine the two sources of the cyclical seasonal effect. The first element is the monthly seasonal effect observed in Figure 4, whereby the winter months gave evidence of increased electricity consumption. The second possible element is autocorrelation within each household's annual electricity consumption values.

In order to further investigate the presence of autocorrelation, another profile plot was examined, this time averaged over each household by reading order, given in Figure 5. From the graph, it can be noted that some form of autoregressive process is taking place. The consumption values at *t=0, 4, 8, 12* and *20* are similar. The same pattern is observed at *t=2, 6, 10, 14* and *18*. Since there are three months between consecutive meter-readings, after four meter readings 12 months have passed. Likewise, after eight readings, it can be assumed that 24 months have passed; after 12 readings 36 months have passed, and so on. One way to account for such an autoregressive pattern in the data is to include some lagged values in a linear model . The current study employed a linear mixed modelling approach which is well-suited to handling repeated measures and accounts for variations both between and within households. Using linear mixed models (LMMs) allows modelling of both the month-to-month seasonality as well as the repetitive pattern occurring in prior consumption values. Moreover, mixed models are flexible, allowing for the both temporal and spatial variations to be modelled.

3. Methodology

Laird and Ware (1982) were the first to illustrate the use of LMMs in longitudinal data analysis. Subsequently, many researchers have used both LMMs and generalised LMMs (GLMMs) to model repeated measures data. The GLMM is the generalised form of the LMM, whereby the response vari-

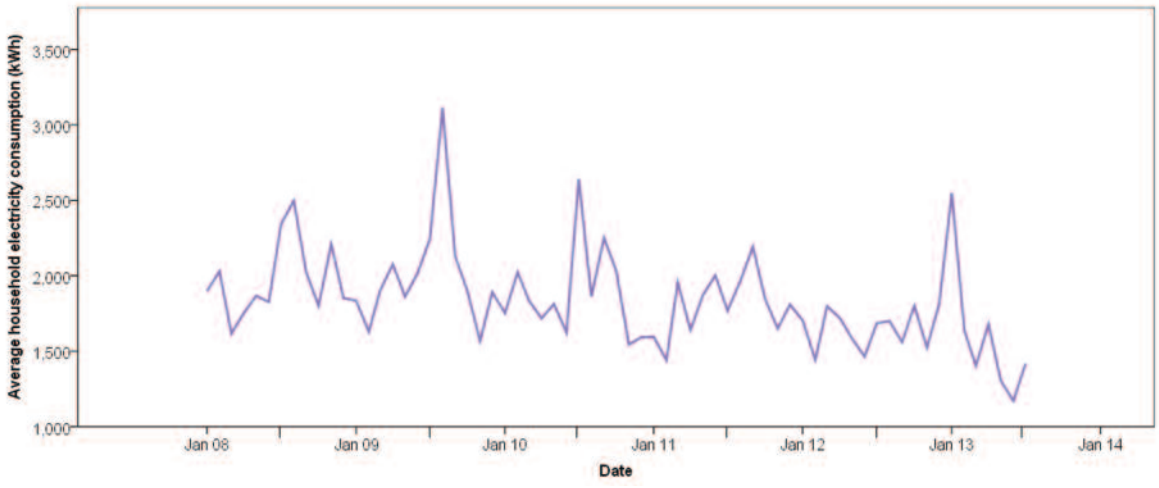

Figure 4: Average reading-batch electricity consumption by month

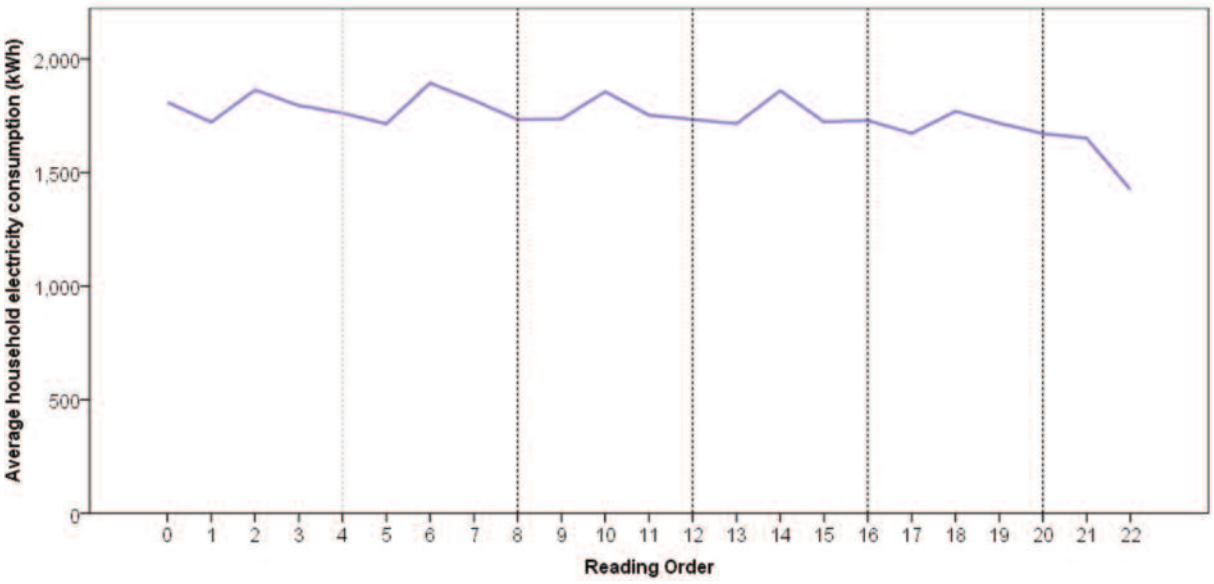

Figure 5: Average household electricity consumption by reading order

able may come from a variety of distributions, provided the distribution is a member of the exponential family . The general form of a linear mixed model, adapted for repeated measures data, is given by Equation 2.

$$y_i = X_i\beta + Z_i b_i + e_i \quad (2)$$

where $y_i = (y_{i1}, y_{i2}, \ldots, y_{in_i})'$, if y_{ij} represents the response of the i^{th} individual measured at time t_{ij} for $i = 1, \ldots, N$ and $j = 1, \ldots, n_i$; Xi is an $(n_i \times p)$ matrix of known covariates associated with the fixed effects; β is a $(p \times 1)$ vector of unknown regression parameters representing the fixed effects; Z_i is an $(ni \times q)$ design matrix associated with the random effects; b_i is a $(q \times 1)$ vector of random effects, representing the random subject-specific effects, such that $b_i \sim N(0, G)$ where G is block diagonal with the i^{th} block being $\sigma_i^2 I_{qi}$; e_i is an $(n_i \times 1)$ vector of residual components where it is assumed $e_i \sim N(0, R)$ and R is positive definite. Furthermore, it is assumed that b_i and e_i are independent. Different variance-covariance structures may be fitted to R, allowing us to model both spatial or temporal variance and correlation. In the GLMM, the conditional expectation of y is related to a linear predictor (η) by means of a monotonic differentiable link function g(.). The general form of such a GLMM for repeated measures data is given by Equation (3).

$$g(E(y_i|b_i)) = \eta_i = X_i\beta + Z_i b_i \quad (3)$$

where η_i represents the linear predictor of the i^{th} individual and $g(.)$ the link function that links the conditional mean, $E(y_i|b_i)$ to the linear predictor.

There are essentially three aspects to consider when specifying and fitting a GLMM to the electricity data: the specifications of the covariates in the model, the selection of the best suited covariance structure, and the selection of the distribution that best fits the response variable. To begin the modelling process current electricity consumption is initially assumed to be normally distributed. That is, it is first established which covariates to include and what covariance structure to fit, then a search is made for the distribution best suited for the electricity data. Having already established that dwelling type, month of meter reading and prior consumption values in some way affect current electricity usage, a marginal linear regression model is tentatively fitted, where current household electricity consumption is modelled as a function of all of these factors. As meters are read at three-month intervals, each household can be expected to have a minimum of 20 measurement occasions for the five-year period. Therefore, each household can be expected to have a minimum of 19 lagged values. To determine whether or not it is necessary to retain all 19 lags in the model, their significance and coefficient values are studied. These values are displayed in Table 1.

Table 1 shows that all the lags except for lags 9 and 11 are significant at a 5% level of significance. However, despite the significance of lags 13 to 19, upon closer examination of their coefficients it can be noted that these lags have, in fact, little overall effect on current household electricity consumption. That is, the coefficients of lags 13 to 19 contribute little, due to the positive coefficients of lags 14, 16, and 19 and the negative coefficients of lags 13, 15, 17 and 18 almost cancelling each other out. This shows that there is little value in retaining more than 12 lagged values in the regression model. Hence, in the interests of parsimony, the modelling process is continued using only 12 lags in the model, which is equivalent to a household's three-year electricity consumption cycle. In addition to the 12 lags, the

Table 1: Coefficients and p-values of the 19 lags

Lag	*Estimate*	*p-values*	*Lag*	*Estimate*	*p-values*	*Lag*	*Estimate*	*p-values*
1	0.4386	<0.0001	8	0.1309	<0.0001	15	-0.05653	0.0049
2	0.2230	<0.0001	9	-0.01415	0.3798	16	0.1873	<0.0001
3	0.06617	0.0001	10	-0.1098	<0.0001	17	-0.1367	<0.0001
4	0.1685	<0.0001	11	0.004017	0.7813	18	-0.1454	<0.0001
5	-0.1026	<0.0001	12	0.1882	<0.0001	19	0.05585	<0.0001
6	-0.06780	0.0001	13	-0.03844	0.0153			
7	0.07944	<0.0001	14	0.1119	<0.0001			

month of the most recent meter reading and dwelling type in the linear model are retained. By including both lags and month of meter reading in the model, two different factors can be analysed. The inclusion of the month of meter reading enables the taking into account of months that may have higher or lower electricity consumption than others. Lags allow for the incorporation and assessment of the cyclical seasonal pattern observed within household electricity usage. Using month of reading, dwelling type and 12 lagged values, the following linear model is specified, noting that two dummy variables have been created for dwelling type and eleven dummy variables for the month of meter reading according to Equation 4.

$$g[E(y_{ij})] = \eta_{ij} = \beta_0 + \alpha_{i0} + \sum_{l=1}^{2} \beta_{1_l} DwellingType_l + \sum_{m=1}^{11} \beta_{2_m} MonthRead_m + \sum_{k=1}^{12} \beta_{3_k} y_{ij-k} \quad (4)$$

where $g(.)$ is the link function, $E(y_{ij})$ is the expected response of the i^{th} household, $i = 1, \ldots, 1478$ at time $j = 1, 2, \ldots, n_i$, where n_i is the number of actual readings for household i; a_{i0} represents a household-specific random intercept; and h_{ij} is the linear predictor. As the data is initially assumed to be normally distributed, a normal distribution is specified and the identity link function is used. By including a household-specific random intercept, the variability of different households within the variance components can be accounted for.

Following model specification, the next focus is on modelling within-household temporal variations. Several temporal covariance structures are fitted to the model, namely unstructured (UN), compound symmetric (CS), first-order autoregressive (AR(1)), autoregressive moving-average of order one (ARMA(1,1)), first-order ante-dependance (ANTE(1)) and Toeplitz (Toep). To determine the best-suited structure, several factors are considered: the Akaike information criteria (AIC), the number of parameters that require estimating and the convergence status of the model. Ideally, the structure selected converges successfully, has a small AIC value and only a few parameters. Amongst the fitted structures, Toep and ANTE(1) failed to converge successfully, so were discarded as viable structures. Table 2 displays the fit statistics of the structures that converged to a solution.

Table 2: Fit statistics for selected covariance structures

Covariance structure	*Iterations*	*AIC*	*BIC*
UN	4	182 924.3	183 279.2
CS	3	184 957.9	184 973.8
AR(1)	2	184 896.9	184 912.7
ARMA(1,1)	6	184 286.0	184 307.2

Table 2 shows that the unstructured model renders the smallest AIC value, but it is discounted as unviable, because it also has the highest number of parameters that require estimating. Following the unstructured form, the next best model is the ARMA(1,1) structure. Not only does this model have the second smallest AIC value, but it also has only three parameters that require estimating. The ARMA(1, 1) structure is therefore selected as the best-suited covariance structure. Having now modelled within-household temporal variation by means of selecting a covariance structure, the third and final aspect of specifying a GLMM for the electricity data is undertaken: searching for the distribution most appropriate for the electricity data. To do so, a variety of link functions are considered, and five distributions that belong to the exponential family, namely the normal, namma, lognormal, inverse Gaussian and exponential distributions. Only two converged to solutions: the normal distribution (AIC=184306.1) and the Lognormal distribution (AIC=3815.57), both with the identity link. However, according to the smaller-is-better Akaike information criteria, the lognormal distribution is clearly to be favoured over the normal distribution. Further support for choosing the lognormal distribution is that it is a distribution that naturally only takes non-negative values, making it compatible

with electricity consumption data which can also only take on non-negative values. Nevertheless, despite the compatibility of the lognormal distribution, it is still necessary and important to assess the goodness of the underlying distribution assumptions. To do so, both the scatter and probability plots of the conditional studentised residuals are examined (Zewotir and Galpin, 2004). These plots are depicted in Figures 6 and 7(a).

For the majority of cases in the scatter plot of Figure 6, an evident random scattering about zero is obvious. This supports the non-existence of any systematic pattern not accounted for by the model. It is also noteworthy, however, that several cases drift away from zero but, given that such cases are few in relation to the large data, these points can be classified as outliers. From the Q-Q plot in Figure 7(a), it is clear that most of the points lie approximately on the straight line, favouring the goodness of the lognormal distribution. The tails that depart from the line are due to a few outlying households in the data. Based on the plots in Figures 6 and 7(a), it can be comfortably concluded that both the distributional and linearity assumptions have been adequately satisfied, except for a few outliers. In repeated measures data analysis it is necessary to ascertain whether or not outlying subjects are influencing the model fit and, more specifically, if they are exhibiting influence in the covariance parameter estimates (see Zewotir & Galpin, 2006; Zewotir , 2008). If an outlying subject is identified as being influential it should be removed from the data, and any inferences ought to be based on the reduced-data model. Such identified subjects must, however, undergo scrutiny in order to determine any case anomalies. The case outliers in Figures 6 and 7(a) belong to households 202 and 1205, and their effect can be examined by running the full-data model and comparing it to subsequent reduced-data models. Influence is measured by the amount of change in covariance parameter estimates, as well as the observed effect on the AIC values and reduced-data Q-Q plots. Both the reduced and full data probability plots are shown in Figure 7, along with the AIC values.

Figure 7 shows that the individual removal of households 202 and 1205 and the simultaneous removal of both result in smaller AIC values. Although suggesting an improved model fit, this alone does not suggest influence, as a reduction in AIC values could be expected when outliers are removed. It is therefore necessary to examine the Q-Q plots and change in covariance parameters. From the near-identical plots in Figures 7(a) and 7(c), it is clear that household 1205 is not effecting influence, as little change is observed upon its removal. Figures 7(b) and 7(d) show that the removal of household 202 results in more model outliers, showing this household is better left in the model. Final evidence of the lack of effect that the removal of these outlying households have is found in the resulting covariance parameter estimates. From the tables within Figure 6, upon removal of households 202 and 1205, it is clear that there are only negligible changes in the covariance parameter estimates. The lack of significant differences in the parameter estimates, as well as the evidence portrayed in the Q-Q plots, shows conclusively that households 202 and 1205 are not influential and are merely model outliers. The data reveal a possible reason for them showing up as outliers: both have consecutive usage periods where electricity

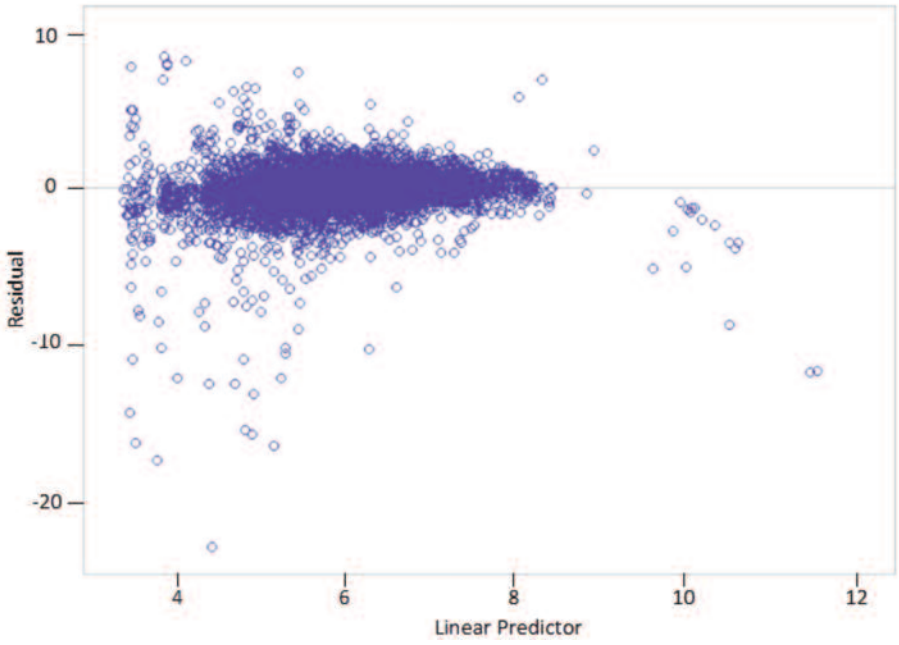

Figure 6: Scatter plot of conditional studentised residuals

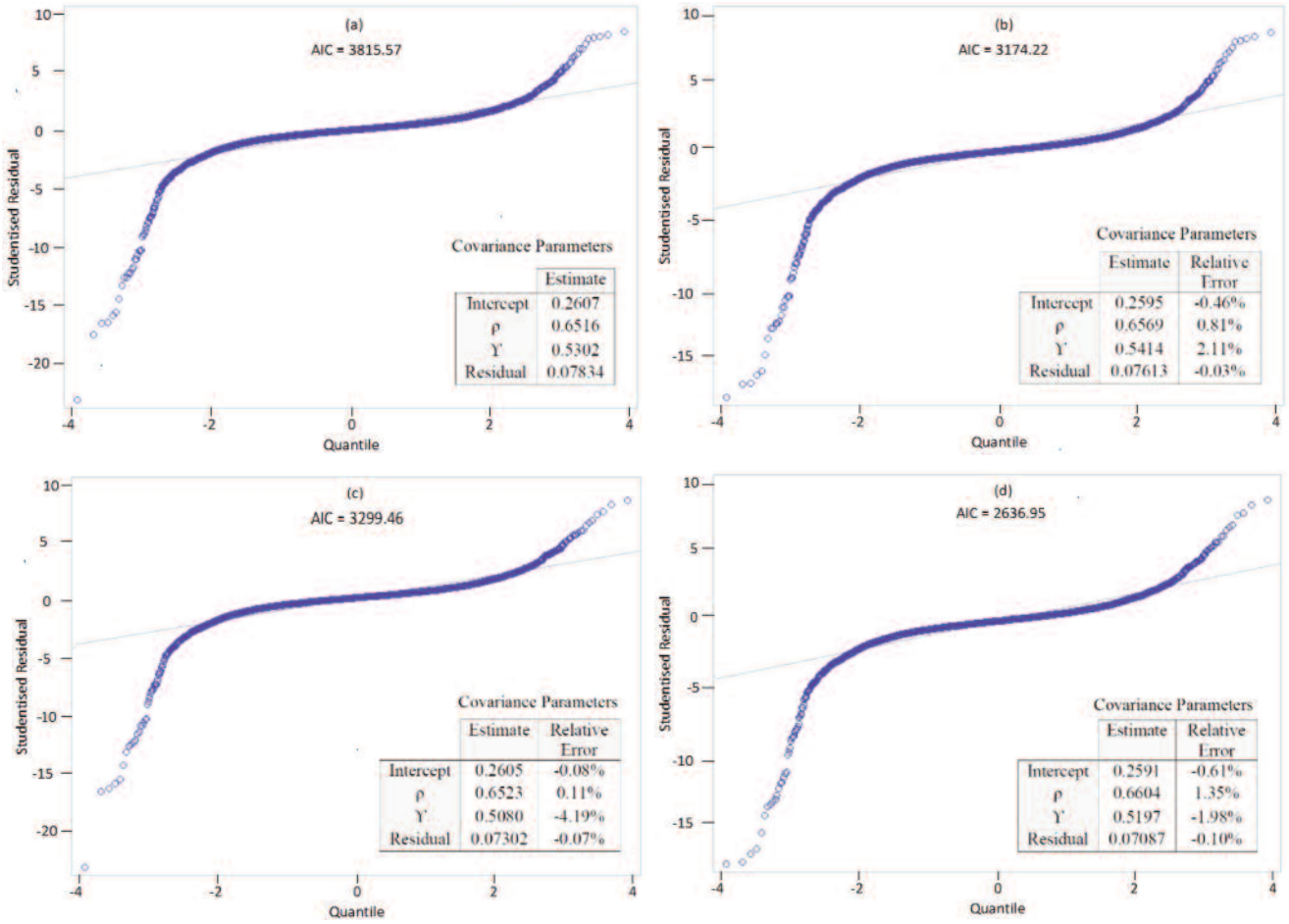

Figure 7: Q-Q plots of conditional studentised residuals, AIC values and covariance parameters when: (a) no households are removed (full-data model); (b) household 202 is removed; (c) household 1205 is removed; (d) both households are removed

consumption is very low, compared to the majority of consumption values in other usage periods for the same households. Having confirmed that households 202 and 1205 are non-influential outliers, they are retained in the model. The conclusion is that, when considering temporal variations within the electricity data, a full-data GLMM fitted to the lognormal distribution that uses an ARMA(1,1) covariance structure and includes a household-specific random intercept is the best-suited model.

Before proceeding with model inference and predictions, however, it should be noted that the current GLMM does not take into account that the number of days in each measurement period varies slightly. Despite carefully selecting the sample data to ensure approximately evenly spaced measurement occasions, a small amount of variation is inevitable. While the variation is negligible enough to still use methods for evenly spaced data, the small variations may result in the parameter estimates no longer being efficient. A possible solution to this problem is to add weights to the estimation procedure. Accordingly, previous estimates are weighted by the length of time (in days) of an approximate monthly measurement period. Upon adding weights, an improved model fit is observed, by which the AIC value was reduced from 3815.57 in the unweighted model to 3781.15 in the weighted model. The weighted GLMM is therefore taken as the final model from which to make inferences.

4. Results

The main inferences are derived from studying the parameter estimates of the fixed effects. The type III test results for the null hypotheses show that, at a 5% level of significance, both hypotheses will be rejected, as both tests render p-values smaller than 0.0001. This indicates that at least one dwelling type and one month are significant to the model and that their individual estimates should be examined along with the lags. All fixed effect estimates are displayed in Table 3.

The first observation to be made from Table 3 is the size and significance of the model intercept, which indicates that not only is a starting value universal to all households necessary but also shows how a household-specific random intercept is likely to improve the model's prediction capabilities for individual households. Next, the estimates for the various dwelling type classifications are examined.

Table 3: Solutions for the fixed effects

Effect	*Weighted estimate*	*Standard error*	*DF*	*t value*	*p-values*
Intercept	5.5425	0.02705	1473	204.93	<0.0001
House	0.3831	0.03428	13303	11.18	<0.0001
Shareblocks ≤ 2 storeys	0.1794	0.03413	13303	5.26	<0.0001
Shareblocks > 2 storeys	0	.	.	.	.
January	-0.02385	0.02004	13303	-1.19	0.2340
February	-0.04305	0.01255	13303	-3.43	0.0006
March	-0.01115	0.006450	13303	-1.73	0.0840
April	-0.04037	0.02058	13303	-1.96	0.0499
May	-0.05540	0.01219	13303	-4.54	<0.0001
June	0.01665	0.006816	13303	2.44	0.0146
July	-0.01354	0.02080	13303	-0.65	0.5150
August	0.01697	0.01244	13303	1.36	0.1726
September	0.06815	0.006820	13303	9.99	<0.0001
October	0.03686	0.02097	13303	1.76	0.0788
November	-0.01162	0.01323	13303	-0.88	0.3798
December	0	.	.	.	.
Lag_1	0.000044	0.000016	13303	2.84	0.0045
Lag_2	0.000081	0.000014	13303	5.76	<0.0001
Lag_3	0.000025	0.000014	13303	1.76	0.0786
Lag_4	0.000202	0.000014	13303	14.74	<0.0001
Lag_5	-0.00002	0.000012	13303	-1.67	0.0940
Lag_6	-0.00004	0.000013	13303	-3.50	0.0005
Lag_7	1.578E-6	0.000014	13303	0.12	0.9081
Lag_8	0.000120	0.000014	13303	8.54	<0.0001
Lag_9	-0.00002	0.000014	13303	-1.80	0.0717
Lag_{10}	0.000012	0.000013	13303	0.90	0.3679
Lag_{11}	1.841E-6	0.000013	13303	0.14	0.8892
Lag_{12}	0.000203	0.000014	13303	14.49	<0.0001

Using share-blocks of not more than two storeys as the reference category, it is shown that houses have a parameter estimate of 0.3831 while such share-blocks have a smaller parameter estimate of 0.1794. This agrees with what was first observed in Figure 2, distinctly showing that, of the three possible dwelling types, households falling under the classification of 'house' have a higher electricity consumption than those under the classification of 'share blocks of not more storeys', provided the reference category remains the same.

The parameter estimates for the months that meters are read in are examined next. Table 3 shows that February, April, May, June and September are significant at a 5% level of significance. Of these months, relative to December, the months May and September are highly significant (having p-values of <0.0001) in the model. Of all the months, September has the highest positive parameter estimate of 0.06815, while May has the highest negative coefficient of -0.05540. This suggests that September is likely to see a rise in electricity consumption, while May is likely to see a decrease, compared to the reference month, December. The meter-reading procedure of three-month intervals and the concept of electricity consumption for a median month (referring to an approximate midpoint between consecutive meter readings) is invoked, to give an understanding that, for May and the two months preceding it, the median month would be April, while for September and two months preceding it the median month would be August. It can be deduced that median month April will likely see a decrease in electricity usage, while median month August will likely see higher electricity consumption. However, this inference depends on the reference month (December) remaining the same and on the concept of a median month being approximate, as it depends on where in the month meters are read. Increased elec-

tricity consumption in August agrees with the original observation from Figure 4 that winter months are periods of higher electricity consumption. The model provided further insight into this aspect of the seasonality by also showing periods of lower consumption.

The last of the fixed effect estimates examined are those of the lags. Table 3 shows that lags 1, 2, 4, 6, 8 and 12 are all significant at a 5% level of significance. Of these lags, however, 1, 2, 4, 8 and 12 have the largest coefficient estimates. The fact that lags 1 and 2 have high estimates indicates that the two most recent consumption values are important. The large coefficients of lags 4, 8 and 12 show that a cyclical seasonal effect is present, as they correspond respectively to 12, 24 and 36 months prior to current electricity consumption. Thus, by including lags in the linear model this aspect of the seasonal pattern can be accounted for. Following the fixed effects, the covariance parameter estimates are briefly examined, recalling that to model temporal variance an ARMA(1,1) structure was fitted, and, to enable better prediction for individual properties, a random household-specific intercept was included. The estimates are displayed in Table 4.

Table 4: Covariance parameter estimates

Covariance parameter	*Weighted estimate*	*Pr Z*
Intercept	0.2607	<0.0001
ρ	0.6506	<0.0001
γ	0.5306	<0.0001
Residual	2.3799	<0.0001

From the ARMA(1,1) structure it can be seen that lag_1 correlation is constant, with the corresponding covariance function being estimated by $(0.2607)+(2.3799)(0.5306)$, where the household-specific intercept is accounted for by 0.2607. Subsequent (lag_2 and onwards) correlations decrease with the amount of time that passes between measurement occasions; that is, the covariance becomes a function of the lag and is estimated by $(0.2607)+(2.3799)(0.5306)(0.6506)^{lag}$.

5. Conclusion

This study used generalised linear mixed models to model electricity consumption of a typical household in eThekwini municipality. The Lognormal distribution was found to be best suited to model the electricity data and an ARMA(1,1) model was well suited to modelling within-household temporal variability. A key interest in this study was to investigate the presence of a seasonal effect in household electricity consumption. Initial data exploration suggested some form of seasonality was present, but it was difficult to distinguish. Further scrutiny of a variety of time plots suggested that there were two elements to the observed cyclical seasonal pattern: a monthly effect and a 12-month form of autocorrelation. To account for both aspects of the seasonality the most recent month of meter reading and 12 prior consumption values in the linear model were included. The inclusion of 12 prior values equated to including a household's three-year cycle of electricity consumption values. Dwelling type and a household-specific random intercept were also included in the linear model. The addition of a household-specific intercept improved the model's overall predictive capabilities, as it allowed for the capturing of some of the between-household variability.

To illustrate the effectiveness of the fitted model, predictions made using both the weighted GLMM and customary eThekwini Electricity estimation method were compared to actual monthly values. For the comparison 50 households were randomly selected and the most recent electricity consumption value that each selected household had from the data was removed, which became a desired value to predict for. Predictions were then made using both prediction methods, and to show which predictions were closest to actual monthly values, a spider graph was constructed (Figure 8), showing the absolute value of the relative errors as a percentage, for both the weighted GLMM and customary eThekwini Electricity method.

In Figure 8, the absolute value of the errors are represented by concentric circles, with the innermost circle representing the smallest error and the others showing increasingly large errors. The graph shows the weighted GLMM to be the method most closely centred in and around the inner circles, indicating that the GLMM is the better performing model, having the smallest errors across the selected households. This means that the GLMM has predictions that are close to the actual monthly consumption values for most households. The municipality's method results in the overall highest errors between predicted and observed values.

Two key findings of this study established a seasonal pattern in the prior consumption values and determined that winter is likely to see a rise in household electricity consumption. The pattern showed that, when modelling current electricity usage, a household's two most recent consumption values, and values 12, 24 and 36 months prior to the current value, are of particular importance out of all the prior values a household has, contributing the most to the prediction. This finding differs from that of the customary estimation method, in which the four most recent consumption values contribute most to the estimate. The model developed in this study provides insight into household consumption patterns as well as serving as the foundation for further studies on modelling and predicting electricity consumption at a household level. Further studies are required to find models that can adapt to less than ideal measurement circumstances that occur in

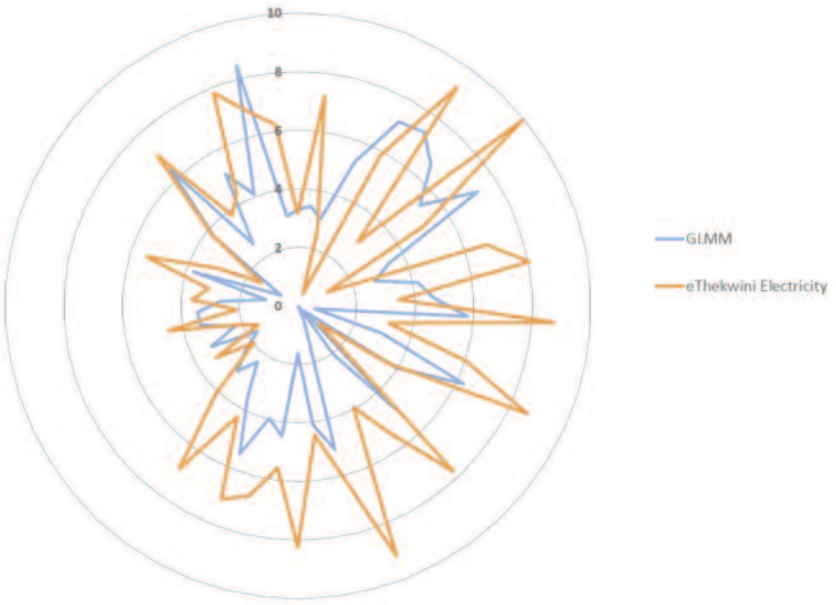

Figure 8: Spider graph showing the relative errors of each prediction method

the meter reading process, such as exceedingly long or unevenly spaced usage periods.

References

Athukorala, P. and Wilson, C. 2010. Estimating short and long-term residential demand for electrcity: New evidence from Sri Lanka. *Energy Economics* 32:34–40.

Chatfield, C. 2004. *The analysis of time series: An introduction.* 6th ed. Boca Raton, Florida, USA: Chapman & Hall/CRC.

Chikobvu, D. and Sigauke, C. 2013. Modelling influence of temperature on daily peak electricty demand in South Africa. *Journal of Energy in Southern Africa* 24(4): 63–70.

Dergiades, T. and Tsoulfidis, L. 2008. Estimating residential demand for electricity in the United States. *Energy Economics* 30: 2722–2730.

eThekwini Electricity. 2013. *2011/2012 Annual Report.* Available: www.durban.gov.za.

Firth, S., Lomas, K., Wright, A., and Wall, R. 2008. Identifying trends in the use of domestic appliances from household electricity consumption measurements. *Energy and Buildings* 40:926–936.

Holtedahl, P. & Joutz, F. 2004. Residential electricity demand in Taiwan. *Energy Economics* 26:201–224.

Inglesi, R. 2010. Aggregate electricity demand in South Africa: Conditional forecasts to 2030. *Applied Energy* 87:197-204.

Laird, N. M. and Ware, J. H. 1982. Random effects models for ongitudinal data. *Biometrics* 38:963–974.

Marvuglia, A. and Messineo, A. 2012. Using recurrent artificial neural networks to forecast household electricty consumtion. *Energy Procedia* 14:45-55.

Narayan, P. and Smyth, R. 2005. The residential demand for electricity in Australia: An application of the bounds testing approach to cointegration. *Energy Policy* 33:467–474.

Nelder, J. and Wedderburn, R. 1972. Generalized linear models. *Journal of the Royal Statistical Society Series A (General)* 135 (3):370–384.

Pouris, A. 1987. The price elasticity of electricity demand in South Africa. *Applied Economics* 19:1269–1277.

Sigauke, C. and Chikobvu, D. 2011. Prediction of daily peak electricity demand in South Africa using volatility forecasting models. *Energy Economics* 33: 882–888.

Yohanis, Y., Mondol, J., Wright, A. and Norton, B. 2008. Real-life energy use in the UK: How occupancy and dwelling characteristics affect domestic electricity use. *Energy and Buildings* 40:1053–1059.

Zewotir, T. (2008). Infinitesimal model perturbation influence in the linear mixed model. *South African Statistical Journal, 41*(2), 105-126.

Zewotir, T. and Galpin, J. (2004). The Behaviour of Normality Under Non-normality for Mixed Models. *South African Statistical Journal, 38*, 115-138.

Zewotir, T. and Galpin, J. (2006). Evalution of linear mixed model case deletion diagnostic tools by Monte Carlo simulation. *Communications in Statistics-Simulation and Computation, 35*(3), 645-682.

Ziramba, E. (2008). The demand for residential electricity in South Africa. *Energy Policy, 36*, 3460-3466.

Overview of predictive CSP spread prospects and its opportunities

Kai Timon Busse

Frank Dinter*

Solar Thermal Energy Research Group, Department of Mechanical and Mechatronic Engineering, University of Stellenbosch, Matieland 7602, South Africa

Abstract

An investigation was carried out to illustrate the prospects and challenges associated with implementation of concentrating solar power (CSP) with storage technology in South Africa. Various factors were examined that have an effect on the cost of CSP plants and offer an overall review of the opportunities CSP has for the country. This paper appeals the general idea that CSP is not cost effective enough and attempts to illustrate the feasibility of this technology in South Africa.

Keywords: concentrating solar power, South Africa, spread scenarios, storage technology

* *Corresponding author: Tel: +27 (0)21 808 4024*
Email frankdinter@sun.ac.za

1. Introduction

Through the last 20 years South Africa has faced numerous power supply problems, especially in late 2007 when there were several rolling power blackouts. As a result, South Africa's Department of Energy (DoE) published the Integrated Resource Plan 2010–30 (IRP) in March 2011, aiming to establish a mix of renewable energy supplies. The IRP attempts to promote steady progress towards an efficient and sustainable power supply for South Africa. The updated 2013 IRP proposed expanding the renewables section to meet nearly 25% of South Africa's energy demand by 2030.

In a first attempt to facilitate this energy supply shift, the DoE introduced the Renewable Energy Independent Power Producer Procurement (REIPPP) programme (Robb & Roberts, 2014), which allows individual bidders to bring their contribution by placing tariff bids on the energy supply objectives of the department. Despite strong support for this initiative as an economically reasonable means of promoting renewable energy in South Africa, this paper reviews the CSP capacity allocated within this framework. Sections 4, 5 and 6 illustrate the advantages of CSP over its energy supply competitors.

The IRP's ambitious modification of South Africa's electricity infrastructure may not be strictly perceived as a challenge, but could present an opportunity for the country, given its natural high solar radiation and the potential of such an innovative modification. Closer examination makes it obvious that a restructuring of the South African energy system is inevitable. Grobbelaar *et al.* (2014: 490) summarise the current situation well: 'CSP is a young technology and there is still space in the global market for South Africa to become involved in technology development and large-scale manufacturing.'

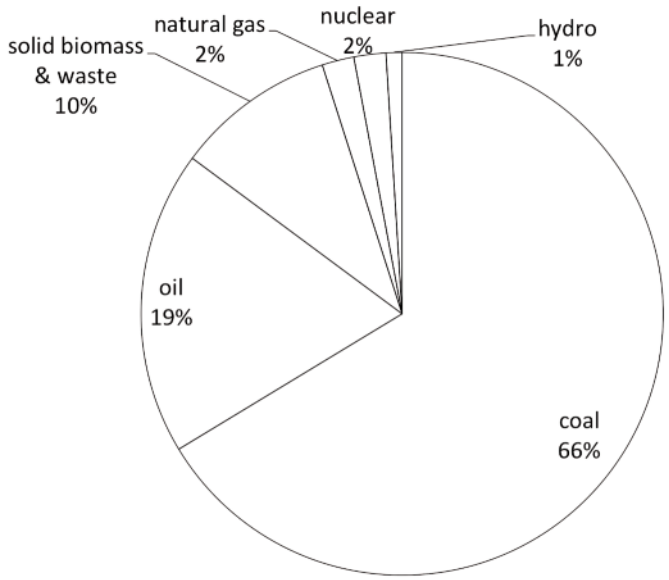

Figure 1: The South African energy mix 2013
Source: Adapted from BP (2013)

Figure 1 shows that the current energy mix in South Africa is dominated by coal. A large proportion of electricity is generated by means of oil used for peak power in open cycle gas turbines. In a scenario where South Africa tolerates fossil fuels, the cost of energy is likely to increase quickly because of decreasing fossil fuel reserves and rising prices. Scenarios envisaging an infrastructural rollout for natural gas imports were made in the updated IRP version (DoE, 2011; 2013a; 2013b). The Mozambican gasfields (Temane and Pande) could deliver what is believed to be a sustainable energy source, although carbon tax costs are likely to be a more pressing issue in the future. An insistence on conventional energy sources could result in dependency on other countries (with possible negative impacts, as in Ukraine, which is currently suffering from its dependency on Russian gas supplies). The consequences must therefore be properly considered, and a near-future turnaround is most desirable in order to acquire a solid position in the global renewable energy market.

In the updated IRP, the CSP is allocated only 1.3% of the generating capacity by the end of the planning period and not considered a suitable electricity source for the future construction of power plants (DoE, 2011; 2013a; 2013b). This is most likely a result of the current levelised cost of electricity (LCOE). At the moment the LCOE of CSP is much more expensive than other intermediate- or base-load energy supply technologies (e.g. ZAR2.0/kWh for a CSP plant (Nersa, 2011)). It is often forgotten, however, that solar technologies – and specifically CSP – offer numerous benefits for South Africa. Figure 2 illustrates typical demand curves for summer and winter days. For winter, the graph displays two power peaks, one in the morning and one in the evening, which reflect challenges associated with inadequate supply that are likely to result in higher power prices. To restore market balance it is necessary to provide a supply curve approximated to the demand, and in order to meet these power peaks, peak power plants (see Pegels, 2010) are required.

A conventional photovoltaic (PV) system generates electricity only while the sun is shining, making it impractical to meet the average electricity demand. During the evening peak, when most power is required, the power network is in need of a flexible and sustainable electricity source. Currently, peak demands are met by several open-cycle gas turbines (OCGTs) which make use of expensive electricity generation technologies with a LCOE up to ZAR 5/kWh. In 2014, Eskom was forced to spend ZAR 10.5 billion on diesel fuel to enable the OCGTs, which contributed 3621 GWh of the 230 938 GWh produced by the coal-heavy utility (Creamer, 2014). As part of an alternative solution to this problem, CSP could significantly contribute to South Africa's future energy mix.

2. Concentrating solar power technology

In contrast to photovoltaic or wind energy, CSP is able to store thermal energy (normally by means of liquid salt in a two-tank system), which can provide electricity after sunset. Concerning cost- and energy-efficiency aspects, thermal energy storage has an advantage over electrical, chemical or potential energy storage systems. Despite the technical experience with wind and PV plants, CSP is the only established energy source with an efficient combination of energy generation and energy storage (Viebahn et al., 2011). This uniqueness makes CSP potentially valuable for South Africa. Due to its capability to supply electricity when needed, it is possible to provide the necessary grid stability and

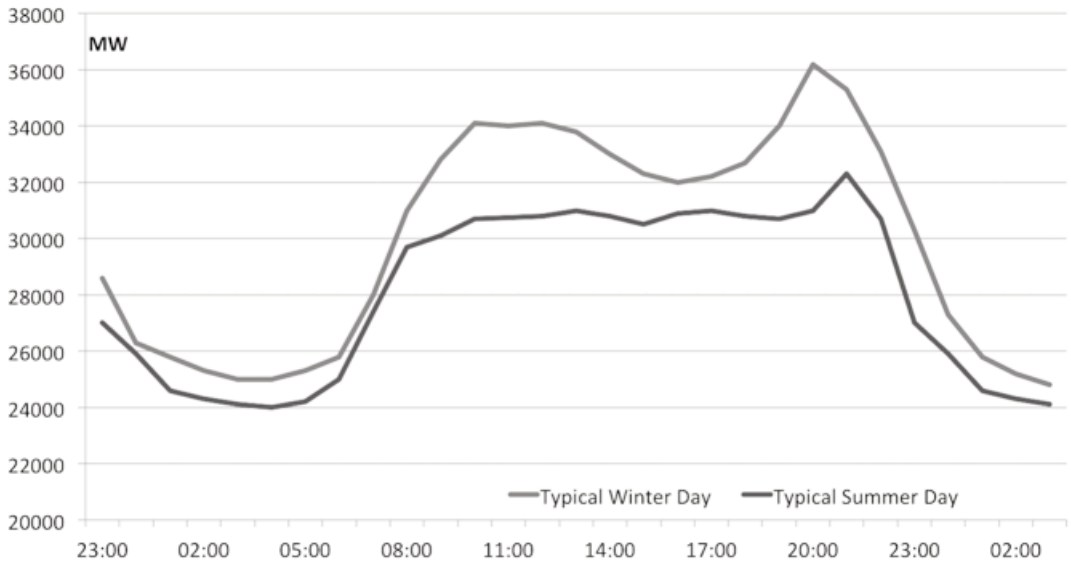

Figure 2: Demand of typical winter and summer days in South Africa
Source: Eskom (2014)

flexibility required to meet South Africa's peak demand. The dispatchable nature of the technology makes CSP preferable to other renewables.

A solar thermal power plant usually consists of three major components, namely the solar field, a conventional power block, and an energy storage system. The technology can be classified into two general types of CSPs: line-focus and point-focus.

2.1 Parabolic trough technology

Parabolic trough technology focuses sunlight on a receiver pipe (line-focus), which contains a heat transfer fluid. The fluid (usually oil) is used to generate power by means of a steam turbine or to heat up the thermal energy storage tank. Based on this technology, plants that operate with flat mirrors instead of parabolic troughs are being tested. This so-called Fresnel technology holds a further cost reduction potential, although its performance is far below the performance of parabolic troughs.

2.2 Solar towers

Solar towers use a large number of mirrors to concentrate the light beams onto a receiver (point-focus) positioned in the middle of the field. The heat transfer fluid flows through the receiver, where it is heated, and is used to either generate power or be stored inside the thermal energy storage tank. Both the line-focused and tower systems should be placed in an area with intense DNI and nearby grid connection. Each of the systems needs a substantial amount of water for steam circuit operation and for keeping the reflectors clean.

3. Geographic factors favouring CSP

South Africa offers some of the world's best areas of high irradiation, making solar energy, especially CSP with storage, a particularly fitting technology for the its electricity supply system. In Figure 3 the direct normal irradiation of South Africa is visualised and a grid map of high voltage lines is added (black lines). An area's DNI is directly linked to the amount of electricity a plant is able to deliver in that specific area. As a consequence, South Africa can provide more power with the same reflector size than other countries.

Judging by the DNI distribution, the northwestern region is highly suitable for CSP power plants. A DNI exceeding 2500 kWh/m^2 could result in a lower LCOE for plants located in this area.

There are, however, several other factors affecting the profitability of an energy source. The LCOE illustrates the cost-effectiveness of a certain power plant, expressed by Equation 1 (Hernández & Martínez, 2013).

$$LCOE = \frac{\sum_{t=1}^{n} \frac{I_t + M_t + F_t}{(1+r)^t}}{\sum_{t=1}^{n} \frac{E_t}{(1+r)^t}} \quad (1)$$

This mathematical approach contrasts the investment expenditures I_t, the operation and maintenance expenditures M_t and the fuel expenditures F_t to the electricity E_t generated over a certain time t, which represents the life-cycle time of a CSP plant.

At this point, for reasons of fairness, it has to be mentioned that issues have been raised about the validity of using LCOE as a comparison tool of different energy sources. Indeed, the LCOE does not consider the 'hidden benefits' of a project (European Solar Thermal Energy Association (ESTELA), 2016). These include factors like the lifetime of components, degradation of performance, impact of temperature on performance,

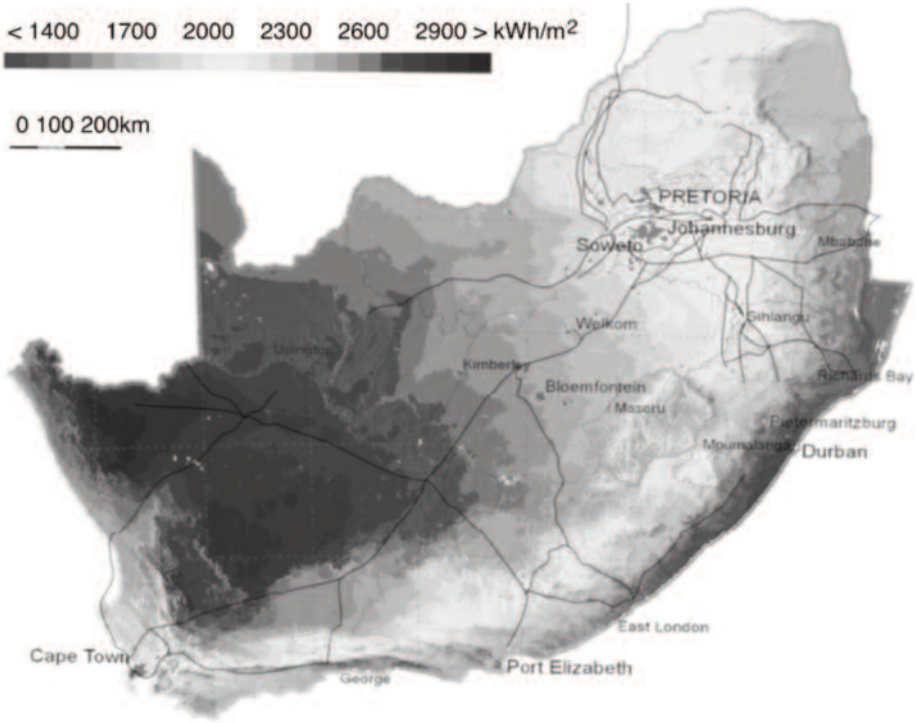

Figure 3: The DNI of South Africa with a shimmed grid map
Source: GeoModel Solar (2013)

losses in charging and discharging batteries and pumping stations. The present investigation accepts and promotes the cost-vs-value approach, as introduced in the ESTELA publication, for comparing energy production means. The LCOE is, however, a widely accepted measurement of the direct, production-associated costs a power plant generates. For this reason, the LCOE is used here as a valid metric of comparison, while the feasibility of a cost-vs-value approach in order to incorporate hidden benefits is explicitly highlighted. Concerning the allocation problem of CSP, the ratio of electricity production and its generation costs can help to determine suitable locations for plants. In order to reduce the LCOE, efforts are made to either reduce the investment, maintenance and fuel costs of a plant or increase its electricity generation. Increasing electricity supply can be achieved by providing the power plant with a high DNI level. The correlation between the DNI a CSP plant receives and the amount of power it produces is illustrated in Figure 4.

In order to establish the correlation between generated power and DNI, as seen in Figure 4, monthly average data was collected and projected for a whole year. The result is a disproportionately high relation between increasing DNI and generated power (see E_t in equation 1). As Figure 4 shows, the plant gains efficiency, which can be measured by Equation 2 at higher DNIs, where W_{out} defines the electricity output and W_{in} the irradiation input.

$$\eta = \frac{W_{out}}{W_{in}} \qquad (2)$$

To apply this with respect to LCOE, a suitable choice of location in a high DNI area will lead to a lower price of electricity, provided that costs remain constant. The high DNI of South Africa provides an opportunity that is almost unique, since smaller power plants are required to produce the same amount of power a bigger plant would produce in, for example, Europe (Fluri, 2009). In other words, fewer reflectors are needed for the same design output, which leads to a better LCOE.

Figure 5 shows the suitable areas where a high DNI level is combined with a good link to the grid. These locations are along several grid lines and are shown as white lines. High costs of grid expansion means that the first CSP plants should be placed close to an existing transmission line. Only when the technology is established in South Africa would enlarging the power system structure by means of grid expansion be an option. In summary, the white lines represent possible locations concerning only the DNI and grid connection factors.

Factors other than suitable grid lines and available water supply that can affect the LCOE include fuel costs (F_t in Equation 1 will be equal to zero in any location) as well as maintenance and investment expenditures, which are highly area-dependent.

Maintenance costs can be subdivided into manpower costs, equipment or service costs and water costs. Two main aspects are relevant here: the plant size that is most likely to affect the manpower and equipment/service costs, and the location of the plant, which has a relatively high impact on opera-

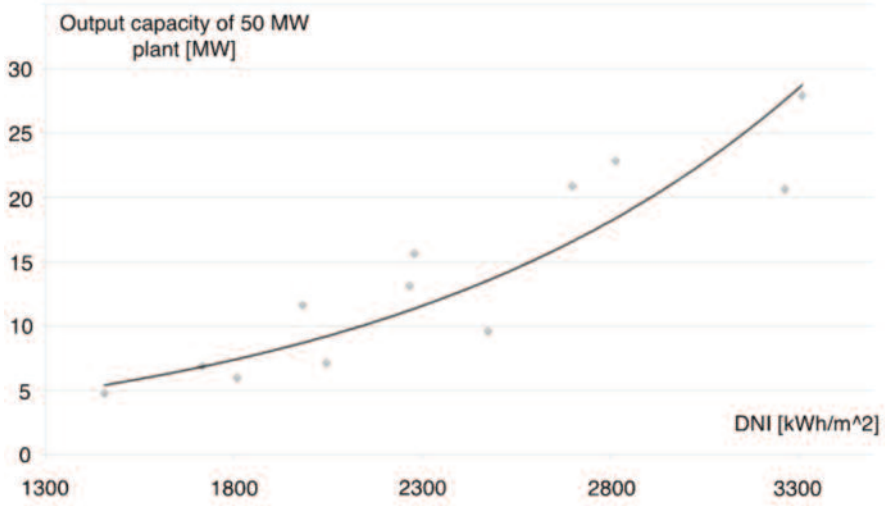

Figure 4: Correlation between generated power and DNI[1]
Source: Dinter et al. (2013)

tion and maintenance costs, on the basis of water availability (Braun, 2011). The demand for water to clean the reflectors and cool the generator turbine is approximately 2.9-3.6 m^3/MWh. Areas that combine grid connectivity with a good water supply are therefore most desirable for establishing CSP plant. In South Africa, not all rivers are perennial, so further research is needed here.

Another factor impacting the LCOE is investment cost, which is only partially influencable. In order to reduce these costs, CSP plants would be placed in an area with good infrastructure, including good transport routes, a solid basis of potential workers and operators, an almost level area to allow a stable foundation, and adequate accommodation. Furthermore, there should be no hills or mountains that could shade the reflectors and thus affect plant efficiency.

Figure 5 furthermore indicates possible plant locations in South Africa, taking into account the factors noted earlier. Locations are strongly based on solar irradiation, representing a first attempt (with the eastern part of the country excluded). More accurate analyses are required to exactly ascertain suitable CSP locations, taking into account Eskom's grid-expansion plans, political and social area-dependent discrepancies, local electricity demands and the global market situation.

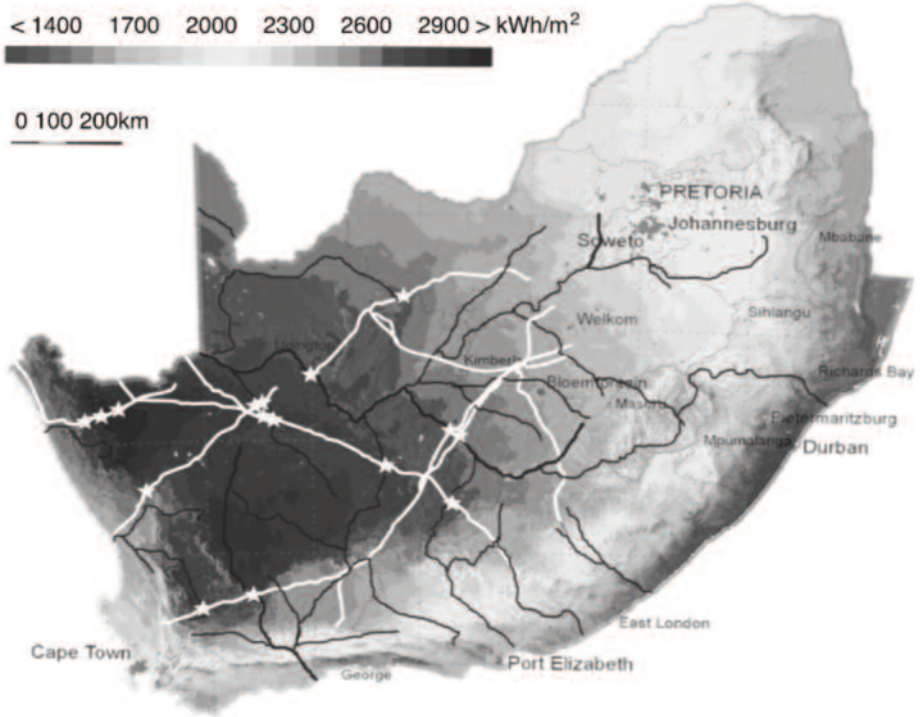

Figure 5: Map of South Africa's suitable grid lines (white) and available water supply (black) *Source: GeoModel Solar (2013)*

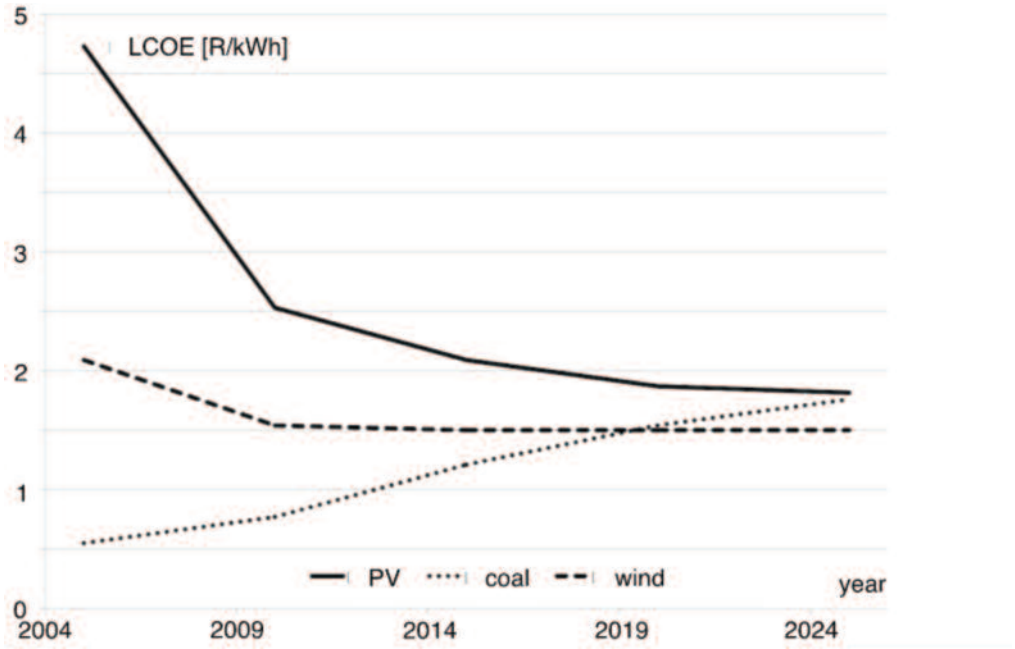

Figure 6: LCOE trends of coal, wind and PV
(Source: Balz et al., 2013)

4. Economic factors favouring CSP

Following an examination of the current situation and of possible locations of CSP plants, it is useful to turn to a consideration of future developments of CSP in South Africa, emphasising the question of whether, and to what extent, CSP could be integrated. Despite CSP still having a higher LCOE than most alternative energy sources, the present study suggests that CSP is set to become a major part of a future South African electricity system. Two aspects justify this view. Firstly, the choice of LCOE is not an instrument of actually comparing the means of energy production, but rather of highlighting the cost reduction potential of CSP. Secondly, the LCOE predictions shown in Figure 6 support the view of CSP as a feasible energy production alternative. The LCOE forecasts for the next ten years are based on several studies that analyse the cost behaviour of innovative technologies, as well as on the trend of fossil power resources. It illustrates the LCOE changes of CSP's main renewable-energy competitors: PV, wind and coal from 2004.

The wind curve is expected to be nearly constant in future because the technology is already at a later stage of maturity. The course of the PV curve is sufficiently representative of 'pioneer technologies', especially in the energy sector, showing a strong cost reduction within the first decade or so, followed by smaller price cuts until it reaches a continuous state prescribed by environmental factors, commodity prices and O&M costs. The wind energy sector has already reached that state.

The dimension of this price-decrease effect depends on the investment and the confidence associated with a specific technology. If the pioneer phase, which CSP is currently in, were followed by a strong adoption phase, it would lead to lower costs, given only a few investors. Many predictions of the LCOE trends of CSP have been made (e.g. Trieb et al, 2009 and Fawer et al, 2011), most of them leading to results similar to the average trend line in Figure 7.

The graph in Figure 7 is based on a DNI of 2500–3000 kWh/m^2. According to the Fraunhofer report studies, additional price cuts are motivated by the five essential cost-reduction potentials, which moreover represent current main research focuses:

1. *Learning effects* is an umbrella term for usual innovative advances. It includes improvement in efficiency and infrastructural upgrading, as well as the continuing education of workers and operators.
2. *Scale-up of component production* describes the procedure of settling and developing businesses, related to a specific technology. Series manufacturing and bigger production lines give cheaper component costs. Heliostats and reflectors, which make up 37% of the whole costs, are believed to profit especially from this effect.
3. *Substitution of oil* as heat transfer fluid by molten salt could lift the efficiency of a power plant by 12–13% due to the fact that a heat-exchanging device is no longer needed to store thermal energy. The salt itself is now heated in the receiver. Researchers are currently verifying various approaches on keeping constant pipe temperatures of >270 °C which would enable molten salt to act as a heat transfer fluid (having a melting point of 260 °C).
4. *Alternative thermal storage technologies* could lead to higher storage temperatures, which go hand in hand with higher energy density and

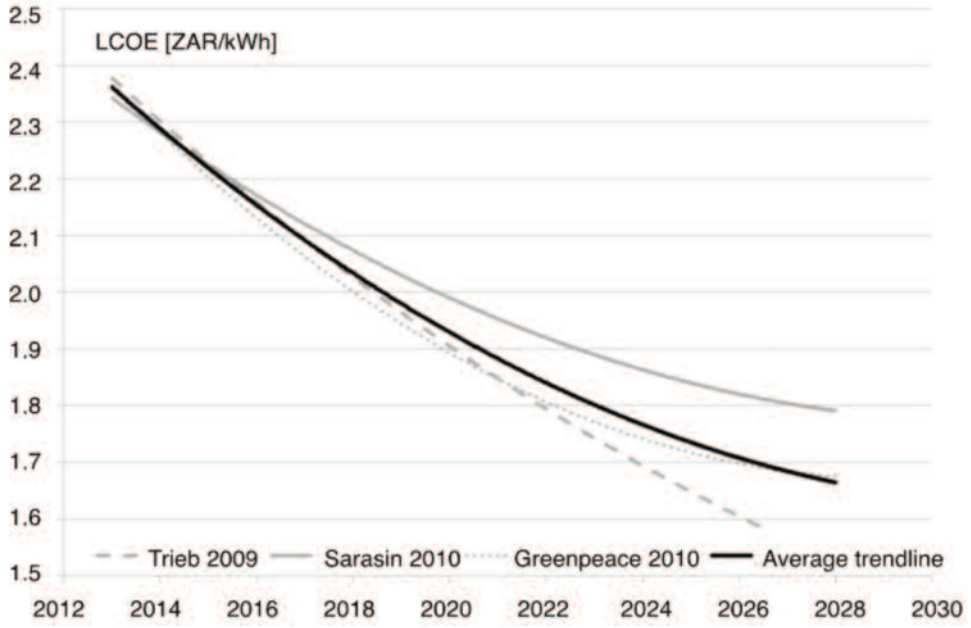

Figure 7: Predictive LCOE trend of CSP, assuming a parallel volume development of the technology
Source: Fraunhofer-Institut für solare Energiesysteme (2013)

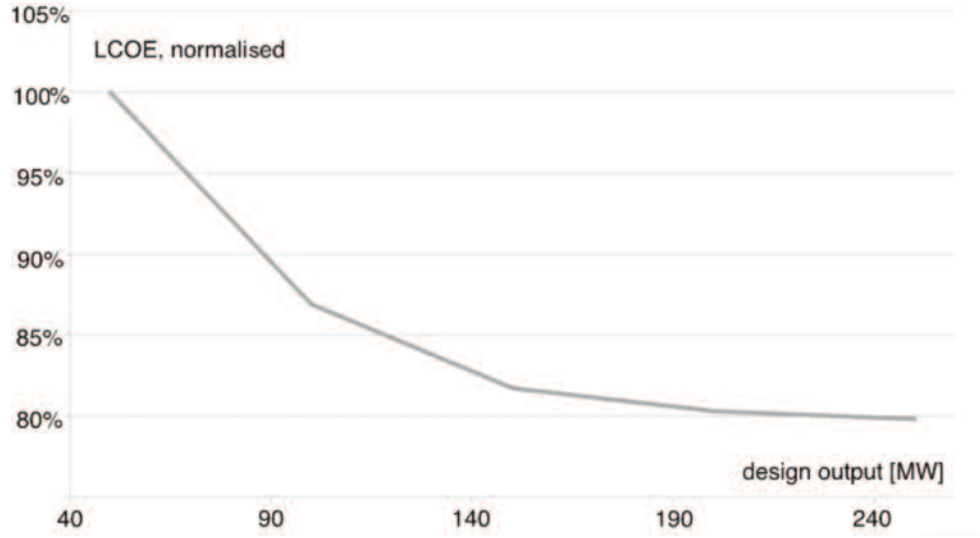

Figure 8: CSP LCOE as a function of design output
Source: CSP Today (2013)

better efficiency.

5. *Scale-up of plant size* is believed to lead to a LCOE decrease of up to 20% (Viebahn et al, 2011). As mentioned, a plant's design output has an influence on O&M costs, as well as investment expenditures. The costs decrease drastically, with increasing plant dimension, up to 150 MW, or even 250 MW, whereas the effect for bigger plants is not that remarkable. This is visualised in Figure 8. Reflector sizes especially are believed to have a big influence on LCOE values (CSP Today, 2013).

Fresnel technology should also be mentioned. Fresnel resorts to known line-focus technologies but features a significant difference in reflector designs. The light is concentrated onto the receiver pipe by several small mirror bars as opposed to one big parabolic trough. Each of these mirrors is tracked and entails the possibility to work with flat surface reflectors. Flat mirrors are about four times cheaper than curved ones, offering further cost reduction potential.

A rather pessimistic cost optimisation based on these parameters could lead to a LCOE projection as shown in Figure 9. It is clear that the LCOE is already beneath the current peak-load level in South Africa, making CSP a valuable energy source for morning and evening and an immediate alternative to OCGTs. The current renewable energy feed in tariff provides a ZAR 3.94 /kWh reward for electricity during peak hours, equal to 270% of the

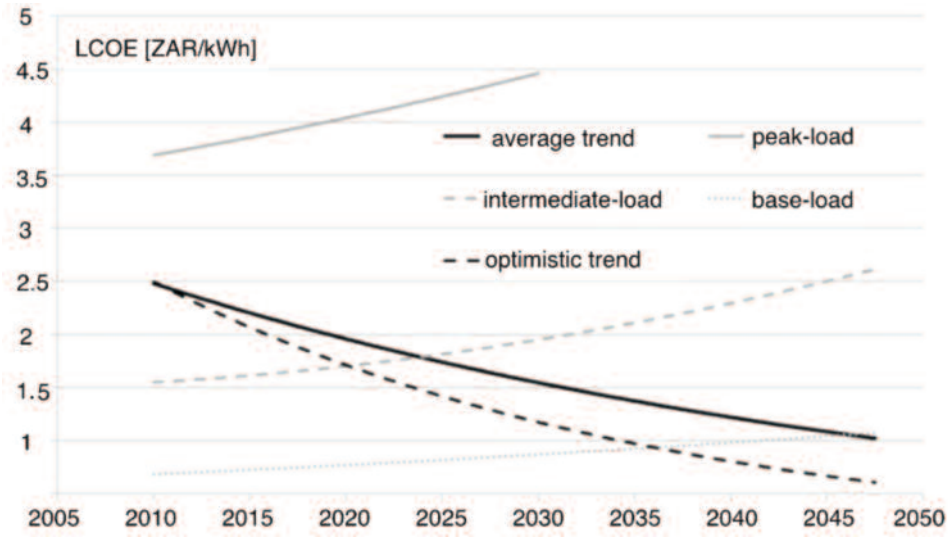

Figure 9: LCOE prediction
(Source: Silinga et al., 2013 and Müller-Steinhagen, 2013)

base-load tariff. This puts CSP in a unique position to benefit from a financial margin, since other renewables do not provide proper energy storage possibilities.

Furthermore, based on a conservative CSP LCOE trend shown in Figure 9, CSP will already match with the intermediate load around 2025. As mentioned above, this prognosis could be enhanced by an advanced adoption phase and result in lower CSP energy costs to a cost-benefit balance in 2020. The graph is partly based on a SolarPACES 2013 study (Silinga et al., 2013), which states that the current peaking LCOE shows a strong dependency on diesel costs. The LCOE of ZAR 3.69 /kWh is based on no increase in diesel costs. An increase of 5% would result in a LCOE > ZAR 10 /kWh. As can be seen, however, the gap between CSP and OCGT costs is1.4 /kWh, even for no increase in diesel costs. Therefore, based on Silinga et al., a peak supply turn-around towards CSP technology is the next logical step for South Africa's energy system.

The problem with the peak supply turn-around is that the LCOE will not necessarily operate as a reliable decision-making tool. Despite the advantage of LCOE, a decision in favour of CSP is accompanied by heavy investment expenditure. Comparatively, OCGTs have low investment costs, but higher O&M costs. In addition to this, there are adequate reasons to favour CSP with storage technology to meet peak demands. As mentioned before, independence from limited resources is a major aspect of this problem. It is impossible to exactly predict diesel fuel prices, although it is certain that costs will sooner or later rise. Assuming that South Africa decides to invest in CSP this will likely result in better LCOE values, due to the cost reduction effects mentioned above.

5. Conclusion

Given South Africa's peak demand, CSP with storage would have substantial benefits for the country's energy system and offer a good and reasonable solution to the problem, due to the system's ability to store energy and supply electricity on demand. Peak demands go hand in hand with high electricity costs, so CSP enables a financial tolerance not shared by other energy sources.

South Africa has one of the world's highest DNI values, providing many potential plant locations along the grid lines. Due to good conducting performances of the South African power grid, it is possible to transport electricity with a loss of only 3% per 1000 km (Oswald, 2010), reducing the impact on choice of location. It is desirable to have good water supply and suitable infrastructure close by, and there are numerous appropriate sites, especially in the northwest. The exact location of CSP plants holds a strong cost reduction potential and should therefore be further researched.

The efficiency of a power plant scales up with increasing capacity, and the number of plants built has a decreasing effect on the LCOE; simply put, the more plants built, the less expensive they will get. The bigger the present investment and confidence in this technology, the better it will develop from a financial perspective.

The locations shown in Figure 5 represent possible plant sites in the phase for meeting peak demand, due to their low financial risks. When CSP becomes a suitable alternative for meeting intermediate load, additional locations away from grid lines could be considered. Gauché et al. (2014) suggest an addition of 3 GW of CSP to South Africa's energy system and that the technology's significant benefits appear to vastly outweigh the risks'.

CSP would be an excellent addition to the South African energy system. Integration of this technolo-

gy in peaking plants would be a viable alternative to current OCGTs, and it even has the potential to serve on intermediate-load level within the next ten years. This opportunity should be pursued with the necessary confidence and patience.

Note

1. Data refers to the Andasol 3 parabolic trough power plant in Spain; design output: 50 MW; storage: salt, 7.5 hours.

References

Balz, M. & Rua, A.B. 2013. *From Moses Mabhida Stadium to solar power generation in South Africa*. Available: http://concentrating.sun.ac.za/wp-content/uploads/2013/12/Lecture-Markus-Balz.pdf [September 2014].

BP plc. 2013. *BP Statistical Review of World Energy June 2013*. Available: http://www.bp.com/content/dam/bp/pdf/statistical-review/statistical_review_of_world_energy_2013.pdf [September 2014].

Braun, B. 2011. Wirtschaftlichkeit solarthermischer Kraftwerke (CSP) am Beispiel Desertec-Projekt unter besonderer Berücksichtigung der Clean Deveopment Mechanism

Creamer, T. 2014. Eskom weighs gas options as diesel costs double to R 10.5bn. Available: http://www.engineeringnews.co.za/article/eskom-weighs-gas-options-as-diesel-costs-double-to-r105bn-2014-07-11 [August 2014].

Aalborg CSP, 2013. *Setting new standards for steam generation with Indian projects* Available from: http://www.aalborgcsp.com/news-events/newstitle/news/setting-new-standards-for-steam-generation-with-indian-projects/?tx_news_pi1[controller]=News&tx_news_pi1[action]=detail&cHash=5ce188e6c895d92500be351a68ad2cf4 Accessed 5 June 2016

Department of Energy. 2011. *Integrated resource plan for electricity (IRP): 2010–2030. Revision 2*. Available: http://www.DoE-irp.co.za/content/IRP2010_2030_Final_Report_20110325.pdf [July 2012].

Department of Energy. 2013a. *Integrated resource plan for electricity (IRP): 2010–2030. Update report 2013.* Available: http://www.DoE-irp.co.za/content/IRP2010_2030_Final_Report_20110325.pdf [December 2013].

Department of Energy. 2013b. Renewable Energy IPP Procurement Programme, Bid Window 3 Preferred Bidders' announcement, 4 November 2013. Available: http://www.record.org.za/resources/doc_download/79-department-of-energy-list-of-ipp-preferred-bidders-window-3-04nov2013.pdf [December 2013].

Dinter, F., & Gonzalez, D. M. (2013). Operability, reliability and economic benefits of CSP with thermal energy storage: first year of operation of ANDASOL 3. *Energy Procedia*, *49*, 2472-2481.

Eskom. 2014. State of the power system quarterly update 'pre-winter'. Available: http://www.eskom.co.za/OurCompany/MediaRoom/Documents/Quarterlysystemstatus25022014.pdf [September 2014].

European Solar Thermal Energy Association. 2016. The value of solar thermal electricity. Availabl: https://issuu.com/estelasolar/docs/estela_ste_value_final-single [May 2016].

Fluri, T. P. 2009. The potential of concentrating solar power in South Africa. *Energy Policy*, *37*(12):5075–5080.

Fraunhofer-Institut für solare Energiesysteme ISE. 2013. *Stromgehstehungskosten Erneuerbare Energien Studie November 2013*. Available: http://www.ise.fraunhofer.de/de/veroeffentlichungen/veroeffentlichungen-pdf-dateien/studien-und-konzeptpapiere/studie-stromgestehungskosten-erneuerbare-energien.pdf [September 2014].

Gauché, P., Brent, A.C. & Backström, T.W., 2014. Concentrating Solar Power: Improving electricity cost and security of supply, and other economic benefits. *Development Southern Africa* 31(5):692–710

GeoModel Solar. 2013. *SolarGIS Solar radiation maps.* Available: http://solargis.info/doc/87 [December 2013].

Grobbelaar, S., Brent, A.C. & Gauché, P. 2014. Developing a competitive concentrating solar power industry in South Africa: Current gaps and recommended next steps. *Development Southern Africa*. 21(3):475–493.

Hernández-Moro, J. & Martínez-Duart, J.M. 2013. Analytical model for solar PV and CSP electricity costs: Present LCOE values and their future evolution. *Renewable and Sustainable Energy Reviews* 20: 119-132.

Müller-Steinhagen, H. 2013. Concentrating solar thermal power. *Philosophical Transactions of the Royal Society of London A: Mathematical, Physical and Engineering Sciences*. doi: 10.1098/rsta.2011.0433.

National Energy Regulator of South Africa (NERSA). 2011. *Review of Renewable Energy Feed – In Tariffs (REFIT)*. Available: http://www.nersa.org.za/Admin/Document/Editor/file/Consultations/Electricity/Presentations/Focused%20Solar%20Power%20Generation%20(SPG).pdf Accessed 16 September 2014.

Oswald, B.R. 2010. Wirtschaftlichkeitsvergleich unterschiedlicher Übertragungstechniken im Höchstpannungsnetz anhand der 380kV-Leitung Wahle-Mecklar, Leibniz Universität Hannover, Hannover.

Pegels, A. 2010. Renewable energy in South Africa: Potentials, barriers and options for support. *Energy policy* 38(9):4945–4954.

Robb, G. & Roberts, S. 2014. Understanding economic regulation and competition in a developing economy: Introduction to special issue. *Journal of Economic and Financial Sciences: Special Issue 7(September)*:501–505.

Fawer, M., & Magyar, B. (2011). Solarwirtschaft: Hartes Marktumfeld–Kampf um die Spitzenplätze. *Bank Sarasin & Cie AG*.

Silinga, C.N. & Gauché, P. 2013. Scenarios for a South

African CSP peaking system in the short term. *Proceedings of Solar Power and Chemical Energy Systems conference (SolarPACES 2013), 17-20 September, Las Vegas, Nevada*:32-44.

Trieb, F., Schillings, C., O'Sullivan, M., Pregger, T., and Hoyer-Klick C., (2009). Global potential of concentrating solar power. *Solar Paces Conference, Berlin, Germany September 2009.*

Viebahn, P., Lechon, Y., & Trieb, F. (2011). The potential role of concentrated solar power (CSP) in Africa and Europe: A dynamic assessment of technology development, cost development and life cycle inventories until 2050. *Energy Policy*, *39*(8):4420–4430.

Synthesis of zirconia-based solid acid nanoparticles for fuel cell application

Rudzani A. Sigwadi[1]*

Sipho E. Mavundla[2]

Nosipho Moloto[3]

Touhami Mokrani[1]

1 *Department of Chemical Engineering, University of South Africa, Christian de Wet Road & Pioneer Avenue, FloridaPrivate Bag X6, Johannesburg 1710, South Africa*

2 *Department of Chemistry, University of Zululand, Private Bag x 1001, KwaDlangezwa, 3886, South Africa*

3 *Molecular Science Institute, School of Chemistry, University of the Witwatersrand, Private Bag 03, Wits 2050, Johannesburg, South Africa*

Abstract

Zirconia nanoparticles were prepared by the precipitation and ageing methods. The precipitation method was performed by adding ammonium solution to the aqueous solution of zirconium chloride at room temperature. The ageing method was performed by leaving the precipitate formed in the mother liquor in the glass beaker for 48 hours at ambient temperatures. The nanoparticles from both methods were further sulphated and phosphated to increase their acid sites. The materials prepared were characterised by X-ray diffraction (XRD), thermo-gravimetric analysis (TGA), Brunauer-Emmett-Teller (BET), transmission electron microscopy (TEM) and scanning electron microscopy (SEM) methods. The XRD results showed that the nanoparticles prepared by the precipitation method contained mixed phases of tetragonal and monoclinic phases, whereas the nanoparticles prepared by ageing method had only tetragonal phase. The TEM results showed that phosphated and sulphated zirconia nanoparticles obtained from the ageing method had a smaller particle size (10–12 nm) than the nanoparticles of approximately 25–30 nm prepared by precipitation only. The BET results showed that the ZrO_2 nanoparticles surface area increased from 32 to 72 m^2/g when aged.

Keywords: nanoparticles, precipitation, zirconium oxide, aging, monoclinic, tetragonal, phosphated zirconia, sulphated zirconia, pore volume, pore diameter

* *Corresponding author Tel : +27 (0)11 670 9462*
Email: sigwara@unisa.ac za

1. Introduction

In the last three decades there has been increased interest in alternative energy research, given that fossil fuels are not going to be with us forever. Among alternative energies, fuel cell technology is one of the most studied because of its potential use in automobiles, electronics and power plants (Wang et al., 2000). The interest in fuel cells has led to an extensive investigation of proton-conducting membranes (e.g. polymeric and organic/inorganic nanocomposite membrane) (Stoychev et al., 2000).

A proton-conducting membrane is the key component of a fuel cell system. Perfluorosulphonated membranes are widely used as proton conductors, including Nafion series (DuPont) with Nafion 117 as the preferred membrane for direct methanol fuel cells. Nafion is the state-of-the-art commercial membrane and performs well in a hydrated environment; its proton conductivity has a strong dependence on water content, but if it is not properly hydrated, proton conduction becomes slow (Zawodzinski, et al., 1995). At higher temperatures, the PEM will dehydrate and lose proton conductivity, and may result in irreversible mechanical damage. However, higher working temperatures are favourable for the kinetics of a platinum Pt catalyst and improve its tolerance to carbon monoxide poisoning (Costamagna et al., 2002). A Nafion membrane has an osmotic swelling problem and is also potentially dissolved in methanol solution when the methanol concentration and temperature are increased (Kleina, et al., 2005).

The efforts to improve membrane properties, e.g. increasing the working temperature above 100 °C, increasing water content and mechanical strength as well as organic and inorganic nanocom-

posite membranes are extensively investigated. Nanoparticles of metal oxides are used to modify a Nafion membrane in order to improve its water retention, thermal stability, proton conductivity and methanol permeability (Savadogo, 2004). It has been demonstrated that the incorporation of metal oxides in the form of nanoparticles improves water retention and the thermo-mechanical stability of the membranes (Savadogo, 2004). These modified Nafion nanocomposite membranes with inorganic nanoparticles have been designed to run at temperatures above 100 °C because higher temperature operation reduces the impact of carbon monoxide poisoning, allows attainment of high power density and reduces cathode flooding as water is produced as vapour (Hara and Miyayama, 2004).

Among metal oxides, zirconium oxide (ZrO_2) nanoparticles have been widely studied because of their high thermal and chemical stability, mechanical strength, chemical inertness, wear and corrosion resistance as well as high water retention (Ranjbar et al., 2012). The ZrO_2 nanoparticles can exist in a number of polymorphs at atmospheric pressure and are monoclinic, tetragonal and cubic (Navarra et al., 2008). The tetragonal phase of ZrO_2 nanoparticles is considered to be the one that is highly catalytic, with low thermal conductivity and thermal expansion coefficient compared with the others, rendering them suitable for use as oxide ion conductors in higher temperature sensors (Adjemian et al., 2006; Adjemian et al., 2002_a; Adjemian et al., 2002_b; Costamagna et al., 2002). This tetragonal ZrO_2 is also used as a catalyst and catalyst support for various gas phase reactions (Casciola et al., 2008; Jian-Hua et al., 2008).

One of the disadvantages of zirconium is its low surface area, acidity and conductivity. This problem can be solved by modifying zirconium nanoparticles with acids such as sulphates (Shao et al., 2006; Xu et al., 2005; Adamski et al.,2008; Mekhemer & Ismail, 2000; Jiao et al., 2003) and phosphates (Ray et al., 2000) to yield solid acids of a wide range of strengths. This acid-modified zirconia has been found to increase water retention, improve proton conductivity and reduce the methanol crossover in the membrane (Zhou et al., 2006; Bondars et al., 1995; Chuah et al., 2001) and be more stable than other solid super acids (Wang et al., 2006).

This aim of the current work is to modify zirconium nanoparticles in order to make them suitable as additives to Nafion membranes, by adding sulphates and phosphates and by also increasing their pore volume and surface area in order to increase water retention in the membrane.

2. Experimental methods

2.1. Reagents

Zirconium diammonium hydrogen phosphate ($(NH_4)_2HPO_4$), Zirconium oxychloride hydrate ($ZrOCl_2 .8H_2O$), silver nitrate ($AgNO_3$), sulphuric acid (H_2SO_4) and ammonia solution (NH_3) were purchased from Merck. All the chemicals were used as received.

2.2. Preparation of zirconium oxide by precipitation.

The ZrO_2 nanoparticles were prepared by the precipitation method; zirconium oxychloride hydrate ($ZrOCl_2.8H_2O$) and ammonia (NH_3) were used as starting materials. Zirconium hydroxide's precipitation ($Zr(OH)_4$) was obtained by adding an NH_3 aqueous solution drop-wise to the aqueous solution of 0.2M $ZrOCl_2.8H_2O$ at room temperature while vigorously stirring until the desired pH of 10 was reached. The precipitate was divided into two parts. The one part of the precipitate was washed with deionised water until the chlorine ions (Cl^-) were not detected by the silver nitrate ($AgNO_3$) test and filtered to obtain a wet powder of $Zr(OH)_4$. The wet powder was dried in an oven at 100 °C overnight. Zirconium oxide nanopowder was obtained through the calcination of the dried zirconium hydroxide at 600 °C for 6 hours.

2.3. Preparation of zirconium oxide by ageing method

The remaining part of the precipitate formed as described in Section 2.2 was aged in the mother liquor by leaving it in the glass beaker for 48 hours at ambient temperature. The precipitate was filtered, then washed and calcined according to the procedure described above.

2.4. Preparation of sulphated zirconia

Sulphated zirconia (S-ZrO_2) nanopowder was prepared by vigorously stirring the dried aged or un-aged ZrO_2 nanopowder obtained from section 2.2 and 2.3 in 0.5 M H_2SO_4 for 30 minutes at room temperature. The resulting solid was filtered and dried at 100 °C for 48 hours. The dried S-ZrO_2 nanopowder was then calcined at 600 °C for 2 hours and the resulting particles were ground to an ultra-fine powder using a mortar and pestle (Roberts et al, 2015).

2.5. Preparation of phosphated zirconia

The phosphated zirconia (P-ZrO_2) nanoparticles were prepared from aged and un-aged ZrO_2 nanoparticles (obtained as described in Sections 2.2 and 2.2) using diammonium hydrogen phosphate ($(NH_4)_2HPO_4$) solution. A portion of the ZrO_2 nanopowder was dissolved in an aqueous solution of $(NH_4)_2HPO_4$. The solution was stirred for 30 minutes using a magnetic stirrer at room temperature for 30 minutes. The P-ZrO_2 nanoparticle suspension obtained was filtered and dried at 100 °C for 48 hours, followed by calcining at 600 °C for 2

hours. The resulting particles were ground to an ultra-fine powder using a mortar and pestle.

3. Characterisation

The XRD analysis was performed using a Philips X-ray automated diffractometer with Cu K radiation source. The analysed material was finely grounded and homogenised. Samples were scanned in a continuous mode from 10–90° (2 theta) with a scanning rate of 0.026°/s. The thermal properties of the samples were studied by thermal gravimetric analysis (TGA) under nitrogen flow. The TGA experiment was carried out using Model 1500 Simultaneous Thermal Analyser (made by Rheometric Scientific limited, United Kingdom), in an inert atmosphere supplied by nitrogen gas at a heating rate of 10 °C/min from 50 °C to 1000 °C.

A BET surface area instrument (Micromeritics Accelerated SA and Porisimetry 2010 system) was used to determine information such as gas uptake, micropore volume (t–plot method), and pore size distribution from adsorption and desorption isotherms. In BET surface area analysis, a dry sample was evacuated of all gas and cooled to 77 K using liquid nitrogen. The particle size was calculated by using Equation 1.

$$S = \frac{6 \times 10^3}{\rho D_{BET}} \quad (1)$$

where ρ is the theoretical density of the materials which equal to 6.27 g/cm^3 (Parera, 1992) and D_{BET} is the particle size in nm.

The matrix surface and cross-section of the synthesised nanopowder morphology were investigated by means of SEM. Scanning electron microscope images were obtained on a Hitachi x650. This technique involves the interaction of the sample with electrons, which results in a secondary effect that is detected and measured. High-resolution transmission electron microscopy (HRTEM) was used to estimate their particle size and observe the morphology.

3. Results

3.1. The X-ray diffraction analysis of ZrO_2, S-ZrO_2 and P-ZrO_2 nanoparticles

Figure 1(i) shows the diffraction patterns of the (a) ZrO_2, (b) S-ZrO_2, and (c) P-ZrO_2 nanoparticles prepared without ageing. The crystallinity of materials in Figure 1(i) is evidenced by sharper diffraction peaks at respective diffraction angles. The XRD did not show any significant difference between ZrO_2 (Figure 1(i)(a)) and other modified ZrO_2 (Figure 1(i)(b) and Figure 1(i)(c)). All the samples exhibited the mixture of monoclinic and tetragonal phase. The major peaks appeared at 24.4°, 28.2°, 30.5°, 34.5° and 62.3° (2theta). The strongest diffraction peak of monoclinic structure which appeared at 28.2° (2theta) was due to the (111) plane, and the major peak for the tetragonal structure seen at 30.5° (2theta) was attributed to the (101) plane. The obtained structures are comparable to the JCPDS data (Card No.37-1484) (Jiao et al., 2003; Ray et al., 2000) for the monoclinic and standard JCPDS data (Card No.17-0923) (Zhou et al., 2006) for the tetragonal structure. Comparing the intensity of the monoclinic and tetragonal peaks shows that the monoclinic peaks are more intense than tetragonal peaks and it can be concluded that the samples contain more monoclinic structure than tetragonal.

The XRD patterns of the samples synthesised by aging method are shown in Figure 1(ii). All the samples showed similar diffraction patterns at 30.2°, 50.2° and 60.2° (2theta) which are characteristics of zirconium in a tetragonal phase and can be indexed to the standard pattern of the tetragonal phase of ZrO_2, which is in good agreement with reported data (JCPDS No.81-1544) (Chuah et al., 2001). The peaks at 30.2°, 50.2° and 60.2° correspond to the planes at 101, 112 and 211 respectively. These XRD patterns show that these materials are amorphous, as evident by peaks and humps. From these results it can be deduced that the slow ageing of samples favoured the tetragonal structure growth, the monoclinic peaks completely disap-

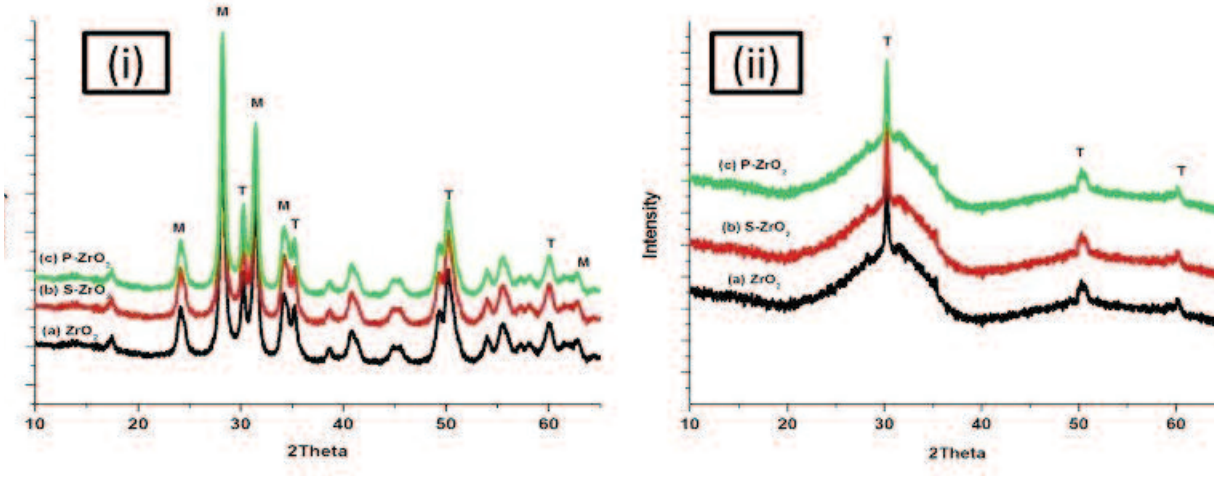

Figure 1: XRD patterns of (a) ZrO_2, (b) S-ZrO_2 and (c) P-ZrO_2 nanoparticles (i) un-aged and (ii) aged

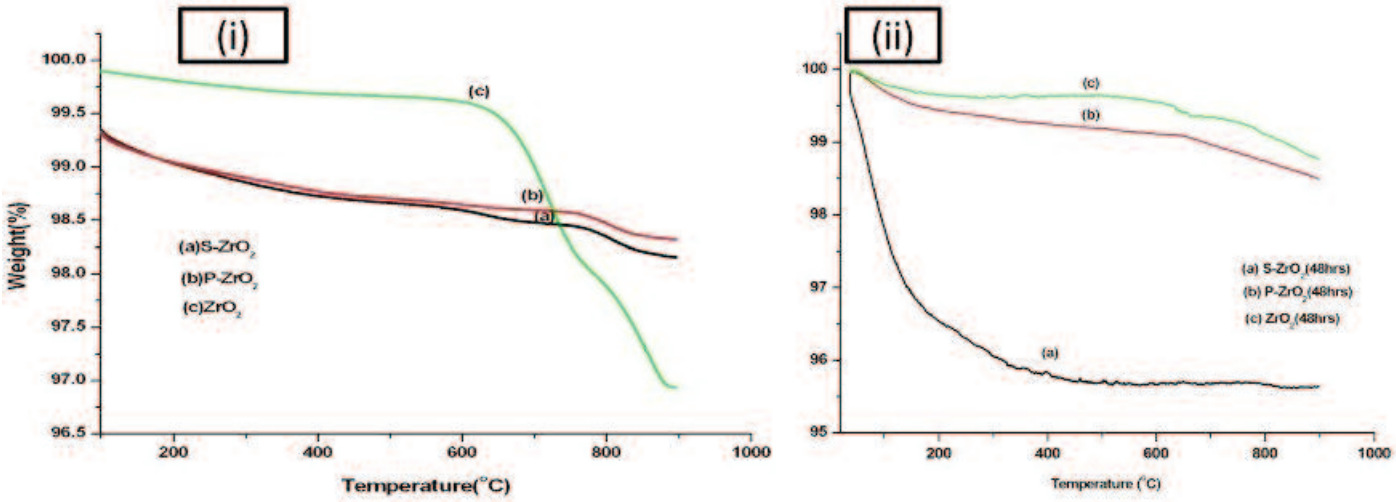

Figure 2: Thermogravimetric analysis of (a) S-ZrO_2, (b) P-ZrO_2 and (c) ZrO_2 nanoparticles (i) un-aged and (ii) aged

peared. This ageing method can be used for single phase zirconium at ambient temperature, whereas other researchers (Hsieh, 1996) find that the single phase can be achieved at temperatures of 950–1230 °C.

3.2. Powder thermo-gravimetric analysis

The ZrO_2, P-ZrO_2 and S-ZrO_2 nanopowder were evaluated by means of thermo-gravimetric analysis (TGA). Figure 2 indicates that the thermal decomposition process occurs in two weight-loss stages. The TGA curve in Figure 2(i)(a) indicates that the thermal decomposition occurs initially between 40 °C and 200 °C, with mass loss of 0.4 % associated to dehydration. The second stage of thermal decomposition is related to decomposition of sulphate and carbonaceous phase decomposition, respectively. The total weight loss of original material reaches about 3.2%. For the phosphated zirconia, Figure 2(i)(b) shows the initial weight loss from 20-300 °C, which can be attributed to the loss of moisture (Smitha et al., 2003). No further weight loss could be detected up to 900 °C, indicating the thermal stability of the phosphate species incorporated. The TGA curve 2(i)(c) indicates that pure ZrO_2 has little loss of its original weight on heating up to 600 °C. This may be due to the dehydration occurring through the loss of water molecules from adjacent -OH groups. Figure 2(ii) also shows two weights loss stages which are the same as in Figure 2(i) except that in Figure 2(ii) the weight losses are more stabilised.

3.3 Brunauer-Emmett-Teller

The BET specific surface areas of ZrO_2, S-ZrO_2 and P-ZrO_2 nanoparticles materials calcinated at 600 °C temperature are listed in Table 1 and Figure 3. The specific surface area of ZrO_2 nanoparticles materials was found to be 33 m^2/g which is larger than the 23 m^2/g obtained by Chuah et al. (1996). The specific surface area of ZrO_2 nanoparticles increased from 33 to 39 m^2/g when they were modified by sulphuric acid. This indicated that the presence of suphate strongly influences the surface acidity of ZrO_2 nanoparticles (Tanabe & Yamaguchi, 1994). Zirconia modified with sulphates exhibits superior catalytic activity. The presence of sulphates increas-

Table 1: BET surface area for ZrO_2, S-ZrO_2 and P-ZrO_2 nanoparticles calcinated at 600 °C

Samples	*BET surface area (m^2/g)*	*Particle size (nm)*	*Pore volume (cm^3/g)*
ZrO_2	33	29	0.08
S-ZrO_2	39	24	0.09
P-ZrO_2	37	26	0.07
ZrO_2(aged)	72	13	0.13
S-ZrO_2(aged)	79	12	0.16
P-ZrO_2(aged)	77	12	0.08

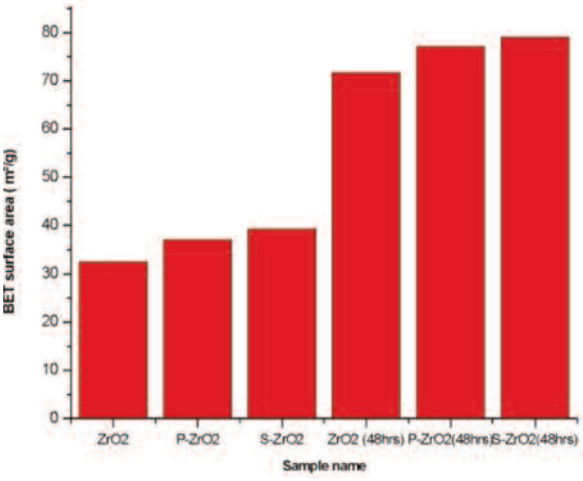

Figure 3: BET surface areas of the nanoparticles calcined at 600 °C

es the stability of zirconia as well as the content of the tetragonal crystal phase, which is the one believed to be catalytically active (Zarubica et al., 2009). It has been reported that S-ZrO_2 exhibited a Hammett acid strength H_0 of -16.03, whereas for 100% sulphuric acid it is only -11.99 and shows higher strength (Yadav & Nair, 1999). The modification with diammonium hydrogen phosphate acid also increases the specific surface areas to 37 m^2/g, which is high in comparison with unmodified ZrO_2, as has also been observed by other researchers (Abbattista et al., 1990). Figure 3 shows that the nanoparticles obtained from the ageing method had an enhanced specific surface area, which is necessary for the application of zirconia nanoparticles as catalyst support in fuel cells. The results show the specific surface area doubled when the aging method was used, going from 33 to 72, 39 to 79 and 37 to 77 m^2/g for ZrO_2, S-ZrO_2 and P-ZrO_2 respectively. Our results are in agreement with the results obtained by other researchers (Jakubus et al., 2003). This indicates that by aging ZrO_2 nanoparticles the surface area also increases, which make them suitable for fuel cell application. The particle size of nanoparticles was reduced by half when the ZrO_2 nanoparticles were aged. A slightly increase of pore volume was observed upon the sulphated zirconia with pore volume ranges of 0.09–0.16 cm^3/g when compared to the un-sulphated zirconia with pore volume ranges of 0.08–0.13 cm^3/g. These properties are good for the application of ZrO_2 in fuel cell membranes.

3.4. Scanning electron microscopy

Figure 4 shows SEM images of aged (Figure 4(a-c) and Figure 4(d-f) un-aged nanoparticles. It is observable that all nanoparticles are aggregated into clusters and their morphology is mostly spherical. This has also been observed elsewhere (Ranjbar et al., 2012; Lim et al., 2013). These nanoparticles are in the form of agglomerates but close inspection reveals that in Figure 4(b) and (c) they are less agglomerated than in Figure 4(a), which might be due to acid solutions in nanoparticles reducing their agglomeration. The aged nanoparticles are more agglomerated than un-aged ones. This might be due to their small size, which was a results of ageing. It was not possible to estimate the particle size, but it can be observed that agglomerates from aged nanoparticles are made up of clusters of smaller nanoparticles. This was confirmed by our BET results, which showed that the aged nanoparticles were half the size of unaged ones.

3.5. Transmission electron microscopy

The morphology and size information of the ZrO_2 nanoparticles was further investigated by TEM

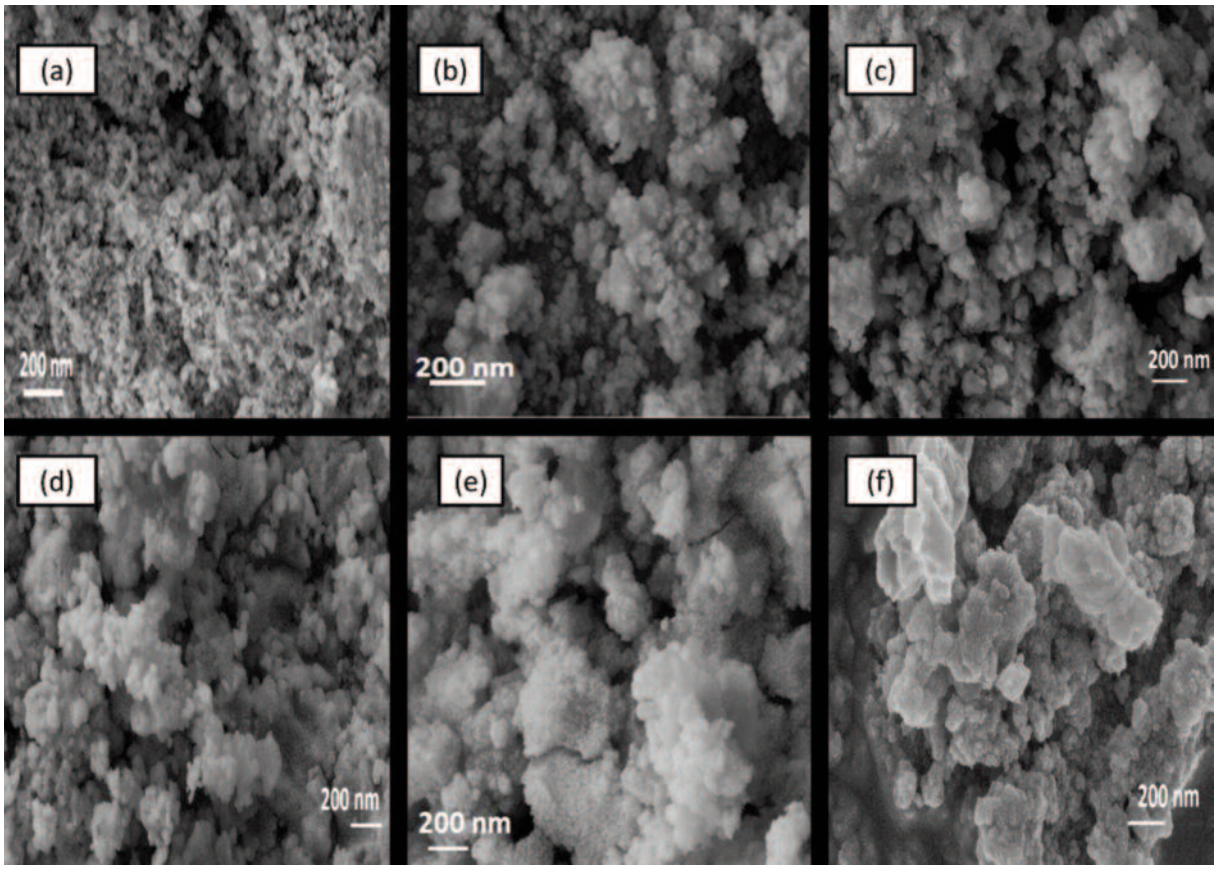

Figure 4: SEM images of (a) ZrO_2, (b) S-ZrO_2 and (c) P-ZrO_2 un-aged nanoparticles and their respective aged nanoparticles (d) ZrO_2, (e) S-ZrO_2 and (f) P-ZrO_2

analysis (see Figure 5). All nanoparticles exhibited a spherical morphology with a particle size diameter which is narrowly dispersed. The un-aged nanoparticles have a particle size distribution of 20–30 nm. The aged nanoparticles had a particle size of 10–13 nm. These results are in agreement with the BET results. Figure 5 (g-i) shows that the nanoparticles are crystalline, which was also confirmed by XRD results.

4. Conclusion

The ZrO_2 nanoparticles were successfully synthesised with varying sizes. The ageing method shows that the single phase of ZrO_2 nanoparticles can be obtained by a simple ageing method at ambient temperatures, which will reduce costs, given that previous researchers have synthesised this single phase at temperatures above 950 °C. This tetragonal phase is useful in catalysis and makes these nanoparticles suitable for use in the Nafion membranes used in fuel cells. The sulphated and phosphated ZrO_2 has been found by other researchers to be suitable for the fuel cell membrane due to their acidic sites. The nanoparticles produced in this work had large pore volume and smaller particle size, which is also useful in fuel cell membrane due to their high capacity for water retention. The ageing method has shown that it is possible to produce small particle size with a higher surface area and single phase (tetragonal) zirconia which is suitable in the fuel cell membrane application.

Acknowledgements

The authors thank Dr James Wesley-Smith for the SEM and TEM results. The financial support of the National Research Foundation, the University of the Witwatersrand, and the Council for Scientific and Industrial Research is acknowledged.

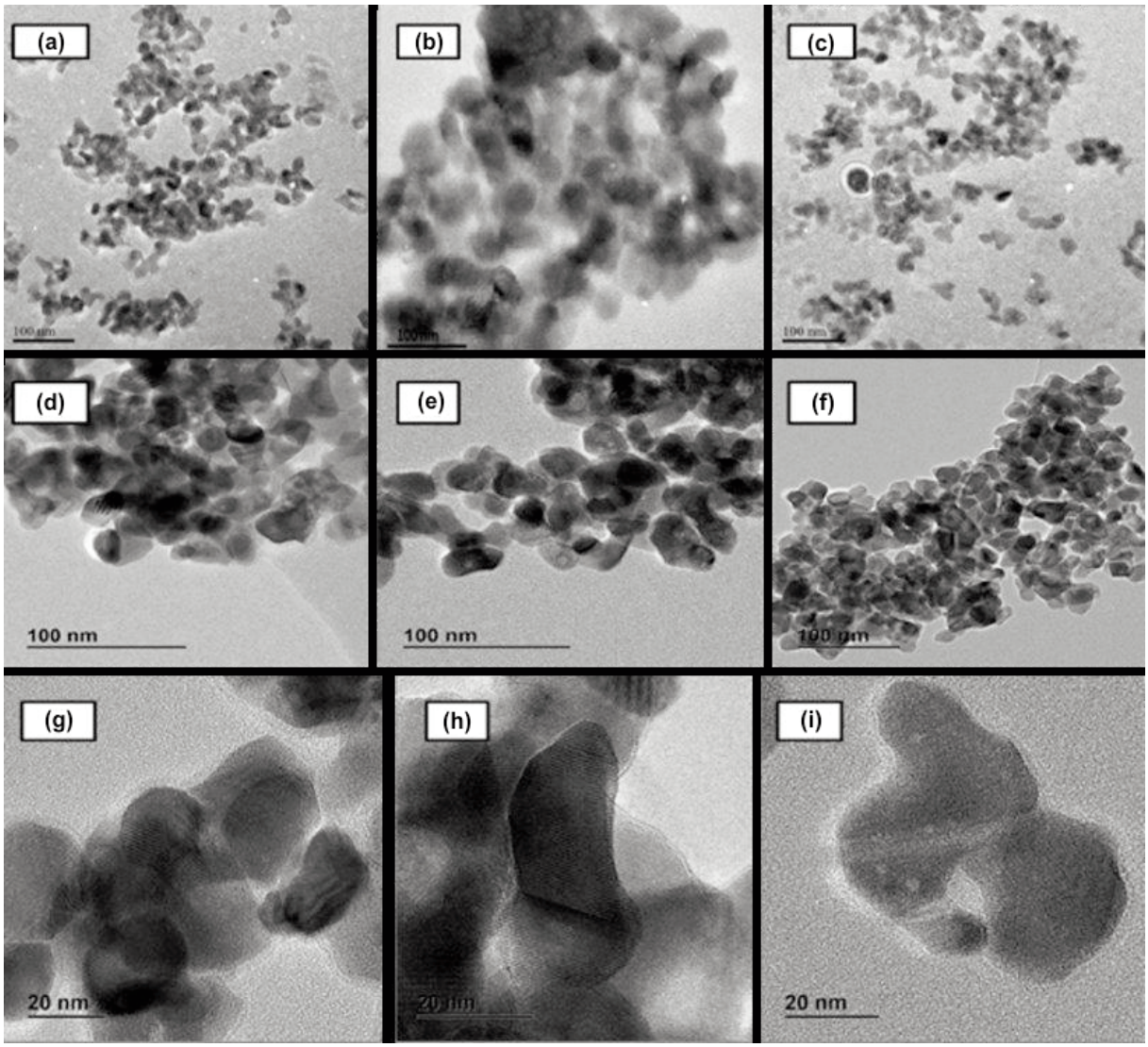

Figure 5: TEM images of (a) ZrO_2, (b) S-ZrO_2 and (c) P-ZrO_2 un-aged nanoparticles and their respective aged nanoparticles (d) ZrO_2, (e) S-ZrO_2, (f) P-ZrO_2 (g) ZrO_2, (h) S-ZrO_2 and (i) P-ZrO_2

References

Abbattista, F., Delastro, A., Gozzelino, G., Mazza, D., Vallino, M., Busca, G. and Lorenzelli, V. 1990. Effect of phosphate ions on the surface chemistry and microstructure of amorphous alumina. *Journal of the Chemical Society*, *Faraday Transactions* 86:3653–3658.

Adamski, A., Jakubus P., Zolka, Z. 2008. Structural and textural evolution of zirconia nanocrystals induced by thermal treatment. *Material science – Poland* 26:273-380.

Adjemian, K. T., Lee, S. J., Srinivasan, S., Benziger, J. and Bocarsly, A. B. 2002_a. Silicon oxide Nafion composite membranes for proton-exchange membrane fuel cell operation at 80–140°C. *Journal of the Electrochemical Society* 149:A256–A261.

Adjemian, K. T., Srinivasan, S., Benziger, J. and Bocarsly, A. B. 2002_b. Investigation of PEMFC operation above 100 °C employing perfluorosulfonic acid silicon oxide composite membranes. *Journal of Power Sources* 109:356–364.

Adjemian, K. T., Dominey, R., Krishnan, L., Ota, H., Majsztrik, P., Zhang, T., Mann, J., Kirby, B., Gatto, L., Velo-Simpson, M., Leahy, J., Srinivasant, S., Benziger, J. B. and Bocarsly, A. B. 2006. Function and characterization of metal oxide-Nafion composite membranes for elevated-temperature H_2O_2 PEM fuel cells. *Chemistry of Materials* 18:2238–2248.

Bondars, B., Heidemane, G., Grabis, J., Laschke, K., Boyesen, H., Schneider, J. and Frey, F. 1995. Powder diffraction investigations of plasma sprayed zirconia. *Journal of Material Science* 30:1621–1625.

Casciola, M., Capitani, D., Comite, A., Donnadio, A., Frittella, V., Pica, M., Sganappa, M. and Varzi, A. 2008. Nafion-zirconium phosphate nanocomposite membranes with high filler loadings: conductivity and mechanical properties. *Fuel Cells* 8: 217–224.

Costamagna, P., Yang, C., Bocarsly, A. B. and Srinivasan, S. 2002. Nafion® 115/zirconium phosphate composite membranes for operation of PEMFCs above 100 °C, *Electrochimica Acta* 47:1023–1033.

Chuah, G. K., Jaenike, S., Cheong, S. A. and Chan, K. S. 1996. The influence of preparation conditions on the surface area of zirconia. *Applied Catalysis A: General* 145: 267–284.

Chuah, G. K., Liu, S. H., Jaenicke, S. and Harrison, L. J. 2001. Cyclisation of citronellal to isopulegol catalysed by hydrous zirconia and other solid acids. *Journal of catalysis* 200: 352–359.

Hara, S. and Miyayama, M. 2004. Proton conductivity of superacidic sulfated zirconia. *Solid State Ionics* 168: 111–116.

Hsieh, H. P. 1996. *Inorganic membranes for separation and reaction*, Amsterdam: Elsevier.

Jakubus, P., Adamski, A., Kurzawa, M. and Sojka, Z. 2003. Texture of zirconia obtained by forced hydrolysis of $ZrOCl_2$ solutions. *Journal of Thermal Analysis and Calorimetry* 72:299–310.

Jian-Hua, T. Peng-Fei, G. Zhi-yuan, Z., Wen-hui, L. and Zhong-qiang, S. 2008. Preparation and performance evaluation of a Nafion-TiO_2 composite membrane for PEMFCs. *International Journal of Hydrogen Energy* 33:5686–5690.

Jiao, X., Chen, D. and Xiao, L. 2003. Effects of organic additives on hydrothermal zirconia nanocrystallites. *Journal of Crystal Growth* 258:158–162.

Lim, H. S., Ahmad, A. and Hamzah, H. 2013. Synthesis of zirconium oxide nanoparticle by sol–gel technique. *AIP Conference Proceeding* 1571: 812–816.

Kleina, L. C., Daikoa, Y., Aparicio, M. and Damay, F. 2005. Methods for modifying proton exchange membranes using the sol–gel process. *Polymer* 46: 4504–4509.

Mekhemer, G.A.H. and Ismail, H.M. 2000. Structure analysis of phosphated zirconia catalysts using XRD and nitrogen adsorption methods. *Colloids and Surfaces A: Physicochemical and Engineering Aspects*, 164:227–235.

Navarra, M. A., Abbati, C. and Scrosati, B. 2008 Properties and fuel cell performance of a Nafion–based, sulfated zirconia–added, composite membrane. *Journal of Power Sources* 183:109–113.

Parera, J. M. 1992. Promotion of zirconia acidity by addition of sulfate ion. *Catalysis Today* 15:481–490.

Ray, J.C., Pati, R.K. and Pramanik, P. 2000. Chemical synthesis and structural characterization of nanocrystalline powders of pure zirconia and yttria stabilized zirconia YSZ. *Journal of the European Ceramic Society* 20:1289–1295.

Ranjbar, M., Yousefi, M., Lahooti, M. and Malekzadeh, A. 2012. Preparation and characterization of tetragonal zirconium oxide nanocrystals from isophthalic icid–zirconiumIV nanocomposite as a new precursor. *International Journal of Nanoscience and Nanotechnology* 8: 191–196.

Roberts, M. J., Everson, R. C., Domazetis, G., Neomagus, H. W. J. P., Jones, J. M., Van Sittert, C. G. C. E., et al. Mathews, J. P., Density functional theory molecular modelling and experimental particle kinetics for CO2–char gasification. Carbon, 2015. 93(0): p. 295–314.

Roberts M. J., Everson R. C. , Neomagus H.W.J.P., Van Niekerk D. , Mathews J. P., Branken D. J. (2015) Influence of maceral composition on the structure, properties and behaviour of chars derived from South African coals. *Fuel* 142: 9–20.

Savadogo, O. 2004. Emerging membranes for electrochemical systems: Part II. High temperature composite membranes for polymer electrolyte fuel cell (PEFC) applications. *Journal of Power Sources* 127:135–161.

Shao, Z., Xu, H., Li, M. and Hsing, I. 2006. Hybrid Nafion–inorganic oxides membrane doped with heteropolyacids for high temperature operation of proton exchange membrane fuel cell. *Solid State Ionics* 177:779–785.

Smitha, V. K., Suja, H., Jacob, J., Sugunan, S. 2003. Surface properties and catalytic activity of phosphate modified zirconia. *Indian Journal of Chemistry* 42A:300–304.

Setare, E., Raeissi, K., Golozar, M. A. and Fathi, M. H. 2009. The structure and corrosion barrier performance of nanocrystalline zirconia electrodeposited coating. *Corrosion Science* 51:1802–1808.

Stoychev, D., Ikonomov, J., Robinson, K., Stefanov, P., Stoycheva, M. and Marinova, Ts. 2000. Surface modification of porous zirconia layers by electrochemical deposition of small amounts of Cu or Co and Co^{+} Cu. *Surface and Interface Analysis* 30:69–73.

Tanabe, K. and Yamaguchi, T. 1994. Acid–base bifunctional catalysis by ZrO_2 and its mixed oxides. *Catalysis Today* 20:185–197.

Wang, S. F., Gu, F., Lü, M. K., Yang, Z. S., Zhou, G .J., Zhang, H. P., Zhou, Y. Y. and Wang, S. M. 2006. Structure evolution and photoluminescence properties of ZrO_2:Eu^{3+} nanocrystals. *Optical Materials* 28:1222–1226.

Wang, W., Guo, H. T., Gao, J. P, Dong, X. H. and Qin, Q. X. 2000. XPS, UPS and ESR studies on the interfacial interaction in Ni–ZrO_2 composite plating. *Journal of Material Science* 35:1495–1499.

Xu, W., Lu, T., Liu, C. and Xing, W. 2005. Low methanol permeable composite Nafion/ silica/ PWA membranes for low temperature direct methanol fuel cells. *Electrochimica Acta* 50:3280–3285.

Yadav, G. D. and Nair, J. 1999. Sulfated zirconia and its modified versions as promising catalysts for industrial processes. *Microporous and Mesoporous Materials* 33:1–48.

Zarubica, A., Jovic, B., Nikolic, A., Putanov, P. and Boskovic, G. 2009. Temperature imposed textural and surface synergism affecting the isomerization activity of sulfated zirconia catalysts. *Journal of the Serbian Chemical Society* 12:1429–1442.

Zawodzinski, T.A., Davey, J., Valerio, J. and Gottesfeld, S. 1995. The water content dependence of electro–osmotic drag in proton–conducting polymer electrolytes. *Electrochemica Acta* 40:297–302.

Zhou, L., Xu, J., Li, X. and Wang, F. 2006. Metal oxide nanoparticles from inorganic sources via a simple and general method. *Materials Chemistry and Physics* 97:137–142.

A life cycle assessment of e-books and printed books in South Africa

Vinesh Naicker

Brett Cohen*

Energy Research Centre, University of Cape Town, Private Bag X3, Rondebosch 7701, South Africa

Abstract

This paper presents the results of a study comparing the life cycle environmental impacts and cumulative energy demands of reading printed books (print system) with those of reading e-books from an Apple Air iPad (digital system), with a specific focus on production of books and use of both options in South Africa. The two systems were compared using the ReCiPe midpoint and cumulative energy demand methods. The findings, which are consistent with international findings, demonstrate that the print system has lower impacts than the digital system in the impact categories of freshwater eutrophication, freshwater ecotoxicity, marine ecotoxicity and metal depletion, whilst the digital system has lower impacts in the categories of climate change, ozone depletion, terrestrial acidification, marine eutrophication, human toxicity, photochemical oxidant formation, particulate matter formation, terrestrial ecotoxicity, ionising radiation, agricultural land occupation, urban land occupation, natural land transformation, water depletion and fossil depletion. The major processes contributing to energy demand and environmental impacts of the print system were paper production and printing. For the digital system the major contributing processes were the production of the iPad and e-book reading. Coal-based electricity and coal-mining-related activities featured prominently in both systems, affecting environmental impacts and energy demand of products and services in South Africa. A change in the electricity mix to be less coal-intensive reduced the impacts of both systems. Finally, the products demonstrate that relatively few additional readers result in printed books becoming preferable to e-books in almost all impact categories, suggesting the need to consider housing print books in libraries to reduce their relative environmental impacts.

Keywords: cumulative energy demand, digital books, print books, life cycle assessment.

**Corresponding author: Tel +27 (0)72 434 2208; Email: brett@tgh.co.za*

1. Introduction

A number of studies around the world have compared the environmental impacts of print media systems with those of digital media systems offering the same services, including those by Kozak (2003), Gard and Keoleian (2003), Enroth (2009), Moberg et al. (2011) and Achachlouei et al. (2013). No similar analyses have, however, been made in South Africa. This paper presents the results of a study that was conducted to determine whether international results are also relevant in the South African context. The work sought to answer three key questions, being:

1. Is it environmentally preferable to read e-books from an iPad or printed books?
2. What is the impact of the future South African electricity mix on both systems, in terms of environmental impacts and cumulative energy demand?
3. What is the effect of multiple users on the environmental impact and cumulative energy demand on both systems?

The remainder of the paper presents details of the approach and key findings, following the ISO 14040 LCA Principles and framework structure (ISO, 2006). The results are compared to the findings of previous studies throughout the paper.

2. Scope

2.1 Introduction

The print and digital systems were compared to each other using life cycle assessment (LCA). LCA is defined as 'an objective process to evaluate the environmental burdens associated with a product, process, or activity by identifying energy and materials used and wastes released to the environment, and to evaluate and implement opportunities to effect environmental improvements' (ISO, 2006).

2.2 LCA methodology

The LCA methodology is built around four major components (Wolf et al., 2012): goal definition and scope; inventory analysis; impact assessment; and interpretation. The methodology is illustrated in Figure 1, which shows the iterative process as indicated by the bi-directional arrows.

2.3 Goal definition

2.3.1 Base case

The purpose of this study is to compare the environmental impacts and cumulative energy demand of 21 university textbooks read as e-books on a digital system with those associated with the same books read in print in South Africa. This figure represents the total number of books required for a four-year commerce degree at a local university. The initial hypothesis was that reading 21 e-books from an iPad has a smaller environmental impact and cumulative energy demand than reading 21 printed books.

2.3.2. Changing the electricity supply mix

This study also serves to investigate the effect that changing the energy mix and increasing the number of users per book has on the results. It was hypothesised that changing the electricity mix to one that includes more nuclear and renewable energy will reduce the differential between the print system and digital system in all of the impact categories considered. The Integrated Resource Plan (IRP) developed in 2010 by the Department of Energy (DOE) forms the planning framework for the installed power production plant capacity in South Africa (DOE, 2011). Several scenarios were developed in the IRP for the period between 2010 and 2030 which assess the impact of installing renewable and non-renewable energy technologies on the price of electricity and the associated greenhouse gas emissions. The 'policy-adjusted IRP' scenario was used to determine how the digital and print systems are impacted by a change in the electricity grid mix.

2.3.3 Impact of multiple readers

If the number of readers per product increases, impacts could either increase or decrease as a multiple of the number of users. The change in impacts may apply to either stages of the life cycle or the entire life cycle, depending on the exchange between users. The print system impacts will decrease with each additional user. The digital system impacts will decrease with each additional user for all stages, except in the reading stage, where additional energy is expended per user to charge the iPad for reading e-books. The third set of analyses was run to determine the impact of multiple readers on the results.

2.4 System boundary and inventory data

2.4.1 Print system

The life cycle of the paper book consists of the following stages:

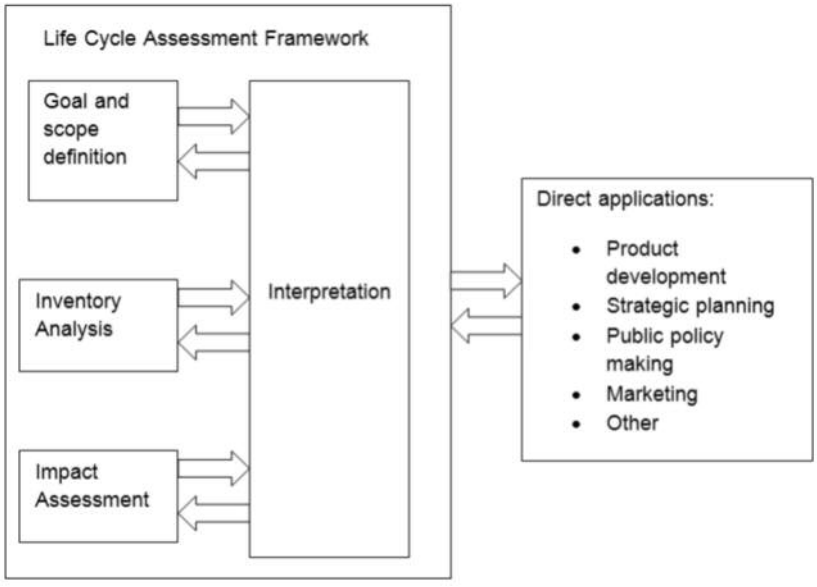

Figure 1: Life cycle assessment phases
(ISO 14040, 2006)

- pulp wood production;
- pulp wood transportation;
- pulp and paper production;
- paper transportation;
- printing;
- personal transportation;
- printed paper book use; and
- waste management.

The system boundary is illustrated in Figure 2. The associated inventory data is shown in Table 1, with the assumptions that underpin this data being presented in the sections that follow.

Pulp wood production

Hardwood is the main feedstock used for writing and printing paper grade in South Africa (Sappi, 2012). It is assumed that the processes used in the production of hardwood in South Africa are equivalent to those used internationally, and hence international data is used in the study.

Pulp wood transportation

Once the wood is harvested it is assumed to be transported a nominal 110 km (Chamberlain et al., 2005) to the pulp and paper mill.

Pulp and paper production

It is assumed that all printed books are made using paper made entirely from sulphite pulp at an integrated paper and pulp mill (The Timber Watch Coalition, 2009). All paper in the book is assumed to be made from wood-free uncoated paper. Wood-free refers to paper that is made from pulp which is free of lignin. This assumption includes the book covers. The weight of the book includes the cover of the book and weight of the paper within.

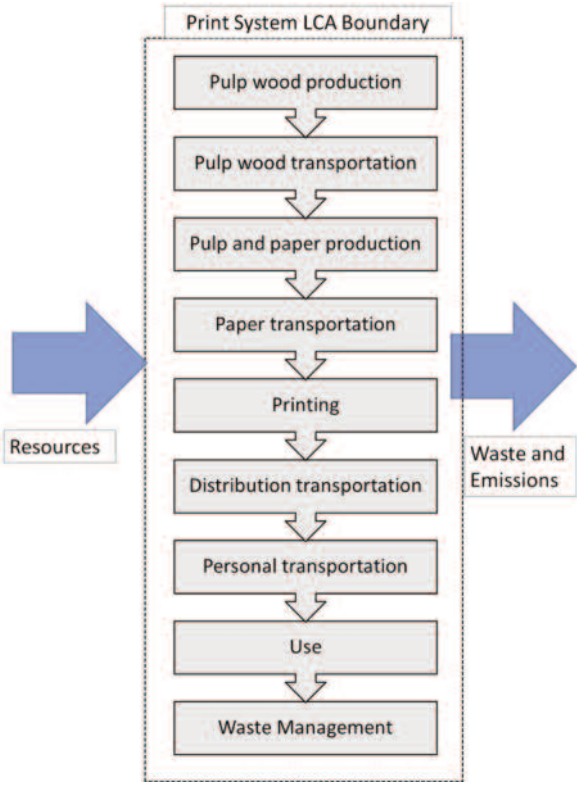

Figure 2: Print system boundary

Paper transportation

Five of the six major book printing houses in South Africa are located in Cape Town. The paper is therefore assumed to be transported 1 600 km

Table 1: Print system data inventory for the functional unit of 21 university books

Stage	*Process*	*Input*	*Value*	*Data regional source*
Pulpwood	Pulpwood	Pulpwood, hardwood, measured as solid wood under bark	1.000 m^3	Global
	Pulp wood transportation	Pulp wood Transport, freight, lorry >32 metric ton	47.520 ton.km	Global
Pulp production	Pulp production	Electricity, medium voltage	0.140 kWh	South Africa
Paper	Paper production	Pulpwood, hardwood, measured as solid wood under bark	0.003 m^3	South Africa
		Water, cooling, unspecified natural origin	0.017 m^3	South Africa
		Water, unspecified natural origin	0.072 m^3	South Africa
		Pulpwood, hardwood, measured as solid wood under bark	0.003 m^3	South Africa
		Sulphite pulp, bleached	0.030 m^3	South Africa
		Hard coal	0.008 kg	South Africa
		Electricity, medium voltage	0.350 kWh	South Africa
		Water, unspecified natural origin	0.052 m^3	South Africa
		Water, cooling, unspecified natural origin	0.056 m^3	South Africa
Paper distribution transport	Paper distribution transport	Transport, freight, lorry 16-32 metric ton, EURO III	41.561 ton.km	Global
Printed paper	Printed paper	Paper, woodfree, coated	1.385 kWh	South Africa
		Electricity, low voltage	0.717 kWh	South Africa
Personal transportation	Personal transportation	Transport, passenger car, medium size, petrol, EURO III	1.905 km	Global
Waste management	Waste management	Treatment of municipal solid waste, landfill	1.000 kg	Global

(Google Maps, 2014), from Durban to printing houses in Cape Town (Chamberlain et al., 2005).

Printing
The publishing and printing process is assumed to be similar to international procedures, so international data was used for this process stage. Only the electricity mix was changed to represent the South African electricity mix. Distribution transport was excluded.

Personal transportation
The personal transportation stage accounts for the consumer travelling in a personal vehicle to a bookshop to purchase books. For modelling the impacts of personal transportation, the data on emissions from EURO III vehicles was used, as South Africa's vehicle parc is a mixture of EURO III and IV vehicles (National Association of Automobile Manufacturers of South Africa, 2012). It was assumed that four two-way trips of 10 km each (Prinsloo, 2010) are made over the four-year period.

Printed paper book use
No impacts have been assumed with the reading of books.

Waste management
Although paper recovery rates in South Africa are high, the recycling of paper or use of recovered paper is not considered in this study as South Africa uses only virgin fibres in the production of writing paper grades and recycled paper is used to manufacture other grades of paper (Sappi, 2003). Hence the benefits of more than one life cycle for recycled paper have been omitted from this study.

2.4.2 Digital system
The life cycle of the iPad consists of the following stages:

- iPad production;
- e-book formatting;
- e-book downloading;
- distribution transportation of the iPad;
- personal transportation;
- use of e-books and the iPad; and
- waste management.

The system boundary is illustrated in Figure 3. The associated inventory data is shown in Table 2, with the assumptions that underpin this data being presented below.

Production of the iPad
The iPad is assembled in Foxconn's Chinese factories, so the Chinese mixes from the Ecoinvent v3.01 database were used for all materials where available. Where Chinese data is not available an average global mix was used. The mass of the iPad was entered as per the iPad Environmental Report (Apple, 2013). The energy and materials associated with the assembly of the iPad were not included as processes in this stage.

Distribution of the i-Pad
The distribution stage only included transportation of the iPad. The iPad is first shipped 32 500 km from China to South Africa via the regional distribution centre in the United Kingdom, and then trans-

Table 2: Digital system data inventory for 21 e-books

Stage	*Process*	*Input*	*Value*	*Data regional source*
iPad production	iPad	Flat glass, coated	61 g	Rest of Europe
		The LCD unmounted	109 g	Global
		Aluminium, wrought alloy	86 g	Rest of world
		Battery cell, Li-ion	161 g	China
		Acrylonitrile-butadiene-styrene copolymer	33 g	Rest of world
		Polystyrene, general purpose	66 g	Rest of world
		Corrugated board box	166 g	Rest of world
		Integrated circuit, logic type	24 g	Global
		Integrated circuit, memory type	8 g	Global
iPad distribution transportation	iPad distribution transportation	Transport, freight, sea, transoceanic ship	5.73 ton.km	Global
		Transport, freight, lorry 16-32 metric ton, EURO III	0.24 ton.km	Global
Personal transportation	Personal transportation	Transport, passenger car, medium size, petrol	10 km	Global
Use	E-book formatting	Operation, computer, desktop, office use	0.05 hr	Global
	E-book download	Electricity, low voltage	8.47 Wh	South Africa
	E-book reading	Electricity, low voltage	19.9 Wh	South Africa
Waste management	Waste management	Municipal solid waste (waste scenario)	100%	Global

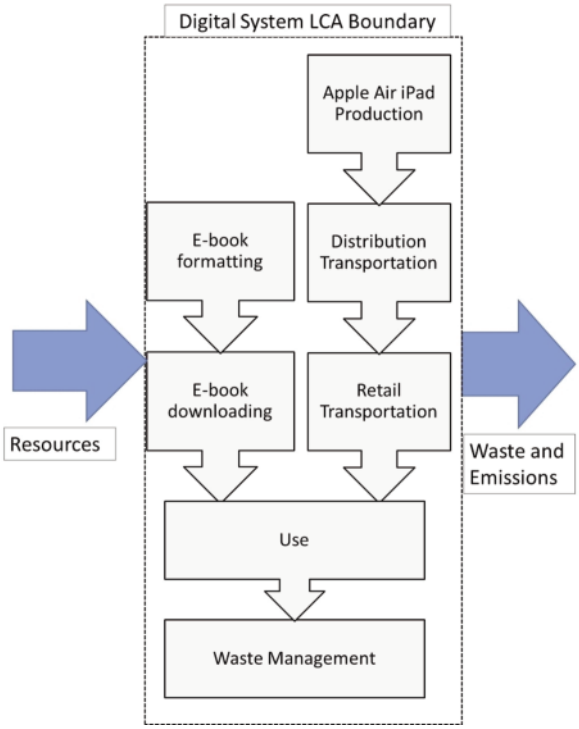

Figure 3: Digital system boundary

ported from Durban harbour (Maharaj, 2013) to Cape Town via truck, a distance of 1 630 km (Google Maps, 2014).

E-book formatting
It is assumed that each e-book is formatted for 50 hours using a computer as per Achachlouei et al. (2013). A further assumption is that one e-book is formatted for a 1 000 readers, i.e. 250 students per year for four years. It is assumed that the e-book will be used over the four-year period and will not undergo subsequent revisions.

E-book downloading
The e-book downloading impact is based on energy use to download the book by the user modem and router, access network DSLAM, internet, data centre, cables and operational activities as per Malmodin et al. (2011). It is also recognised that internet operations and connections are faster and more advanced in Europe than in South Africa, but this consideration is not addressed further in this study, which assumes users to be in middle- and high-income households which can afford high internet bandwidth speed connections. Only the energy usage is modelled for this lifecycle stage. No telecommunications infrastructure associated with the downloading is included.

Personal transportation
The personal transportation stage is the same as that for the purchasing of the books except that only one trip is made for purchasing the iPad.

E-book reading
The impact of charging an i-Pad for reading an e-book is included in the study, based on the battery life of an i-Pad and the time spent reading. This is described in further detail below.

Waste management
After use, most iPad components avoid landfill. It is assumed that only the battery and packaging of the iPad is sent to landfill (DEA, 2012). Whilst previous studies indicate that up to 80% of electronic devices can be recovered and recycled (Achachlouei et al., 2013), this study does not account for these benefits. The recovery stage is excluded because recovered materials will not be shipped back to China but will rather be used in making other products with different applications; as this study deals only with the iPad it would not make sense to include the lifecycle of another product.

2.5 Function, functional unit and reference flows

The study was based on the University of Cape Town Commerce degree booklist that prescribes 21 books over a four-year period. The functional unit can be described as 'the reading of 21 books by a single user two hours per day over a four-year period'.

The reference flow for the print system is 25.4 kg of paper required for the 21 books, and for the digital system it is the energy required to download and read 21 e-books, which is 13 733 Wh, based on Taylor and Koomey (2012).

2.6 Allocation procedure

Whilst there is no allocation required for the printed system, the digital system does have an applied allocation based on use. The iPad is a multifunctional device and this study assumes that it is used for reading for 2 out of 3.1 hours per day, or 64.5% of the time that the iPad is in use. The allocation percentage was applied to the production, distribution and retail transportation associated with the iPad to reflect the potential impacts due to just reading.

2.7 Impact assessment

SimaPro v 8.1 was used for this study. Since this study is concerned with just the environmental impacts and the energy demands of the print and digital system, two methods have been selected, namely the ReCiPe 1.09 midpoint hierarchist method for the environmental impacts and the cumulative energy demand (CED) method for the energy demand. The ReCiPe 1.09 method is one of the many different methods used in LCA, and has the advantage of being able to provide the user with both midpoint and endpoint indicators. The midpoint characterisation method can be described as

'a parameter in the cause-effect chain that or network (environmental mechanism) that is between the inventory data and the category endpoints', while endpoint characterisations factors are computed to indicate 'differences between the stressors at an end-point at a cause effect-chain and may be of direct relevance to society's understanding of the final effect' (Bare et. al, 2000). An example of a midpoint category indicator would be global warming potential in terms of CO_2 equivalents for the impact category for climate change, whilst for the same impact category the endpoint is damage to human health and ecosystems. In this study, however, only midpoint impact category indicators are being used to characterise environmental impacts.

Cumulative energy demand is described as 'the entire demand, valued as primary energy, which arises in connection with the production, use and disposal of economic goods (product or service) or which may be attributed to it respectively in a casual relation' (Frischknecht *et al.*, 2003). It thus focuses on a single parameter in the product's life cycle, represented in a commonly understood metric.

3. Results and discussion

3.1 Base case assessment

The results for the life cycle impact assessments using the ReCiPe midpoint method are shown in Table 4. Print can be seen to have lower impacts than the digital system in the categories of freshwater eutrophication, freshwater ecotoxicity, marine ecotoxicity, and metal depletion, whilst the digital system has lower impacts in the categories of climate change, ozone depletion, terrestrial acidification, marine eutrophication, human toxicity, photochemical oxidant formation, particulate matter formation, terrestrial ecotoxicity, ionising radiation, agricultural land occupation, urban land occupation, natural land transformation, water depletion and fossil fuel depletion.

The findings regarding global warming potential of the digital system as compared to the print system are contrary to those of Enroth (2009). The results of this study indicate that the print system's global warming potential is approximately 251% greater than the digital system's, whilst Enroth's results suggest that the global warming potential of the digital system is 10 times that of the print system. An increase in the amount of paper per book would decrease this gap. This study used an average book weight of 1.2 kg whilst Enroth used an average book weight of 0.8kg; this is taken to be the main cause of the different results. Another contributing factor is the difference in the energy mix between the two systems. South Africa's energy mix is more dependent on fossil fuel than that of Sweden, where Enroth's study was conducted. The findings of this study are also aligned with those of Moberg et al. (2011) who indicated that the digital e-book system with a lifetime of two years was preferred to the print system in terms of energy, abiotic depletion potential, global warming potential, terrestrial ecotoxicity potential, human toxicity potential and terrestrial toxicity potential.

Table 4: Results of the life cycle assessment

Characterisation factor name	*Unit*	*Base case print system*	*Base case digital system*	*IRP energy mix scenario print system*	*IRP energy mix scenario digital system*	*No. of users for print system to equal or better digital system*
Global warming potential	kg CO_2 eq	132.0	375.0	122.0	33.1	3
Ozone depletion potential	kg CFC-11 eq	0.00000512	0.00000118	0.00000557	0.00000139	7
Terrestrial acidification potential	kg SO_2 eq	0.724	0.289	0.633	0.247	2
Freshwater eutrophication potential	kg P eq	0.00935	0.0210	0.00847	0.0206	1
Marine eutrophication potential	kg N eq	0.0951	0.0244	0.9935	0.0237	6
Human toxicity potential	kg 1,4-DB eq	8.38	5.21	8.19	5.12	4
Photochemical oxidant formation	kg NMVOC	0.629	0.166	0.584	0.145	3
Particulate matter formation potential	kg PM10 eq	0.276	0.0892	0.253	0.0784	3
Terrestrial ecotoxicity potential	kg 1,4-DB eq	0.0199	0.00246	0.0198	0.00242	
Freshwater ecotoxicity potential	kg 1,4-DB eq	0.0629	0.206	0.0626	0.206	1
Marine ecotoxicity potential	kg 1,4-DB eq	0.0829	0.272	0.0816	0.271	1
Ionising radiation potential	kBq U^{235} eq	3.27	1.36	4.23	1.80	3
Agricultural land occupation potential	m^2a	462.0	0.557	462.0	0.547	
Urban land occupation potential	m^2a	4.50	0.249	0.249	0.237	
Natural land Transformation Potential	m^2	0.0347	0.00117	0.00117	0.00113	
Water depletion potential	m^3	193.0	86.2	86.2	85.7	4
Mineral resource depletion potential	kg Fe eq	0.465	15.2	15.2	15.2	1
Fossil resource depletion potential	kg oil eq	32.2	9.58	9.58	8.47	3

The land use impacts for the print system are also noted to be much larger than those of the digital system. The print system impact is approximately 827 times greater for agricultural land occupation, 17 times greater for urban land occupation and 29 times greater for natural land transformation. This would be expected, given the large land areas required for forestry.

The main observations regarding the print system can be summarised as follows:

- Paper production featured as a prominent stage in all categories except in agricultural land occupation and urban land occupation.
- Printing is also prominent, featuring in all categories except in agricultural and urban land occupation, and natural land transformation.
- Pulpwood is the major contributing stage in the impact categories concerning land use such as agricultural land occupation and urban land occupation.
- Personal transportation is a major contributor in ozone depletion, marine ecotoxicity, ionising radiation and fossil depletion.
- Waste management is the biggest contributor in marine eutrophication and global warming contributing to 46% and 15% of the total potential, respectively.

The following notes relate to contributions of the different life cycle stages to each impact category as shown in Table 4.

- The production of the iPad features as the major contributor in most impact categories. Impact categories almost entirely attributed to the production stage are metal depletion potential, freshwater eutrophication potential, marine ecotoxicity, freshwater ecotoxicity and agricultural land occupation.
- The e-book reading stage was the second-greatest contributor of impact potential. It has a large impact in global warming potential, terrestrial acidification potential, photochemical oxidation formation potential, particulate matter formation potential and fossil resource depletion potential.
- Personal transportation has a notable impact in global warming potential, ozone depletion, terrestrial ecotoxicity, ionising radiation, and fossil depletion.
- In comparison to the above stages, e-book formatting and downloading contribute little or nothing to any of the impact potentials.

3.2 Base case cumulative energy demand

The results from the CED analyses are shown in Table 5, which shows that the print system requires approximately three times more energy (1 525 MJ) to offer the same service as the digital system (473 MJ). This result is similar to the findings of Moberg et al. (2011) who report a difference of approximately 3.5 times.

The paper and printing processes are responsible for the greatest energy demand contribution to the life cycle of the paper system, contributing 41% and 39% respectively to the total life cycle energy demand (Figure 4). These results are in line with Enroth (2009) who suggests that half the energy demand for printed textbooks is within the paper and pulp production stage and a further 35% is consumed in printing.

In the digital system, the production of the iPad is the most prominent process, contributing 53% of the total CED. This is followed by e-book reading, which contributes 37% (Figure 5). These results seem to agree with the findings of Moberg et al. (2011) who also indicate that the production stage of the electronic device is the most prominent in energy consumption. According to the CED calculations, 94% of the print system energy is provided by fossil fuels and approximately 6% is from nuclear energy, whilst in the digital system 87% of the CED is obtained from fossil fuel and 13% from nuclear fuel. This observation is as a result of the print system being largely dependent on the South African

Table 5: Results of cumulative energy demand analysis

Print system			*Digital system*		
Process	*Base case energy (MJ)*	*IRP energy (MJ)*	*Process*	*Base case energy (MJ)*	*IRP energy (MJ)*
Pulpwood	31	31	iPad production	251	251
Pulp	19	18	iPad distribution transportation	1	1
Paper	617	597	Personal transportation	41	41
Paper distribution transportation	96	96	E-book formatting	0	0
Printing	594	563	E-book downloading	2	2
Personal transportation	166	166	E-book reading	176	153
Waste management	4	4	Waste management	0	0
Total	1525	1474	Total	473	450

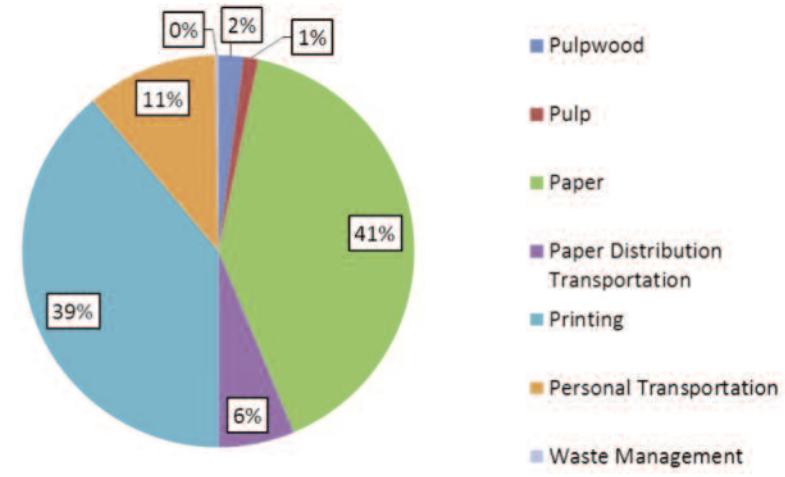

Figure 4: Print system cumulative energy demand (MJ)

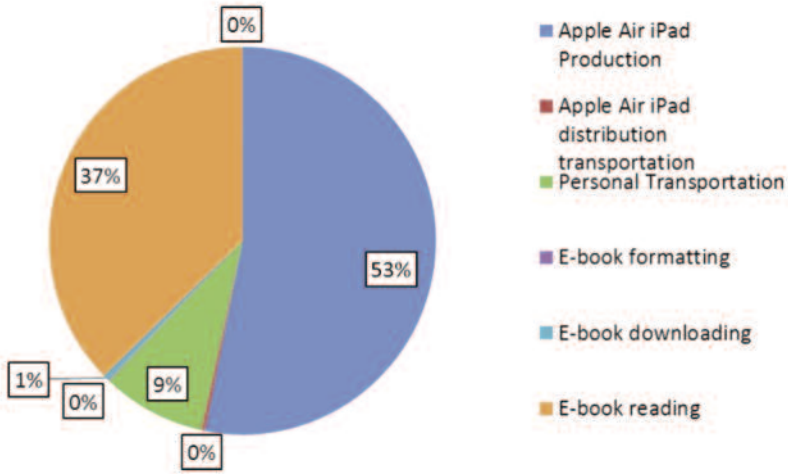

Figure 5: Digital system cumulative energy demand (MJ)

electricity mix, while the digital system is dependent on a global, and to some extent a Chinese, electricity mix (which are both less coal-dependent than the South African mix).

3.3 The IRP energy mix scenario

The introduction of a new energy mix as proposed in the 'policy-adjusted IRP' scenario for 2030 reduces the relative difference of the impacts between the digital and print systems, in most impact categories, as seen in Table 4. The 2030 IRP mix assumes a greater reliance on nuclear energy and renewable energy and a reduced reliance on coal energy. Coal processes feature in most of the impact categories as a significant contributor to the impact potentials. The CED (Table 5) for renewable energy sources is less than that of fossil fuels because of the less energy-intensive processes upstream. By changing the electricity mix, the way in which the demand is met also changes, and hence the cumulative energy demand changes.

The print system improves relative to the digital system when compared to the base case for certain of the impact categories, being ozone depletion and agricultural land occupation. There is little or no change to terrestrial acidification, metal depletion, water depletion, marine ecotoxicity, freshwater ecotoxicity and ionising radiation. The impact categories that see relative increases between the print and the digital system are global warming potential, fossil depletion, urban land occupation, photochemical oxidation formation, freshwater eutrophication and terrestrial acidification. The changes in the results can be attributed to the increase in the use of gas for proposed gas power plants and also from the nuclear fuel, energy production and waste that come with the increased use of nuclear power, as proposed in the IRP electricity energy mix.

The CED results in Table 5 indicate that the change to the 2030 IRP electricity energy mix has a positive impact on both systems, with the print system having a total reduced CED of 3% and the digital system having a total CED reduction of 5%. Since the CED is met with fewer inputs of primary energy commodities, the stages that are most dependent on electricity in the print system, paper and printed paper, have reduced cumulative energy demands. The pulpwood, book distribution trans-

portation, personal transportation and waste management are not affected.

3.4 Multiple users per book scenario

The break-even point is defined here as a measure of the point at which the number of users sharing books causes the print system to have lower impact than the digital system. This point differs between the different impact categories (Table 4). As indicated previously, in the impact categories of freshwater eutrophication, freshwater ecotoxicity, marine ecotoxicity and metal depletion, even with one user per book the digital system impacts are greater than those of the print system. Two users per system is the break-even point for the impact category of terrestrial acidification; three users per system is the break-even point for climate change, photochemical oxidant formation, particulate matter formation, ionising radiation and fossil depletion; four users per system is the break-even point for water depletion and human toxicity potential; six users per system is the break-even point for marine eutrophication; and seven users per system is the break-even point for ozone depletion. The impact categories associated with land cannot reach the break-even point within the maximum of eight users. This can be explained by the print system using a large amount of wood and hence the impacts associated with land use for the forest wood plantations are far greater than the digital system, which depends more on metal and mineral resources.

The LCA results thus suggest that a book used in a library could prove environmentally preferred to reading an e-book on iPads, for the same number of users. The greater the number of users per book, the more beneficial it is to read from a printed book. This result confirms the findings of Kozak (2003), Gard and Keoleian (2003) and Toffel and Hovarth (2004). The CED results also indicate that the print system is increasingly favoured as the number of users increase. In contrast, the digital system energy demand increases almost linearly with each additional user as would be expected. The break-even point for the number of users seems to be approximately three users sharing their books. The CED results thus also indicate that reading a printed book in a library could, for a large number of users, prove more environmentally preferred and be less energy demanding than reading e-books on an iPad.

4. Conclusions and recommendations

The objective of the study was to establish which of the systems, digital or print, had less of an environmental and energy demand impact. The initial hypothesis of this study was that reading 21 e-books from an iPad would have a smaller environmental impact and energy consumption than reading them in printed form.

When the two systems are compared in terms of impact potentials, the digital system emerges as the environmentally preferred system for certain impact categories, including climate change, ozone depletion, terrestrial acidification, marine eutrophication, human toxicity, photochemical oxidant formation, particulate matter formation, terrestrial ecotoxicity, ionising radiation, agricultural land occupation, urban land occupation, natural land transformation, water depletion and fossil depletion. The study's initial hypothesis is therefore proved partially correct, as each system is preferable in terms of certain impacts.

The stages with the highest contribution to the impact potentials and cumulative energy demand for the print system are the printing and paper stages. Electricity produced in South Africa using hard coal also features as a one of the main contributing processes in these stages. Mining also features prominently in fossil depletion potential and urban land occupation, and the disposal of coal-mining waste is the main contributing process for freshwater eutrophication potential.

The other major finding is that the print system has much larger land-based impacts than the digital system, because of the large amount of wood needed to produce books. The impact potentials for agricultural land occupation, urban land occupation, and natural land transformation are significantly higher for the print than the digital system.

The digital system is influenced by both local and international processes. The iPad production stage is the prominent contributor in most impact categories. The e-book reading stage is the second-greatest contributor in terms of impact potentials. It has a large impact in global warming potential, terrestrial acidification potential, photochemical oxidation formation potential, particulate matter formation potential and fossil resource depletion potential. The main processes are the production of electricity using coal, coal-mining and coal waste disposal. The digital system is also dependent on coal processes because it is based on the Chinese electricity mix, which has a large dependency on coal (although recognising this dependence is not as high as South Africa's). In the digital system, the production of the iPad in China has the greatest energy demand and is responsible for 53% of the total cumulative energy demand, followed by e-book reading (37%).

The results of the IRP 'adjusted policy' scenario reveal that the IRP electricity mix change reduces the environmental impacts and cumulative energy demand of both systems. As expected, however, the digital system realised a greater reduction.

The final scenario assessed the effects of multiple users reading each book. The break-even point was reached for most impact categories at four users whilst a break-even point for impacts associated with land-use could not be reached even with

eight users. This was because the print system has a much greater reliance on wood products compared to the digital system, and even with multiple users this gap cannot be overcome.

Reading e-books from an iPad could be encouraged in universities because the findings of this study suggest that the environmental impact of e-books read on iPads is less than that of reading printed books. However, this will depend to an extent on the amount of reading material and whether the re-use of books or sourcing books from the library is actively promoted at the university.

References

Achachlouei, M.A., Moberg, A. & Honschhorner, E. 2013. Climate change impact of electronic media solutions: Case study of the tablet edition of a magazine. Centre for Sustainable Communications, Royal Institute of Technology, Stockholm, Sweden.

Apple. 2013. iPad Air Environmental report, Apple. October 2013. Available: https://www.apple.com/environment/reports/docs/iPadAir_PER_Oct2013.pdf.

Bare, J.C., Hofstetter, P., Pennington, D. W. & de Haes, H. A.U. 2000. Life cycle impact assessment workshop summary: Midpoint versus endpoints: The sacrifices and benefits. *International Journal of LCA* 5(6):319–326.

Chamberlain; D., Essop, H., Hougaard, C., Walker, R. 2005. The contribution, costs and development opportunities of the forestry, timber, pulp and paper industries in South Africa: Part III: Technical notes and appendices. Genesis Analytics, Johannesburg. Available: http://www.daff.gov.za/doaDev/sideMenu/ForestryWeb/dwaf/cmsdocs/Elsa/Docs/FED/SA%20Forestry%20Industry%20Market%20Analysis%202005.pdf.

Department of Environmental Affairs. 2012. Identification of the magnitude of the electrical and electronic (e-waste) situation in South Africa: A strategic approach to international chemicals management (SAICM) e-waste as an emerging policy issue. Africa Institute for Environmentally Sound Management of Hazardous and Other Wastes, and the Department of Environmental Affairs. Available: http://africainstitute.info/wp-content/uploads/2013/02/E-WASTE-South-Africa-2012.pdf

Enroth, M. 2009. Environmental impact of printed and electronic teaching aids, a screening study focusing on fossil carbon dioxide emissions. *Advances in Printing and Media Technology* 36, 2009.

Frischknecht, R., Jungbluth, N., Althaus, H., Doka, G., Dones, R., Hirschier, R., Hellweg, S., Humbert, S., Margni, M., Nemecek, T., Spielmann, M. 2003. Implementation of life cycle impact assessment methods. EcoInvent Report 3, Swiss Centre for LCI, Duebendorf, Switzerland. Available: http://www.ecoinvent.org/fileadmin/documents/en/03_LCIA-Implementation-v2.2.pdf

Gard, D.L. & Keoleian, G. A. 2003. Digital versus print: Energy performance in the selection and use of scholarly journals. *Journal of Industrial Ecology* 6(2): 115–132.

International Standards Organisation. 2006. ISO 14040:2006: Principles and framework of LCA. International Standards Organisation.

Kozak, G. 2003. Printed Scholarly books and e-book reading devices: A comparative life cycle assessment of two book options. Centre for Sustainable Systems, University of Michigan, Report No. CSS03-04. Available: http://css.snre.umich.edu/css_doc/CSS03-04.pdf [2014, July 6].

Malmodin, J., Lundén, D., and Andersson, G. 2011. Lifecycle assessment of ICT networks and primary subscription services in Sweden. In Presentation slides and Abstract to the 3rd NorLCA Symposium (Helsinki, Finland, September 15-16 2011).

Moberg, Å., Borggren, C. & Finnveden, G. 2011. Books from an environmental perspective – Part 2: e-books as an alternative to paper books. *International Journal of LCA* 2011(16):238–246. DOI: 0.1007/s11367-011-0255-0.

National Association of Automobile Manufacturers of South Africa. 2012. Current and future trends of the South African car parc. Paper presented by Eckart Kruger, 30 March 2012. Available: http://www.energy.gov.za/files/IEP/presentations/CurrentFutureTrends_SA_CarParc_30MArch2012.pdf [2014, August 9].

Prinsloo, D. 2010. Classification and hierarchy of retail facilities in South Africa. Available: http://www.urbanstudies.co.za/wp-content/uploads/2014/07/New-Retail-Classification-2010.pdf [2014, August 9].

Sappi. 2003. The paper making process from wood to coated paper. Available: http://www.sappi.com/regions/sa/service/mediadownloads/Pages/default.aspx [2014, July 6].

Sappi. 2012. Frequently asked questions about: eucalyptus trees. Available: http://www.sappi.com/group/Sustainability/FAQs/Sappi-FAQs-Eucalypts.pdf [2014, July 6].

Taylor, C. & Koomey, J. 2008. Estimating energy use and greenhouse gas emissions of internet advertising. February 14th, 2008 Working Paper. IMC2.

The Timber Watch Coalition. 2009. Pulp mills and plantations: Environmental, social and economic impacts of the pulp and paper industry globally and in South Africa. The Timber Watch Coalition, Mayville, South Africa. Available: http://www.timberwatch.org/userfiles/Social%20impacts%20of%20certified%20timber%20plantations%20in%20South%20Africa%20-%20TW(2).pdf [2014, July 6].

Toffel, M.W. & Horvath, A. 2004. Environmental Implications of Wireless Technologies: News Delivery and Business Meetings. *Environmental Science & Technology* 38(11): 2961- 2970.

Wolf, M., Pant, R., Chomkhamsri, K., Sala, S. & Pennington, D. 2012. The international reference life cycle data system handbook. Institute for Environment and Sustainability in the European Commission Joint Research Centre. Available: http://eplca.jrc.ec.europa.eu/uploads/JRC-Reference-Report-ILCD-Handbook-Towards-more-sustainable-production-and-consumption-for-a-resource-efficient-Europe.pdf.